Review

Combined Radiations: Biological Effects of Mixed Exposures Across the Radiation Spectrum

Orfeas Parousis-Paraskevas , Angeliki Gkikoudi , Amer Al-Qaaod , Spyridon N. Vasilopoulos , Gina Manda , Christina Beinke , Siamak Haghdoost , Georgia I. Terzoudi , Faton Krasniqi , Alexandros G. Georgakilas *

Posted Date: 25 June 2025

doi: 10.20944/preprints202506.2020.v1

Keywords: mixed radiation fields; ionizing radiation; non-ionizing radiation; DNA damage; combined irradiation; simultaneous irradiation; synergistic effects; radiation protection

 doi:10.20944/preprints202506.2020.v1

Review

Combined Radiations: Biological Effects of Mixed Exposures Across the Radiation Spectrum

Orfeas Parousis-Paraskevas [1,†], Angeliki Gkikoudi [1,2,†], Amer Al-Qaaod [3], Spyridon N. Vasilopoulos [1], Gina Manda [4], Christina Beinke [5], Siamak Haghdoost [6], Georgia I. Terzoudi [2], Faton Krasniqi [3] and Alexandros G. Georgakilas [1,*]

[1] DNA Damage Laboratory, Physics Department, School of Applied Mathematical and Physical Sciences, National Technical University of Athens (NTUA), Zografou Campus, 15780 Athens, Greece; ge17035@mail.ntua.gr (O.P.-P.); angelikigkikoudi@mail.ntua.gr (A.G.); svasilopoulos@mail.ntua.gr (S.N.V.)

[2] Laboratory of Health Physics, Radiobiology & Cytogenetics, Institute of Nuclear & Radiological Sciences & Technology, Energy & Safety, National Centre for Scientific Research "Demokritos", 15341 Agia Paraskevi, Greece; gterzoudi@rrp.demokritos.gr (G.I.T.)

[3] Physikalisch-Technische Bundesanstalt (PTB), Bundesallee 100, 38116 Braunschweig, Germany; amer.al-qaaod.ext@ptb.de (A.A.-Q.); faton.krasniqi@ptb.de (F.K.)

[4] Radiobiology Laboratory, "Victor Babes," National Institute of Pathology, 99-101 Splaiul Independentei, 050096 Bucharest, Romania; gina.manda@ivb.ro (G.M.)

[5] Bundeswehr Institute of Radiobiology, University of Ulm, Neuherbergstraβe 11, 80937 Munich, Germany; christinabeinke@bundeswehr.org

[6] ABTE/ToxEMAC Laboratory, University of Caen Normandy, F-14050 Caen, France; siamak.haghdoost@unicaen.fr (S.H.)

* Correspondence: alexg@mail.ntua.gr; Tel.: +30-210-7724453

† Equal contribution.

Abstract

The growing use of mixed radiation exposures in medicine, space exploration, and environmental contexts has emphasized the need to understand their biological effects. This review compiles and analyzes findings from over 170 studies examining combinations of ionizing and non-ionizing radiation types, including ultraviolet light, X-rays, gamma rays, alpha and beta particles, protons, neutrons, and heavy ions. Through a structured literature survey, we organized studies into three main domains: radiobiological, therapeutic, and space radiation. Results reveal frequent additive and/or synergistic interactions—especially when radiation types are applied sequentially within short intervals—that affect DNA repair kinetics, cell survival, and gene expression. The degree of synergy often depends on dose, exposure sequence, and the involvement of specific repair pathways. Therapeutic combinations, such as carbon ion–proton therapy or radiotherapy–photodynamic treatment, show enhanced efficacy and tolerability in preclinical and clinical settings. In contrast, space and environmental studies illustrate the complexity of mixed-radiation effects, including immune suppression and persistent DNA damage. This review provides a consolidated reference framework for the diverse and evolving field of combined radiations, emphasizing the need for mechanistic studies and standardized protocols to guide safe and effective implementation across applications, such as radiation protection, therapy, and space mission planning.

Keywords: mixed radiation fields; ionizing radiation; non-ionizing radiation; DNA damage; combined irradiation; simultaneous irradiation; synergistic effects; radiation protection

1. Introduction

Different types of radiation can be combined in various contexts, whether therapeutic or experimental; they may be applied to biological or non-biological targets, simultaneously or

 doi:10.20944/preprints202506.2020.v1

sequentially, with intervals between irradiations ranging from minutes to weeks. The dose of each combined radiation type is another important factor, as are other dosimetric features of a given experimental configuration. For biological targets, a number of endpoints (specific measurable biological outcomes) can be utilized to determine the induced effects, the specification of which is typically the main aim of most related research articles. "Combining different radiation types" thus constitutes a broad set of practices, involving a variety of methods developed and applied for distinct purposes.

Yet despite this diversity, no comprehensive review has systematically assembled the relevant literature according to clearly defined criteria for combined radiation exposures to date. In many respects, this review pursues a rather ambitious aim: to create a concise map of the published studies on the radiobiological and therapeutic utilization of combined radiation exposures, discussing and analyzing the qualitative and quantitative characteristics of this highly promising, long-standing set of practices. It aims to provide a succinct depiction of the diverse processes and outcomes that define the use of mixed irradiation in biological systems, reflecting our current scientific understanding of this multifaceted field.

2. Methodology

The challenges impeding an instantaneous compilation of all relevant publications required for such an extensive review arise from a range of factors, including the dispersion of publications across a wide variety of databases, shifting terminology and evolving epistemological frameworks. The selection criteria applied during the literature review are presented here to clarify the rationale behind the inclusion of each study in the compiled database. First, we determined which types of combined radiations to include—specifically, which wavelength and/or energy ranges were relevant. Our focus aligned with conventional and space radiobiology, as well as several combined therapeutic modalities. Consequently, other forms of mixed exposure, such as environmental exposure to extremely low-frequency electromagnetic fields (ELF-EMF) or microwave radiation in combination with other types, were intentionally excluded from this review. Similarly, combinations involving radiation and non-radiation agents, such as chemicals or microgravity, were also excluded, as they fall outside the scope of radiation–radiation interactions. In rare cases where non-radiation factors were present (e.g., the NASA Twins Study), the inclusion of those publications was primarily justified by their focused investigation of combined radiation exposures, with any additional variables considered secondary. Regarding the combinatorial nature of the exposures, studies involving the sequential application of radiations with time intervals longer than those typically defining combinatorial exposure (e.g., >24 h) were mostly excluded.

The radiation types included in the search were near-infrared (NIR), visible (VIS), ultraviolet (UV), X-rays, gamma rays (γ), alpha radiation (α), beta radiation (β), protons (p), neutrons (n), and heavy ions. In addition, space-relevant mixed fields—such as high atomic number and energy (HZE) particles and simulated ion beam combinations (e.g., 5-ion or 33-ion beams)—were incorporated to reflect realistic space radiation exposures. Therapeutic modalities considered included conventional radiotherapy (RT), intensity-modulated radiation therapy (IMRT), boron neutron-capture therapy (BNCT), carbon ion radiation therapy (CIRT), radionuclides therapy (RNT), proton therapy (PT), photodynamic therapy (PDT), photothermal therapy (PTT), near-infrared photoimmunotherapy (NIR-PIT), helium ion radiation therapy (HIRT), electron beam radiation therapy (EBRT), fast neutron therapy (FNT), megavoltage X-ray therapy (megavoltage XRT), and californium-252 neutron therapy (Cf-252 NT).

The methodological approach for the literature review involved several phases. Initially, databases and search engines—such as PubMed, Google Scholar, Semantic Scholar, bioRxiv, and Europe PMC—were searched manually using combinations of keywords, Boolean operators, and filters, covering publications available up to June 20, 2025. Titles were extracted and categorized based on radiation combinations. The "related articles" or "related results" features were also used to locate additional relevant publications. In categories that initially included only one or very few

 doi:10.20944/preprints202506.2020.v1

studies, targeted searches were conducted to retrieve further publications, aiming to achieve a more representative sample for each radiation combination. Despite these efforts, some combinations remain represented by a single study; however, their inclusion was preferred over omitting a radiation combination entirely from the review.

A master table was created, consisting of columns detailing the combined radiation types, doses, biological systems, biological endpoints, and effects recorded for each study. Abstracts and relevant sections of the selected publications were reviewed to extract key data, which were organized into structured entries corresponding to the table's columns.

In the final phase, the master table was split into separate tables, each corresponding to a specific combination of radiation types as studied across the selected publications. Rows were redistributed accordingly and reviewed manually. No specific order—chronological or otherwise—was applied to either the newly created tables or their rows. The tables were then regrouped into three overarching categories: "Radiobiological Studies" (with the sub-categories *Non-Ionizing–Ionizing*, *Non-Ionizing–Non-Ionizing*, and *Ionizing–Ionizing*), "Therapeutic Studies," and "Space Radiation Studies". This regrouping resulted in five new tables, which were inserted into the manuscript. Subsequently, the finalized dataset underwent analysis, processing, and discussion.

3. Results

Over 170 studies were retrieved and reviewed. The compiled data spanned a wide spectrum of exposures, including combinations of ionizing and non-ionizing radiation, as well as high- and low-LET (Linear Energy Transfer) modalities. In this review, *synergy* refers specifically to biological effects that exceed additive expectations based on responses to individual radiation types. These include outcomes such as increased chromosomal aberrations, reduced cell survival, or gene expression changes that cannot be explained by a simple summation of single-exposure effects. Quantitatively, synergy was inferred when the combined effect was statistically greater than the predicted additive response, or when modeled interaction terms (e.g., interaction index > 1) indicated non-linear enhancement. Studies showing that the effect of combined exposure depended on irradiation order or specific DNA repair pathways were also considered synergistic, provided the damage exceeded what would be expected from the individual exposures alone. The following tables summarize key findings across the reviewed studies, organized by radiation type and dose, biological systems, endpoints and observed effects. These are presented first, followed by detailed commentary on the results.

Table 1. Radiobiological Studies on Combinations of Non-Ionizing and Ionizing Radiation.

Type & Dose	Biological systems	Biological endpoints	Effects	Ref.[1]
X-rays: 150 rad; UV-C (254 nm): 70 erg/mm²; irradiations 2–6 h post-PHA stimulation	PHA-stimulated human lymphocytes (G_1 stage)	Dicentric and chromatid-type chromosome aberrations (first mitosis)	• No synergistic effect observed • Dicentric yields from combined exposures matched X-rays alone • UV induced only chromatid-type aberrations • Suggests G_1 cells possess enhanced repair capacity preventing UV–X-ray interaction	[1]
X-rays (260 kV): 125–200 rad; UV-C (253.7 nm): 40–100 erg/mm²; exposures ≤30 sec apart	Human peripheral blood lymphocytes (unstimulated, G_0 stage)	Dicentric chromosome formation (cytogenetic analysis)	• ~2-fold synergistic ↑ in dicentrics vs. X-rays alone • Synergy consistent across UV doses and exposure order • Suggests interaction between X-ray-induced breaks	[2]

 doi:10.20944/preprints202506.2020.v1

			and UV-mediated repair inhibition or lesion overlap	
UV-C (254 nm): up to 1000 ergs/mm²; X-rays (50 kVp): up to ~10 krads/min	*E. coli* K-12 wild-type; DNA repair mutants (uvrA, uvrB, uvrC, recA, recB, recC, exrA, polA)	Cell survival; DNA single-strand break repair (alkaline sucrose gradients)	• ↑ X-ray sensitivity after UV pretreatment (wild-type and uvr mutants) • UV inhibits Type III repair of X-ray-induced DNA SSBs • No synergism in recA, recB, recC, exrA mutants	[3]
Near-UV (365 nm): up to 2.5× 10^6 J/m²; X-rays (250 kVp): up to 19.6 krad (2 krad/min); UV administered ~3–5 min before X-rays	*E. coli* K12 strains (wild-type W3110, polA mutant P3478, recA recB mutant SR111)	Clonogenic survival; single-strand break rejoining (alkaline sucrose gradients); DNA degradation (TCA-insoluble material)	• Pre-treatment with 365 nm UV enhanced X-ray lethality (up to 3.4× slope ↑ in survival curves) • Synergism absent in recA recB mutants • 365 nm inhibited type II and III DNA repair • Full-medium incubation partially restored repair in wild-type and recA recB but not in polA	[4]
UV-C (254 nm): up to 960 ergs/mm²; X-rays (150 kVp): up to 40 krads	*E. coli* B/r and Bs-1 strains; 5-BU substituted DNA and purine-starved cells	Cell survival; UV-X-ray synergism; repair inhibition by 5-BU and purine starvation	• ↑ X-ray sensitivity after UV pretreatment in B/r (up to 3×) • No synergism in 5-BU substituted or purine-starved cells • UV and 5-BU inhibit X-ray repair • No effect in Bs-1 cells	[5]
UV-C (254 nm): 65–95 erg/mm²; X-rays (260 kVp): 150 rad; exposures given in sequence with <30 sec interval	Human peripheral blood leukocytes from healthy donors; human peripheral blood leukocytes from Down's syndrome patients	Chromosome aberrations (dicentrics); DNA repair synthesis ([3H]thymidine incorporation); synergistic aberration induction	• ↑ Dicentrics after combined UV + X-rays vs X-rays alone (2× in controls, 27% in Down's syndrome) • ↓ UV-induced DNA repair synthesis in Down's syndrome cells, synergism suggests shared repair pathways	[6]
X-rays (260 kVp, 0.5 Gy/min): 1.5 Gy; UV-C (254 nm): 6 J/m²; timing between irradiations varied from <30 sec to 90 min	Human peripheral blood lymphocytes in G_0 phase; cultured and analyzed for chromosomal aberrations	Yield of dicentric chromosomes per cell; timing dependence of synergistic chromosome aberration induction	• UV followed by X-rays produced a stable 2-fold ↑ in dicentrics across all timing intervals • X-rays followed by UV showed decreasing synergistic effect with ~20 min half-life • Indicates short-lived DNA lesions responsible for early chromosome exchange events	[7]
UV-C (254 nm): 1–120 J/m²; X-rays (100 kVp): 6.7–26.6 krad or alpha particles (4.5 MeV, LET 140–180 keV/μm): 4–48 krad	Diploid *Saccharomyces cerevisiae* strains (wild-type, rad2 mutant, rad9 mutant)	Colony-forming ability; survival curves; synergism analysis (shoulder reduction, slope changes)	• ↑ Synergistic loss of colony-forming ability when X-rays precede UV • Reduced UV survival shoulder, altered slopes depending on repair genotype	[8]

 doi:10.20944/preprints202506.2020.v1

			• Synergism absent or reduced in rad2 and rad9 mutants	
X-rays (50 kVp): up to 8000 rads; UV-C (254 nm): up to 1620 erg/mm²	HeLa cells (G_1 phase)	Premature chromosome condensation (PCC); chromosome fragmentation, unscheduled DNA synthesis	• ↑ Chromosome fragmentation with X-rays (linear with dose), no DNA synthesis • UV causes elongation to "S-like" PCC and ↑ unscheduled DNA synthesis, no fragmentation	[9]
Gamma rays: 90 krad; UV-C (254 nm): 170 J/m²; exposures sequential, no delay	*Schizosaccharomyces pombe* (wild-type 972h⁻) and rad1 mutant	Inactivation (colony survival); recovery kinetics; involvement of recombinational repair	• Strong synergistic interaction in wild-type cells • Survival dropped >100× beyond additive prediction • No synergism in recombinational repair-deficient rad1 mutant • Recovery kinetics depend on second radiation type, not first	[10]
Gamma rays: 0.1–0.3 Mrad; UV-C (253.7 nm): 270–810 J/m²; exposures ≤5 min apart	*Micrococcus radiophilus*	Survival/colony-forming ability	• Synergistic killing effect with UV pre-treatment (3.5× increased gamma ray sensitivity) • Additive effect with gamma pre-treatment	[11]
Gamma rays: 200–600 krad; UV-C (254 nm): 140–560 J/m²; exposures ≤2 min apart	Wild-type and mutant *Bacillus velezensis* strains from soil and oil samples; screened for surfactin production and antifungal activity	Hemolytic activity, emulsification index, oil spreading, antifungal zone diameter, MALDI-TOF for surfactin isoforms	• Mutant AF-UVγ2500 showed ~2× higher surfactin yield (1.62 g/L vs. 0.85 g/L) • Stronger antifungal activity, 3× isoform abundance • Combined mutagenesis more effective than single-agent treatment	[12]
Electron beam (32 MeV): 21–28 krad; UV-C (254 nm): 450 erg/mm²; exposures ≤2 min apart	*E. coli* B/r	Survival/colony-forming ability	• Synergism observed • Inhibited by 3 h liquid holding between irradiations regardless of order • Attributed to excision repair activity	[13]
Beta particles (^{32}P, internal): time-integrated decay (up to 25 mc/mg P); UV-C (254 nm): 120–530 erg/mm²; exposures sequential with varied timing and order	*Salmonella typhimurium* strain LM2	Inactivation (colony-forming ability); synergy quantified via survival slopes and modeling	• Strong synergistic effect between ^{32}P decay and UV damage • Reciprocity observed (UV→^{32}P and ^{32}P→UV) • Synergy eliminated by photoreactivation, suggesting interaction between nonlethal DNA lesions (e.g., thymine dimers and p^{32}-induced strand breaks) within ~25 nucleotide pairs	[14]

 doi:10.20944/preprints202506.2020.v1

UV-C (254 nm): 150 ergs/mm²; Protons (LET 20 keV/μm): 8–40 krads	*E. coli* B/r (wild-type, log-phase)	Survival (loss of reproductive capacity)	• UV pre-exposure sensitized cells to protons • Survival curve slope increased 1.5–1.7× • Synergy not observed when reverse order applied or with other radiation types • Suggests repair system involvement	[15]
NIR (600–1400 nm, non-thermal): 360 kJ/m² (30 min); X-rays (90 kV, 5.23 Gy/min): 1–4 Gy; sequential exposure with NIR pretreatment 30 min before X-rays; temperature-controlled setup	Human full-thickness skin model (primary dermal fibroblasts and keratinocytes)	DNA double-strand breaks (53BP1, γH2AX); cell proliferation (BrdU, Ki-67); apoptosis (TUNEL); morphology (H&E)	• NIR pretreatment delayed repair of X-ray–induced DSBs • Protected fibroblasts from apoptosis • Counteracted X-ray–induced proliferation inhibition in keratinocytes • No morphological disruption observed • Photobiomodulation modulated radiation stress response	[16]
Gamma rays: 1–3 Gy; low-intensity laser (670 nm): 5.3–10.6 J/cm²	Human full-thickness skin model (primary dermal fibroblasts and keratinocytes)	Cell counts (RBC, WBC, LYM); enzyme activity (SOD, catalase); blood oxygenation	• No synergistic toxicity • Laser pretreatment ↑ leukocyte counts, antioxidant enzyme activity, and oxygenation • Evidence of radioprotective effects from laser pre-irradiation	[17]

[1] Reference.

Table 2. Radiobiological Studies on Combinations of Non-Ionizing and Non-Ionizing Radiation.

Type & Dose	Biological systems	Biological endpoints	Effects	Ref.
UV-A (365 nm): 49 W/m²; UV-B (311 nm): 8 W/m²; simultaneous exposure for 6–8 h/day	*E. coli* MG1655 (wild-type and mutant strains)	Photoinactivation (colony survival); genetic basis of UV-A-UV-B synergy	• Strong synergistic inactivation effect (~100× more than UV-B alone) • Synergy traced to thiouridine (s^4U) in tRNA absorbing UV-A and impairing protein synthesis, reducing DNA repair • Mutants with *thiI* gene alterations lost synergy, confirming mechanistic link	[18]
UV-A (365 nm): 700 W/m²; UV-C (254 nm): 0.7 W/m²; simultaneous irradiation for 6 min in 96-well plate format	*Vibrio parahaemolyticus* WT and recA/lexA mutants; cultures in LB broth	DNA damage (CPDs, 8-OHdG); colony-forming assay (log survival); SOS response analysis	• Simultaneous UV-A+UV-C caused synergistic bactericidal effect (log survival −3.3) vs. additive effects of single/seq. exposure (−2.1) • CPD repair suppressed • Synergy absent in SOS-deficient mutants, implicating RecA/LexA-dependent repair in survival	[19]

 doi:10.20944/preprints202506.2020.v1

UV-B (280–315 nm): 1080–3600 J/m²; UV-C (100–280 nm): 280–930 J/m²	*Sclerotinia sclerotiorum*; tomato plants	Disease suppression, plant health, gene expression	• Combination had strongest pathogen suppression and yield/quality improvement • ↑ defense gene expression and antioxidants	[20]
UV-B (290–320 nm): physiologic; UV-A (320–400 nm): physiologic; Visible light (400–740 nm): physiologic; Near-infrared (IRA, 770–1400 nm): physiologic; simultaneous full-spectrum exposure	Human skin cells and tissue (keratinocytes, fibroblasts, full skin models)	Photoaging biomarkers (MMP-1, collagen expression), gene expression (MAPK signaling), pigmentation, oxidative stress	• Marked synergistic effects across wavelengths • Combined exposure → responses distinct from single or sequential exposures • Enhanced MMP-1, ROS, angiogenesis, pigmentation • Molecular cross-talk shown between UV-B, UV-A, IRA pathways affecting MAPK signaling and DNA repair	[21]
UV-A (379.68 nm): ~11.65 μW/cm²; UV-B (305.22 nm): ~8.65 μW/cm²; 6 h/day exposure for up to 27 days	Scyphozoan jellyfish polyps (*Aurelia* sp.)	Asexual reproduction (budding rate), polyp detachment, survival, qualitative health (tentacle retraction, feeding)	• Strong synergistic effect: combined UV-A + UV-B caused 100% mortality by day 21 • No budding, total loss of attachment and feeding • UV-B alone reduced reproduction and health • UV-A alone had minimal impact • Combined exposure drastically worsened all outcomes	[22]
UV-A (365 nm): 600–1200 mJ/cm²; UV-C (268 nm): 2.5–20 mJ/cm²; sequential exposure with UV-A first, intervals 0–24 h; LED-based setup	*E. coli* K12 MG1655 (wild type) and SP11 (*ThiI* mutant)	Inactivation (CFU assay), growth delay (OD600), single-cell division time, tRNA photodamage	• Strong synergistic inactivation in wild type (up to 5.7 $\log_{10}$ reduction with UV-C after UV-A) • Effect absent in *ThiI* mutant lacking s^4U tRNA modification • Synergy linked to UV-A-induced translational arrest via tRNA damage • Effect persists up to 24 h post UV-A	[23]
UV-LEDs (267 nm, 275 nm, 310 nm): 0.384 mW/cm²; combined exposures (267/275, 267/310, 275/310 nm) matched for irradiance; fluences of 8.78–23.04 mJ/cm² for 3–4 log inactivation	*E. coli* (strain CGMCC 1.3373) in water suspension	Inactivation efficiency (log reduction), photoreactivation and dark repair, electrical energy consumption	• No synergistic effect observed for combined wavelengths • 267 nm UV-LED had highest inactivation efficiency • 275 nm showed strongest resistance to reactivation, likely due to protein damage • Photoreactivation was dominant over dark repair	[24]
UV-C doses: 5–20 mJ/cm²; irradiance: 0.194 mW/cm² (260 nm), 0.314 mW/cm² (280 nm), 0.473 mW/cm² (260/280	Enteroviruses (CVA10, Echo30, PV1, EV70) in water suspension; propagated in BGMK cells	Log_{10} inactivation (infectivity via ICC-RTqPCR); ANOVA comparison across wavelengths	• No synergistic effect observed • 260 nm alone was most effective	[25]

 doi:10.20944/preprints202506.2020.v1

combined); simultaneous exposure			• Dual 260/280 nm either matched or underperformed vs. 260 nm • 280 nm less effective overall • Results consistent with nucleic acid absorption peak near 260 nm	
UV-C (222 nm): 0.32 mW/cm²; UV-C (275 nm): 0.50 mW/cm²; delivered simultaneously for 12–20 s	*E. coli* ATCC 15597 (bacteria) and PR772 (bacteriophage) in PBS suspension	Log_{10} microbial inactivation; photoreactivation and dark repair; DNA damage; Reactive Oxygen Species (ROS) production	• Marked synergistic inactivation of *E. coli* (synergism coefficient up to 1.92) • No synergism for PR772 • DWUV suppressed photoreactivation in both organisms • Enhanced ROS and protein damage likely mechanism for synergy in bacteria	[26]
UV-C (260 nm): 38–122 mJ/cm²; UV-C (280 nm): 41–89 mJ/cm²; UV-C (260∣280 nm): 41–105 mJ/cm²	*E. coli*, MS2 coliphage, Human adenovirus type 2 (HAdV2), *Bacillus pumilus* spores	Inactivation kinetics (log_{10} reduction), DNA/RNA damage (qPCR); electrical energy per order (EEO)	• No synergistic effect observed • Combined 260∣280 nm inactivation matched additive sum of individual wavelengths • No enhanced DNA/RNA damage or energy efficiency • Supports fluence-based independence of dual UV wavelengths	[27]
UV-C (222 nm): 1.0–2.4 mJ/cm²; UV-C (282 nm): 0.8–2.1 mJ/cm²; fluences for 5-log inactivation: *E. coli* 2.4–2.6 mJ/cm², *E. faecalis* 3.6–5.4 mJ/cm²	*E. coli* and *Enterococcus faecalis* in synthetic water (pH 6.4–7.0)	Log_{10} microbial inactivation (CFU count); photoreactivation and dark repair; synergistic coefficient φ	• Strong time-based synergistic effect in all dual-wavelength combinations (φ = 1.3–3.8) • No dose-based synergy • Complete inactivation achieved rapidly • Synergy linked to combined protein damage and DNA damage mechanisms • No repair observed after DWUV exposure	[28]
UV-C (222 nm): 0–25 mJ/cm²; UV-C (254 nm): 0–25 mJ/cm²; UV-C (255/265/285 nm): 0–25 mJ/cm² each	MS2 bacteriophage (virus surrogate) in water suspension (host: *E. coli* Famp)	Log_{10} inactivation (PFU count); modeled dose responses; energy efficiency (EEN)	• Significant synergy observed for LP or excimer lamps followed by LEDs • Enhanced disinfection vs. additive predictions • Reverse sequences less effective • Excimer + LP sequence showed highest energy efficiency • Supports order-dependent synergy in UV-UV disinfection	[29]

 doi:10.20944/preprints202506.2020.v1

UVA (365 nm): 1.7–52 J/cm²; UVC (265 nm): 4.2–20 mJ/cm²	*E. coli* (ATCC 11229) and coliphage MS2 (ATCC 15597-B1) in PBS suspension	Log_{10} inactivation; photoreactivation and dark repair; ROS role via scavengers	• UV-A pretreatment significantly enhanced UV-C inactivation of *E. coli* (up to +2.2 log) • Eliminated photoreactivation by impairing self-repair (via hydroxyl radicals inside cells) • No synergy observed for MS2 • Simultaneous UV-A+UV-C decreased *E. coli* inactivation (photoreactivation effect)	[30]
UVA (369 nm), UVB (288 nm), UVC (271 nm), Dual UV (288/271 nm, 369/288 nm, 369/271 nm): 0.75–6.75 mJ/cm²	*E. coli*, *Staphylococcus epidermidis*, *S. Typhimurium*, *Serratia marcescens*, *Pseudomonas alcaligenes* on agar (simulated food surface)	Log_{10} inactivation (colony count); synergy ratios; inactivation rate constants (k)	• Significant synergistic effect observed only for 288/271 nm (UV-B/UV-C) on E. coli, *S. epidermidis*, and *S. Typhimurium* • Synergy ratios 0.20–0.87 • No synergy with 369/271 or 369/288 combinations • Pulsed and continuous modes equally effective at same dose	[31]
UVC (222 nm or 280 nm); 405-nm blue light; pre-treatment: 30 s (222-nm: 7.1 mJ/cm², 280-nm: 1.2 mJ/cm²); 405-nm: up to 48 h, 86.4 J/cm²	*E. coli*, *Listeria monocytogenes*, *Staphylococcus aureus*, *S. Typhimurium*, *Pseudomonas aeruginosa* (in vitro)	Survival/colony counts; membrane integrity; ROS generation	• Synergistic bactericidal effect for *E. coli*, *L. monocytogenes*, *S. Typhimurium* • Minor for *S. aureus* • Antagonistic for *P. aeruginosa* • Synergy linked to ↑ ROS and membrane damage	[32]
UVA (320–400 nm): 0.5, 1, 2 J/cm²; VIS (395–600 nm): 2, 4, 6, 8 J/cm²; Mixed UVB (5%, 310–320 nm est.), UVA (25%, 320–400 nm), VIS (70%, 395–600 nm) = mUV/VIS: 2, 4, 6, 8 J/cm² (i.e., 0.1–0.4 J/cm² UVB)	Human volunteers (ragweed-allergic patients, n=19); forearm skin tested	Skin prick test (SPT) wheal size; allergen-induced immediate hypersensitivity response	• Only mUV/VIS (not UV-A or VIS alone) caused significant, dose-dependent inhibition of allergen-induced wheal formation (up to 83% at 8 J/cm²) • Inhibition occurred even at suberythematous doses • Suggests synergistic action of UV and VIS light on mast cell-mediated response	[33]
Blue light (405 nm): 1, 3, 5, 10, 15 J/cm²; Blue light (470 nm): 1, 3, 5, 10, 15 J/cm²	*S. aureus*, *P. aeruginosa*, *Propionibacterium acnes* (in vitro)	Survival/colony counts	• Dose-dependent bactericidal effect on *S. aureus* and *P. aeruginosa* • Up to 96.5% and 90% kill • No effect on anaerobic P. acnes	[34]

Table 3. Radiobiological Studies on Combinations of Ionizing and Ionizing Radiation.

Type & Dose	Biological systems	Biological endpoints	Effects	Ref.

 doi:10.20944/preprints202506.2020.v1

Alpha particles (LET 100–238 keV/μm): 0.1–0.2 Gy; X-rays (80 keV): 0.1–0.6 Gy	Human TK6 cells (wild-type and hMYH knockdown)	Clonogenic survival, mutant frequency	• Mixed beams show synergy in wt cells (survival) • MYH− cells resistant to survival loss but show high mutant frequency • Oxidative stress role unclear	[35]
X-rays: 0.25–1.0 Gy; alpha: 0.166–0.994 Gy; mixed beam 1: 75% X-rays + 25% alpha (0.333–1.327 Gy); mixed beam 2: 50% X-rays + 50% alpha (0.249–0.999 Gy); simultaneous exposure using custom MAX irradiator at 37 °C	Chinese hamster ovary (CHO) cells (AA8)	Clonogenic survival (colony formation assay)	• No synergistic effect observed • Mixed beam survival data fell within or near predicted additive models • Envelopes of additivity and mathematical modeling confirmed additivity for both mixed beam conditions	[36]
1–10 Gy total dose; alpha particles (11%–45% of total dose); X-ray dose rate 0.1 Gy/min; sequential exposure (alpha then X-ray)	T-1 human kidney cells; aerobic and hypoxic conditions; survival measured by colony formation, scoring of DNA damage (clonogenic assay)	Survival fraction (10% survival), RBE (relative biological effectiveness), OER (oxygen enhancement ratio)	• Alpha particle irradiation ↑ RBE (~2.3 at 10% survival) and ↓ OER sharply (~1.0) • Mixed radiation ↓ OER further • Observed trends aligned with theory for mixtures of high and low LET radiations	[37]
0.5–2 Gy total dose; mixed beam is 1:1 dose ratio (e.g., 1 Gy = 0.5 Gy alpha + 0.5 Gy X-rays); simultaneous exposure using custom irradiation setup	Human peripheral blood lymphocytes (from 4 donors)	DNA damage response gene expression (FDXR, GADD45A, MDM2, BBC3, CDKN1A, XPC); qPCR at 24 h post-exposure	• Mixed beams induced gene expression levels ≥ alpha alone • Synergy detected in 3 of 4 donors using “envelope of additivity” • FDXR most responsive • ATM inhibition decreased response, indicating role in synergistic effect	[38]
X-rays: 0.20–0.40 Gy; alpha: 0.07–0.27 Gy; mixed beams included 0.20X + 0.07 alpha, 0.40X + 0.13 alpha, and 0.40X + 0.27 alpha Gy; simultaneous exposure via dual-source setup	Human peripheral blood lymphocytes (PBL) from 1 donor	Chromosomal aberrations (simple vs complex) via FISH in chromosomes 2, 8, and 14	• Significant synergistic effect at the level of complex aberrations for two highest mixed doses • Linear-quadratic dose–response for complex events • ↑ damage complexity suggests higher-than-additive biological effect	[39]
Alpha particles (LET 97–238 keV/μm): 0.13–1.33 Gy; X-rays (190 kV): 0.25–2.00 Gy; mixed beam doses: 0.38, 0.77, 1.53 Gy; simultaneous exposure using custom dual-source irradiator at 37 °C	Human peripheral blood lymphocytes (1 male donor)	Micronucleus (MN) frequency in binucleated cells; MN size	• All mixed beam doses showed statistically significant synergistic effects (average 1.8× higher MN than additive prediction) • Linear dose-response • Synergy attributed to impaired repair of X-ray-induced damage by prior alpha exposure	[40]
X-rays (280 kVp, 0.75 Gy/min): 0–15 Gy; Alpha particles (0.18 Gy/min): 0–3 Gy; mixed	Rat lung epithelial cells (F344, LEC)	Cell survival (clonogenic), micronuclei	• Simultaneous exposures caused greater-than-additive effects on cell killing and	[41]

 doi:10.20944/preprints202506.2020.v1

exposures: 0.06 or 1 Gy alpha + graded X-ray doses		induction (FISH), mitotic delay	micronuclei frequency • High-dose alpha (1 Gy) removed shoulder from survival curve • Synergistic slopes observed in micronuclei assays even at low alpha dose (0.06 Gy)	
Alpha particles (LET 100–172 keV/μm): 0–1 Gy; X rays (80 keV): 0–1 Gy (always 1:1 ratio in mixed exposures)	Human osteosarcoma U2OS cells expressing 53BP1-GFP	DNA double-strand break focus formation and decay (53BP1 foci); ATM and p53 activation	• Strong synergistic interaction observed in both small and large DSB foci • Slower focus decay and prolonged ATM/p53 signaling suggest overwhelmed DNA repair • Synergy most pronounced at lower total doses	[42]
Alpha: 0.13–0.32 Gy; X-rays: 0.20–0.80 Gy; Mixed beams: 25% alpha + 75% X-rays (e.g., 0.53 Gy = 0.13 alpha + 0.40 X); simultaneous exposure using MAX dual-source system	Human VH10 fibroblasts (immortalized)	γ-H2AX foci formation and repair kinetics (IRIF); small vs. large foci quantification	• No dose response synergy detected at 1 h • Mixed beam exposure delayed formation and decay of large foci compared to predicted additive effect, indicating a transient impairment of DNA damage response	[43]
Total dose of 0-2 Gy: 50% alpha (0.223 Gy/min, LET ~91 keV/μm) + 50% X-rays (0.052–0.068 Gy/min); exposures via dual-source platform on blood discs (simultaneous delivery)	Human peripheral blood lymphocytes (PBLs, from 3 donors)	DNA damage (alkaline comet assay), repair kinetics, phosphorylated DDR proteins (ATM, DNA-PK, p53), gene expression (qPCR)	• Mixed beams caused significantly more DNA damage than additive prediction (synergy via envelope analysis) • Delayed repair kinetics • Highest activation of DDR proteins and gene expression vs. either radiation alone • Results support synergistic impairment of repair by clustered + dispersed DNA damage	[44]
1 Gy exposure: 0.5 Gy alpha (LET 100–238 keV/μm) + 0.5 Gy X-rays (peak 80 keV); simultaneous delivery using a dual-source irradiator on U2OS cells stably expressing 53BP1-GFP	Human osteosarcoma U2OS cells (live cell imaging)	53BP1-GFP foci kinetics, area, intensity, mobility (live microscopy), chromatin dynamics	• Mixed beam foci showed unique dynamic behavior • Intermediate size, highest intensity, low mobility, and persistent signal • Distinct from additive prediction • Results support synergistic effect via impaired repair and complex DSB clustering at chromatin domains	[45]
Alpha priming doses (LET ~140 keV/μm): 0.5, 2, or 2.5 Gy; X-rays (3 Gy/min): multiple doses; irradiations separated by ≤3–4 min	V79 Chinese hamster lung fibroblast cells	Clonogenic survival; survival curve parameters (Dq, Do)	• Sequential exposure with ≤4 min delay showed strong synergistic effect at 2.5 Gy alpha • Survival curve shoulder (Dq) nearly eliminated	[46]

 doi:10.20944/preprints202506.2020.v1

			• X-ray survival curve slope (Do) unchanged • Synergy attributed to alpha-induced damage interfering with sublethal damage repair from X-rays	
Alpha particles (LET 91 keV/μm); X-rays (190 kV, 3:1 ratio): 2 Gy total, acute or 0.4 Gy × 5 fractionated	Human microglial HMC3 cells; cultured in vitro on Mylar-covered disks	γH2AX foci, qPCR (CDKN1A, MDM2), IL-1β ELISA, NF-κB/STING phosphorylation, phagocytosis assay	• Fractionated alpha or alpha+X-ray exposure → stronger pro-inflammatory response and DNA damage signaling than acute • ↑ IL-1β, CDKN1A, MDM2, STING/NF-κB activation, and phagocytosis • Responses returned to baseline by day 14	[47]
Alpha particles (high LET, Am-241 source): 0.05–1 Gy; X-rays (150 kVp): 0.05–1 Gy	BEAS-2B (human lung epithelial) and SVEC4-10EHR1 (mouse endothelial) cells; in vitro foci analysis via immunofluorescence microscopy	γ-H2AX foci count, size distribution, and decay (dephosphorylation rate) over 24 h	• Alpha-induced foci were larger and dephosphorylated slower than X-ray-induced foci • Radiation type correctly identified in >80% of blinded tests • Individual alpha and X-ray doses estimated within 12% error using mixed-beam exposure data	[48]
0.83 Gy alpha (0.223 Gy/min) 1.02 Gy gamma (0.372 Gy/min), total of 1.85 Gy; 5-minute transfer time between irradiations	U2OS human osteosarcoma cells stably expressing NBS1-GFP	Live-cell imaging of DNA damage response: NBS1-GFP foci number, area, intensity, mobility	• Stronger synergistic effect observed for α → γ sequence • Slower repair kinetics, larger and more persistent foci • ↑ Intensity and ↓ mobility • γ → α induced faster decay and lower focus intensity • Results suggest order-dependent DDR engagement and impaired repair after alpha priming	[49]
Alpha particles (LET ~91 keV/μm): 2.5 Gy; gamma rays (0.73 Gy/min): 2.5 Gy; fractionated regimens used as well	Breast cancer (MDA-MB-231), Osteosarcoma (U2OS)	γH2AX foci (TEM, immunofluorescence), colony formation, viability	• Mixed beam causes more γH2AX foci • Stronger reduction in viability/colony formation • Delayed chromatin recompaction enhances cell kill	[50]
Alpha (LET ~126 keV/μm, 50 rad/min): ~25% of total dose; gamma (LET ~0.31 keV/μm, 154 rad/min): ~75% of total dose	Diploid yeast (*S. cerevisiae*, strain BZ34)	Mutation frequency (reversion to arginine independence)	• Statistically significant synergistic effect observed • Reversion frequency 1.34× higher than additive prediction • Enhanced mutagenic effect attributed to interaction between low- and high-LET damage pathways	[51]

 doi:10.20944/preprints202506.2020.v1

Alpha particles (high LET): 0.89–4.81 kBq/g lung; beta particles (low LET, E^{-} = 0.062 MeV): 0.52–2.11 MBq/g lung	F344/Crl rats (inhalation, in vivo)	Mortality from radiation pneumonitis; respiratory function (vital capacity, compliance, CO diffusion)	• Combined exposure produced additive effects • Validated hazard models for lethality and morbidity • Alpha radiation ~7× more biologically effective than beta • Respiratory dysfunction and fibrosis observed	[52]
Alpha + beta + gamma radiation (mixed radionuclides from Chernobyl fallout including 134Cs, 137Cs, 144Ce, 154Eu, etc.): total dose 1–515 mSv (chronic); gamma (from 60Co source): 0.1–29,600 mSv (chronic)	Barley (Hordeum vulgare, waxy mutant line); field-grown in contaminated plots and gamma-field controls; waxy-reversion assay in pollen	Pollen waxy-reversion frequency; mutation rate per mSv; beta/gamma/alpha soil activity; dose–response and RBE comparison	• Combined radionuclide IR caused higher mutation rates per mSv than external gamma • Mutagenicity not explained by dose alone • Enhanced genotoxicity linked to multi-type exposure, chemical synergies, and heterogeneous contamination	[53]
Beta (^{90}Sr-^{90}Y, low LET): 1.2–4.8 krad; gamma (^{60}Co, low LET): 1.2–4.8 krad; beta and gamma combined (varied proportions): total 1.2–4.8 krad at 8.4 or 17.8 rad/min	Soybean plants (Glycine max cv. Hill) at unifoliolate leaf stage; grown to maturity in field; assessed for vegetative and reproductive traits	Survival, plant height, lateral growth frequency and length, vegetative yield, seed yield	• Combined exposure affected lateral growth and yield depending on beta/gamma dose component • Gamma slightly more damaging overall • Interaction effects seen in vegetative vs. reproductive response • Dose rate and composition sensitivity evident	[54]
X-rays (250 kVp): 3 Gy; Neutrons (IND-spectrum, broad energy range simulating Hiroshima 1–1.5 km epicenter): 0.75 Gy or contributing 5% (0.15 Gy), 15% (0.45 Gy), or 25% (0.75 Gy) of 3 Gy total mixed dose	Mice (C57BL/6, peripheral blood, 7 days post-exposure)	Gene expression (microarray, RT-qPCR); pathway and ontology analysis (IPA, PANTHER)	• Strong synergistic effect at gene expression level • Mixed exposures → unique suppression of mRNA translation, tRNA processing, EIF2/mTOR signaling, and ribosomal protein genes linked to bone marrow failure • Effects not seen in pure X-ray group • Synergy evident even at 5% neutron	[55]
Monoenergetic neutrons (0.35, 0.45, 5.9, 13.7 MeV): 0.1 or 0.3 Gy; X-rays (250 kVp): 1 or 3 Gy; sequential exposures with <2 min delay (neutrons always first)	C3H 10T½ mouse fibroblast cells	Oncogenic transformation (type II/III foci); clonogenic survival	• No significant synergistic effect • Transformation frequencies matched additive prediction across all neutron energies • Low-dose combined exposures showed additive behavior even with high-LET neutrons	[56]
X-rays (140 kVp): variable dose per fraction (up to ~30 Gy total); Neutrons (3 MeV): variable dose per fraction (up to ~25 Gy total); Mixed fields included combinations with photon	Mouse foot skin (WHT/Gy fBSVS mice)	Acute skin reaction scoring; dose-response curve modeling; α/β analysis	• Strong synergistic interaction during simultaneous exposure • Full quadratic-term interaction confirmed • Synergy declined but	[57]

 doi:10.20944/preprints202506.2020.v1

contamination levels of 11%, 32%, 53%, and 72%			persisted up to 6 h delay • Dose-response curves shifted with increasing photon content, supporting sublethal damage interaction model	
Neutrons (14 MeV): up to ~430 rad; X-rays (180 kVp): up to ~635 rad; various single and sequential doses used; exposures spaced by 5–10 minutes	L5 mouse fibroblast cell line (subclone of L cells); suspension culture in Eagle MEM	Cell reproductive capacity (colony formation >50 cells); survival curves; RBE at 50–1% survival	• Survival lower in sequentially irradiated cells vs. single modality • Combined exposures showed interaction • RBE values for neutrons 2.5–1.5 vs. X-rays • Evidence of partial overlap but mechanistic differences between neutron and X-ray cell killing	[58]
X-rays (250 kVp): 0.2 Gy priming and 1 Gy challenge; neutrons (LET = 60–70 keV/μm): 0.2 Gy priming and 1 Gy X-ray challenge; Bragg-peak negative pi mesons (LET = 35–55 keV/μm): 0.2 Gy priming and 1 Gy X-ray challenge	V79-379A Chinese hamster fibroblasts; monolayer culture survival assay	Colony-forming ability (>50 cells); plating efficiency; survival after challenge; induction of adaptive response	• Sequential high-LET priming (neutrons/pions) ↑ resistance to subsequent X-rays if 4–6 h elapsed • Adaptation required minimum 0.2 Gy priming • Effect was transient, protein synthesis–dependent, and indicative of inducible DNA repair mechanisms	[59]
X-rays (250 kVp): 3 Gy; neutrons (IND-spectrum, high-LET): 0.15–0.75 Gy (5%–25% of total 3 Gy dose); Neutrons (83%) + gamma (17%): total 0.75 Gy	Human peripheral blood (ex vivo from 5 donors)	Gene expression profiling (microarray, RT-qPCR); TP53 signaling; immune suppression	• Neutron-photon mixtures caused increasing transcriptomic alterations with higher neutron % • 25% neutron had strongest TP53 and immune effects • 22 genes uniquely responded to neutron-containing exposures, suggesting gene-level synergism even without simultaneous irradiation	[60]
X-rays (250 kVp, 3 Gy/min): up to 8.5 Gy; fast neutrons (3.15 MeV, 0.47 Gy/min; 11.3% gamma contamination): up to 3.75 Gy; sequential exposures with 6-minute delay (room temp), or 3-hour delay (with recovery at 37 °C)	V79 Chinese hamster fibroblasts (in suspension)	Clonogenic survival; survival curve parameters (Do, Dq); sublethal damage interaction	• Synergistic interaction observed with 6-minute delay • ↓ X-ray survival curve shoulder (Dq), especially after neutron priming • No interaction with 3-hour delay • Effects consistent with partial inhibition of repair between exposures	[61]
Fast neutrons (25 MeV, Fermilab): 280 or 420 rad; fast neutrons (0.86 MeV, JANUS): up to ~1.6 krad; X-rays (250 kVp, 150 rad/min): doses combined with neutrons in split exposures	V79 Chinese hamster cells	Survival curve, colony-forming ability	• ↑ in survival after dose fractionation, repair of sub-lethal damage	[62]

 doi:10.20944/preprints202506.2020.v1

X-rays (250 kVp): 1250 rad; fast neutrons (produced by 16 MeV deuterons on Be target): 540 rad; sequential irradiation with 15 min to 4 h interval	Mouse jejunum (crypt cells)	Crypt survival	• Combined effect is additive after full repair of sub-lethal damage	[63]
Gamma rays (60Co, low-LET): up to 7.5 Gy; fast neutrons (~6 MeV, 2–3% photon contamination): up to 7.5 Gy; mixed exposures with 60% gamma + 40% neutrons and vice versa, delivered sequentially with < 3 min interval	Chinese hamster V79 cells	Clonogenic survival (colony formation assay); survival curve slope and shape	• Survival after mixed exposure was independent of sequence • Synergistic effects reflected in altered survival curve slopes • Zaider-Rossi model accurately described both sequential and simultaneous outcomes	[64]
Gamma-neutron radiation (from IR-8 nuclear reactor, mixed field of neutrons and gamma rays): 25–500 mGy; comparison made with gamma-only radiation in same dose range	Neonatal mouse neural stem/progenitor cells (NSCs/NPCs) cultured in vitro; neurosphere assay; immunocytochemistry for γH2AX	DNA double-strand breaks (γH2AX foci), foci size and repair kinetics, neurosphere formation, cell survival	• Low doses (25–50 mGy) stimulated proliferation • >100 mGy reduced survival • Gamma-neutron IR had higher RBE (max 9.7) vs. gamma alone • Induced large γH2AX foci with slow repair • Sensitivity of NSCs/NPCs to mixed radiation highlighted	[65]
Neutron beam (HB11, mixed field of protons from neutron capture and induced/incident gamma): 0.25–1.7 Gy; ^{60}Co photons (for calibration): 0.25–3 Gy; exposures in water phantom at 37 °C	Human peripheral blood lymphocytes (PBLs) from 6 donors	Chromosomal aberrations (dicentric chromosomes); RBE estimation	• No synergistic effect observed • Mixed beam-induced dicentric yields matched additive predictions from gamma + calculated proton components • RBE values: 3.0 (mixed beam), 7.2 (protons) • Results consistent across varying neutron:gamma ratios	[66]
Mixed field: fission neutrons and gamma rays (MUTR reactor); neutron dose: 0.32 Gy/min, gamma dose: 0.42 Gy/min; ^{60}Co gamma (control): 0.15–1.3 Gy/min; total doses up to ~7 Gy	V79-4 Chinese hamster lung fibroblast cells (monolayer culture)	Clonogenic survival; survival curve fitting with nanodosimetric LQ model	• Interaction term (βnγDnDγ) fits synergistic behavior better than traditional additive RBE model	[67]
Gamma: 150 rad/min; neutrons: 10–15 rad/min (5 ± 2% gamma contamination); combined doses with 50% or 75% gamma ray contribution; exposures sequential with immediate succession or extended up to 45 min	Chinese hamster ovary cells (in flasks, room temperature)	Clonogenic survival; survival curve modeling; interaction index (I) based on Katz delta-ray theory	• Significant synergistic effect observed at both 50% and 75% gamma ray mix • Survival lower than additive prediction • Minimal impact of sequence or delay up to 45 min • Katz model predictions matched experimental interaction magnitude	[68]
Total dose: 0.5, 0.75, or 1.0 Gy; mixed beams were 50:50 neutron:gamma; sequential	Human peripheral blood mononuclear cells (PBMCs) from 3 donors	Gene expression (RT-qPCR of FDXR, BBC3, etc.); Dicentric	• No synergistic effect detected in either endpoint • Mixed beam responses were	[69]

 doi:10.20944/preprints202506.2020.v1

exposure (within 8 min) in both orders (γ→n and n→γ); neutron: 0.02 Gy/min, gamma: 0.1 Gy/min		chromosome assay (DCA)	additive regardless of sequence • RBEs for neutrons ranged from 1.39–3.91 (gene expression) and 7.30 (dicentrics) • Gamma-neutron order had no significant influence	
Simultaneous and sequential exposures; 60% gamma (8 rad/min) + 40% neutrons (4.8 rad/min); sequential interval ~5 min; total dose varied	V79 Chinese hamster lung fibroblast cells (monolayers at 37 °C)	Clonogenic survival; survival curve modeling; RBE estimation	• Simultaneous exposure produced a supra-additive effect • 29% lower survival at 10% level vs. additive prediction • Sequential exposures (either order) matched additive model • Results indicate dose-rate sensitive synergism when beams are mixed	[70]
Simultaneous and sequential exposures; 60% gamma rays (3 cGy/min) + 40% neutrons (2 cGy/min); delivered via pulsed beam in 3-min intervals; total doses varied	V79 Chinese hamster lung fibroblasts (monolayers at 37 °C)	Clonogenic survival; survival curve modeling; maximum likelihood fitting	• Simultaneous exposures caused significantly more cell killing than sequential • Dose ratio at 1% survival = 1.08 • Survival curves fitted better with quadratic models • Confirms supra-additive effect under simultaneous delivery • Supports interaction between damage types	[71]
Mixed gamma-neutron radiation (TRIGA Mark-F reactor; ~60% gamma, ~40% neutron): 570–30,000 rad; delivered in steady-state (1000 rad/min) or pulsed mode (88% of dose in <40 ms)	Male Sprague-Dawley rats; serum and urine sampled 6–72 hours post-exposure	Fluorescence intensity in serum (360, 465 nm) and urine (400, 425 nm); dose- and time-dependent changes	• Serum fluorescence at 465 nm ↓ dose-dependently at 24 h (570–9300 rads) • 360 nm peak ↑ at 72 h (non-dose-dependent) • Urine fluorescence at 425 nm ↑ with dose (1000–30,000 rads) • Limited utility as biological dosimeter	[72]
Mixed neutron-gamma radiation (light water-moderated research reactor; neutron peak energy 0.4–0.6 MeV; ~30% gamma component): 0.5, 2, or 4.5 Gy total dose; whole-body exposure in rotating cage	Male F1 (C57BL × DBA2) mice; erythrocytes, lymphocytes, platelets isolated from whole blood	3H-concanavalin A membrane binding; SEM/TEM ultrastructure of plasma and intracellular membranes	• ↑ lectin-binding observed as early as 30 min • Lymphocytes most sensitive (up to 2.5× increase) • Dose- and time-dependent oscillatory membrane responses • Membrane ultrastructure altered (filopodia, vacuolization, ER dilation) • Effects not dose-proportional above 0.5 Gy	[73]

 doi:10.20944/preprints202506.2020.v1

Gamma (60Co, ~2.0–2.5 MeV): 0.1 Gy; mixed gamma (2.0–2.5 MeV) and neutron (0.5–10 MeV): 1 Gy	C57BL/6J male mice; hippocampus and brain immune cells analyzed	Open field and Morris water maze behavior; flow cytometry for microglia and astrocytes; qPCR/ELISA for cytokines and neurotrophins	• Combined irradiation impaired hippocampus-dependent memory (unlike gamma, neutron alone) • ↑ M2 microglia, astrocytes, BDNF and NT-4 expression • ↓ TNF-α and IL-1β vs. gamma, neutron • Suggests anti-inflammatory neuroadaptation post gamma-priming	[74]
Neutrons (2.5 MeV): 1.42 Gy; gamma rays (137Cs): 1.42 Gy; combined neutron + gamma: 0.71 Gy each; 252Cf neutrons: 0–0.71 Gy	A: Human peripheral blood from 3 healthy adult males; B: AHH-1 human lymphocytes	Gene expression profiling (RNA-seq, qPCR); KEGG pathway enrichment; dose–response of BAX, DDB2, FDXR	• Neutrons induced more differentially expressed genes and pathways than gamma rays • Combined exposure activated genes overlapping with both mono-exposures • BAX, DDB2, FDXR showed neutron-specific dose-responses, suggesting their role as molecular targets of neutron damage	[75]
Mixed neutron-gamma radiation (neutrons: 0.5–3.0 MeV, ~85% of dose; gamma: <10% of dose): 375 rads or 1000 rads	ICR female mice (germfree and conventional); small intestine examined histologically	Mucosal atrophy, crypt regeneration, diarrhea, survival time	• At 375 rads, mucosal recovery occurred in both groups before death • At 1000 rads, lesion progression and death occurred earlier in conventional mice • Villus atrophy, lipid-filled cells, and delayed regeneration observed in germfree mice • Epithelial denudation not seen	[76]
Neutrons: 4–8.5 Gy; gamma rays: up to 12 Gy; delivered sequentially with short intervals (0–3 h) between modalities	V79 Chinese hamster cells in plateau phase (G_1 arrest)	Cell survival; survival curve parameters (Dq, n, slope); repair of potentially lethal damage (PLD)	• Interaction effect shown as significant reduction or elimination of survival curve shoulder • Damage from both modalities appears to involve similar PLD • Response mimics that seen with β-araA treatment	[77]
Epithermal neutron source (Studsvik: includes fast neutrons >1 MeV and γ-rays): total dose 8.2–16.2 Gy/h, depth-dependent; epithermal neutron source (Birmingham: neutrons ≤1 MeV and γ-rays): total dose 0.58–1.04 Gy/h, depth-dependent	Chinese hamster V79 fibroblast cells	Clonogenic survival, relative biological effectiveness (RBE), repair inhibition	• ↓ Clonogenic survival with depth • ↑ RBE values (Studsvik > Birmingham) • Evidence of high-LET and low-LET interaction enhancing biological damage	[78]

 doi:10.20944/preprints202506.2020.v1

Mixed fields totaling 3 Gy (e.g., 0.15–0.75 Gy neutrons + 0.03–0.15 Gy gamma rays + 2.1–2.82 Gy X-rays); equitoxic 0.9 Gy (0.75 Gy neutrons + 0.15 Gy gamma rays)	Mouse (C57BL/6J) serum	Lipidomic dysreg.; inflammation marker	• Synergistic pro-inflammatory and hyperlipidemic lipidomic changes • ↑ LPC/PC ratio • ↑ TG and PS	[79]
Fast neutrons (14.5 ± 1.04 MeV, high LET): 0.7 Gy (2 Gy EQD); Protons (67–83 MeV, spread-out Bragg peak): 2 Gy (2 Gy EQD); Combined sequential exposure (neutron → proton, 2 h interval): 4 Gy EQD	Human breast cancer cell lines (MCF-7, MDA-MB-231)	Cancer stem cell fraction (ALDH+/CD44+/CD24−); stemness gene expression (OCT4, NANOG, SOX2)	• Combined exposure decreased CSC fraction additively in MCF-7 and antagonistically in MDA-MB-231 • No significant changes in stemness gene expression • Response depended on cell line and radiation sequence	[80]
X-rays (225 kVp, 270 rad/min): up to 8 Gy; Neon ions (425 MeV/amu, LET ~234 keV/μm, 500–600 rad/min): up to 6 Gy; sequential exposures with 0–24 h interval	V79 Chinese hamster lung fibroblasts (asynchronous monolayer)	Clonogenic survival; survival curve fitting (Do, Dq); repair kinetics	• Synergistic reduction in survival with both sequences • Strongest effect with minimal delay • High-LET priming eliminated shoulder of X-ray curve • Low-LET priming steepened neon-ion curve • Synergy diminished with 3–24 h interval, indicating repairable, interacting damage types	[81]
Neon ions (425 MeV/u, LET ~ 234 keV/μm): 3.3 Gy; X-rays (225 kVp): 5.5 Gy; Argon ions (570 MeV/u, LET ~ 117 keV/μm): 2.04 or 3.57 Gy	Chinese hamster V79 fibroblasts (synchronized at GI/S, mid-S, and late-S phases)	Clonogenic survival; survival curves; timing and cell-cycle phase interaction analysis	• Strong synergistic effect; greatest in late S-phase • Interaction diminished with ≥3 h delay • Survival response depended on cell-cycle stage and priming radiation type • Supports repairable, phase-specific sublethal damage interaction	[82]
Deuterons (50 keV/μm): 2 or 5.6 Gy; ^{3}He ions (96 keV/μm): 2.5 or 4 Gy; ^{3}He ions (160 keV/μm): 4 Gy; X-rays (50 kVp): graded doses following each high-LET dose	Chinese hamster V79 cells (synchronized in late S-phase)	Clonogenic survival; enhancement ratio (ER); survival curve modeling	• Strong synergistic effects observed across all LETs and doses •↑ ER with LET and priming dose • Mixed irradiation decreased survival more than additive prediction • Results consistent with interaction of sublethal damage from high- and low-LET radiation	[83]
Priming dose: 7 Gy neon ions (557 MeV/u, LET 115–240 keV/μm) or 20 Gy X-rays (225 kVp, 6 Gy/min); top-off X-ray	Rat rhabdomyosarcoma tumors (R2C5 subline in WAG/Rij rats)	Tumor growth delay (doubling time to 2× volume); RBE and interaction analysis	• No significant synergistic effect • Growth delays similar regardless of whether X-rays followed neon ions or X-rays	[84]

 doi:10.20944/preprints202506.2020.v1

doses: 7.5, 15, or 25 Gy given at 0.5, 4, or 24 h later			• Top-off doses produced near-additive outcomes even at 0.5 h interval • Rapid sublethal damage repair likely prevented interaction	
Carbon ions (290 MeV/u, LET ~ 75 keV/μm): 1, 4, 7 GyE; X-rays: 1, 4, 8 Gy	Head & neck cancer cell lines (squamous cell carcinoma, salivary gland cancer, malignant melanoma, normal keratinocyte)	PCR-LOH on chromosome 17; microarray gene expression analysis	• X-ray caused LOH on one homolog • Carbon ion caused homo-deletion • Both altered gene expression	[85]

Table 4. Therapeutic Studies Involving Combined Radiation.

Type & Dose	Biological systems	Biological endpoints	Effects	Ref.
Protons (delivered to CTV): 50.4 GyE in 28 fractions; Carbon ions (boost to GTV): 12, 15, or 18 GyE in 4, 5, or 6 fractions	Locally advanced pancreatic cancer (10 patients, in vivo, clinical trial)	Tumor control, toxicity, survival	• Well tolerated with no dose-limiting toxicities • 1-year overall survival (OS) 80%, median OS 17.3 months • Modest improvement in tumor control • Carbon ions suggested more effective than proton alone	[86]
Intensity Modulated Proton Therapy (IMPT) 50–70 GyE + Intensity Modulated Carbon Therapy (IMCT) boost 15–21 GyE [total up to ~69 GyE in 21–23 fractions (fx)]	Chordoma and chondrosarcoma of skull base/cervical spine (91 patients)	Tumor control, survival, toxicity	• 2-year OS 87.2%, Progression-Free Survival (PFS) 76.8%, Local Control (LC) 86.2% • Worse survival with re-irradiation and tumor volume >60 cc • Low toxicity with mostly grade 1–2 side effects	[87]
Protons: median 44 GyE in 22 fx; Carbon ions: median 23.1 GyE in 7 fx (total median dose: 67.1 GyE); concurrent chemotherapy (etoposide + platinum)	Small cell lung cancer (25 patients, limited-stage, in vivo clinical study)	Overall survival, progression-free survival, toxicity	• 2-year OS 81.7%, PFS 41.2%, Local Progression-Free Survival (LPFS) 66.7% • Well-tolerated • Main grade 3 toxicities hematological • 1 case of grade 3 esophagitis, 1 late bronchial obstruction	[88]
Protons (95–105 MeV); carbon ions (^{6}C, 400 MeV/n); total RBE-weighted dose ≈8.4±0.2 Gy; four sequential exposure schemes with 30–45% ^{12}C contribution; intervals: 0–4 h; sequence: p→C or C→p	Chinese hamster fibrosarcoma cells (B14-150)	Clonogenic survival; survival curves; synergy coefficient K	• Significant synergistic effect observed only in C→p sequence with 45% ^{12}C contribution (K=0.65) • Effect diminished with 30% ^{12}C • Antagonism seen in p→C sequence (K>1) • ↑ Survival with longer interval in p→C, but ↓ in C→p	[89]
Proton Beam (OPTIS2; Bragg Peak; LET ≈ 0.5–2 keV/μm): 7.5 Gy or 5 Gy; Targeted Radionuclide	CD1 nude mice with KB xenografts; BALB/c nude	Tumor growth delay (TGDI2/5), survival,	• Combination therapy showed additive or synergistic effect depending	[90]

 doi:10.20944/preprints202506.2020.v1

Therapy with 177Lu-Folate or 177Lu-PSMA-617 (β^-, E_{max} ≈ 0.5 MeV; LET ≈ 0.2 keV/μm): ~7.5 Gy (8.5 MBq) or ~5 Gy (1.25 MBq)	mice with PC-3 PIP xenografts	tumor volume monitoring	on tumor model • KB model showed significant synergy (↑ TGDI2/5, no endpoints) • PC-3 PIP model showed additive trend only • Combination well tolerated in both cases	
Fast Neutron Therapy (p→Be, 50.5 MeV, high-LET ~ 70–100 keV/μm): 18.4 nGy in 16 fractions; Proton Therapy Boost (Pencil Beam, RBE = 1.1): 25 Gy (RBE) in 10 fractions	Patients with locally advanced unresectable salivary gland tumors involving the base of skull (n=29)	Local control (LC), progression-free survival (PFS), overall survival (OS); acute and late toxicity (CTCAE v4.03)	• At 18.9 months: LC 89.7%, OS 93.1%, PFS 79.3% • Acute toxicities mostly grade 1–3 • No grade 5 toxicity in de novo group • Late toxicities included vision loss (25%) and hearing loss (8.3%) • Combined approach was feasible with acceptable toxicity in this high-risk cohort	[91]
Protons (1 GeV, 60%); 16O ions (250 MeV/n, 20%); 28Si ions (263 MeV/n, 20%); total dose: 6.6–6.8 Gy (RBE); varying p/HR ratios (60/40%, 80/20%, 40/60%, 20/80%); intervals: 0–8 h	B14-150 Chinese hamster fibrosarcoma cells; confluent monolayers irradiated in vitro	Cell survival (clonogenic assay); regression modeling of post-irradiation recovery	• HR→p sequence with 40% HR most effective for reducing survival • p→HR sequence showed partial recovery (T½ ~1.1–1.3 h) • Combinations showed mostly antagonistic interaction (K > 1) • Survival inversely related to HR dose contribution	[92]
Proton Pencil Beam Scanning (96–104 MeV; LET ≈ 0.5–1 keV/μm): 40 Gy × 2 (total 80 Gy); Neutron Radiation (14.1 MeV; High-LET ≈ 100 keV/μm): 5 Gy; sequential exposure in mice with 3 h interval: neutrons before or after protons; neutron dose ~15% of total; CT-guided tumor targeting	SHK mice with solid Ehrlich ascites carcinoma	Tumor growth suppression, skin radiation reactions (RTOG/EORTC), relapse frequency, remission duration, survival	• All groups showed tumor suppression • Neutron-after-proton group had milder skin toxicity and better tolerance • Neutron-before-proton group had severe toxicity and shortest survival • Combined exposures ↑ relapse rate and ↓ lifespan vs. protons alone	[93]
Protons (88–109 MeV); neutrons (14.5 MeV, D-T generator); total dose ~8.6 Gy; neutron:proton dose ratios of 30:70 or 40:60; sequential exposures with 0–8 h delay; survival modeled vs. independent action	Chinese hamster fibrosarcoma cells (B14-150)	Clonogenic survival (colony assay); synergy coefficient K	• All neutron–proton schemes showed synergistic effects (K < 1) • Strongest synergy when neutrons delivered first and comprised 40% of dose • Survival significantly below additive prediction • No recovery observed in neutron-first sequence	[94]

 doi:10.20944/preprints202506.2020.v1

Priming dose: 0.075 Gy X-rays; challenging dose: 1.75 Gy 137Cs gamma rays; 6-hour interval between doses; exposures in mice and ex vivo human thymocytes	Mouse thymocytes (C57BL/6J); Human pediatric thymocytes (1 mo–3 yrs)	Cell cycle (sub-G_1), DNA damage (γH2AX), apoptosis (Caspase-3, PARP1), ferroptosis (xCT, GPX4), epigenetic markers (DNMTs, TDG, MBD4)	• Strong synergistic response: earlier and enhanced apoptosis, cell cycle arrest, ferroptosis, and DNA damage response in combined vs. single dose • Priming dose → sensitized "radiation awareness" state • Consistent mouse–human similarity in response	[95]
X-rays (320 kVp, whole thorax): 12.5 or 13 Gy; soft X-rays (10 kVp, dorsal skin, 10% surface): 30 Gy	WAG/RijCmcr rats; lung and skin monitored for 210 days post-irradiation	Survival (IACUC criteria), breathing interval, lung collagen (fibrosis), mast cell count, skin wound area	• Combined lung+skin irradiation delayed pneumonitis onset and improved survival vs. thorax alone (13 Gy) • Lung collagen ↓ by skin co-irradiation • Captopril enhanced skin healing and delayed lung injury further	[96]
X-rays (150 kV, orthovoltage): 9 Gy; Photodynamic therapy (THPTS, 760 nm): 20 J/cm²	Bladder cancer organoids (T-24, RT-112)	Organoid viability, death markers, immune migration	• IR + PDT showed additive/synergistic cytotoxicity • Multimodal cell death • Non-malignant tissue unaffected • ↑ T cell infiltration	[97]
PDT (non-coherent light, 370–680 nm): 30 mW/cm², 90–180 s; RT (gamma rays, 60Co source, 1.0–1.62 Gy/min): 2 Gy (range tested: 0–15 Gy)	Ehrlich ascites carcinoma	Tumor growth inhibition, membrane vs DNA damage	• PDT damaged membranes • RT caused DNA breaks • Combo had additive tumor inhibition (~33–38%) • HPde acted as dual sensitizer	[98]
X-rays: 2, 10, 20 Gy; PDT: 2.5 J/cm² at 690 nm; PDT given ~10 min before RT	Heterocellular pancreatic cancer spheroids (MIA PaCa-2, Capan2, AsPC-1) co-cultured with patient-derived fibroblasts	Viability (live/dead staining), necrosis, apoptosis (flow cytometry), DNA damage (γ-H2AX), proliferation (PCNA)	• Low-dose PDT and RT showed synergistic effects • PDT → necrosis and apoptosis • RT decreased spheroid growth • Combination → smaller, less viable spheroids than expected additively • Effects varied by cell line	[99]
X-rays (50 kV): 0–10 Gy; nanoparticles: MC540-SAO:Eu@mSiO2 at 50 μg/mL; X-PDT combines RT and nanoparticle-mediated PDT; applied 5 min after injection	Radioresistant human NSCLC cells (H1299); subcutaneous and intrathoracic mouse tumor models	Cell viability (MTT), clonogenic survival, apoptosis/necrosis, DNA damage (comet, γ-H2AX), lipid peroxidation (ROS), tumor growth delay	• Strong synergistic effect: X-PDT significantly more effective than RT alone in vitro and in vivo • Enhanced apoptosis, necrosis, DNA, and lipid damage • Tumor suppression in deep tissues • No systemic toxicity observed	[100]

 doi:10.20944/preprints202506.2020.v1

PDT (non-coherent light, 730 nm): 45 mW/cm², 30–108 J/cm²; indocyanine green (ICG) 50 μM; RT (X-rays, 100 kVp): 2–8 Gy; combination: 4 Gy X-rays + 60 J/cm² light + 50 μM ICG	MCF-7 breast cancer cells	Cell viability (MTT assay)	• ICG alone non-toxic but effective photosensitizer • Combo of ICG + light + X-ray killed 96.6% cells • Low-dose X-ray enhances PDT efficacy	[101]
RT (X-rays): 4 or 8 Gy; UV-C (200-280 nm)-emitting nanoscintillators ($LuPO_4$:Pr^{3+},Nd^{3+}): 2.5 mg/ml	A549 lung cancer 3D spheroid model	Tumor spheroid growth; cell death pathways (apoptosis, necrosis); cell cycle arrest (G2/M)	• ↑ Tumor growth inhibition • ↑ apoptosis and necrosis • ↑ G2/M arrest • No nonspecific toxicity from nanoparticles alone	[102]
RT (X-rays, 320 kVp): 2–4 Gy; UVC (220–285 nm, via $LuPO_4$:Pr^{3+} NPs, generated in situ by X-rays; NP concentration: 0.5–7.5 mg/mL (optimal: 2.5 mg/mL)	HFF1 normal human fibroblasts, XP17BE UV-sensitive fibroblasts	Clonogenic survival, CPD formation (ELISA), radiosensitization, nanoparticle cytotoxicity	• ↑ Cell killing with combined treatment (↓ survival to ~2% at 7.5 mg/ml NPs + 2 Gy) • ↑ CPD formation (~50% equivalent to 15 J/m² UV-C) • ↑ effect in XP17BE vs HFF1 cells • NPs alone cause mild dose-dependent toxicity at ≥5 mg/ml	[103]
RT (X-rays (6 MV): 2 Gy; NIR laser (808 nm): 2 W/cm² for 3–20 min at 43 °C	Human glioblastoma U87MG cells	Colony formation; cell viability; nanoparticle uptake (Prussian blue stain); radiosensitization	• ↓ Plating efficiency with IUdR-PLGA-NGO + X-ray + NIR vs all other groups • ↑ nanoparticle uptake • Enhanced radio- and thermo-sensitization • No cytotoxicity from laser or nanoparticles alone	[104]
CIRT: 16.6 Gy (RBE) in 4 fractions [4.15 Gy(RBE)/fraction]; IMRT (X-rays, ~6 MV): 45–50.4 Gy in 1.8–2 Gy/fraction	High-risk prostate cancer patients (n=15) enrolled at 3 Italian oncology centers; follow-up up to 12 months	RTOG/EORTC acute toxicity grading; Prostate-Specific Antigen (PSA) kinetics; Quality of Life (QoL) via IPSS, QLQ-C30, QLQ-PR25, IIEF-15	• No acute GI/GU toxicity > G2 • 53% had no GU toxicity • QoL improved or stable post-RT • PSA median 0.08 ng/ml at last follow-up • Mixed-beam approach feasible and well-tolerated	[105]
CIRT (LET ~50–80 keV/μm): 16.6 Gy (RBE) in 4 fractions [4.15 Gy(RBE)/fraction]; IMRT [X-rays, 6 MV, volumetric modulated arc therapy (VMAT) mode]: 50 Gy in 25 fractions (2 Gy/fraction)	High-risk prostate cancer patients (n=5); multi-center prospective Phase II protocol	Target coverage and OAR dose metrics; DIR accuracy (DSC, CI, TRE); comparison with IMRT-only plan	• CIRT+IMRT plans showed lower doses to rectum, bladder, anal canal, penile bulb vs. IMRT-only • DIR accuracy varied by OAR and patient • Femoral heads least deformed • Rectum most deformed mixed-beam approach enables OAR sparing but introduces DIR-related uncertainty	[106]
RT (IMRT, photons): 54–60 Gy; RT (proton therapy, active scanning, RBE=1.1): boost to 70–74 Gy;	27 patients with locally advanced nasopharyngeal cancer (LANPC, T3–T4, N0–	RTOG/CTCAE acute and late toxicity; local control, PFS, LPFS; oral cavity,	• Grade 3 mucositis: 11% (MB) vs. 76% (IMRT-only) • Significantly lower doses to oral cavity and supraglottic	[107]

 doi:10.20944/preprints202506.2020.v1

RT (IMRT-only cohort, photons): 69.96–70 Gy	N3); compared to historical IMRT-only cohort (n=17)	esophagus, larynx dosimetry	larynx • 2-year LC: 96% (MB) vs. 81% • No Grade ≥3 late toxicities • Mixed-beam ↓ acute toxicity with comparable efficacy	
Bolus Electron Conformal Therapy (BECT) + IMRT (6 MV X-rays) + VMAT (6 MV X-rays); 20 fx BECT to chest wall (40 Gy) + parallel opposed IMRT to supraclavicular (40 Gy) + 5 fx VMAT boost (10 Gy); total dose: 50 Gy in 25 fx	Left-sided postmastectomy breast cancer patients (n=9); retrospective planning study	Target coverage (CI, DHI), OAR dose (lung, heart, contralateral breast), NTCP, SCCP	• Mixed-beam plans ↓ NTCP for cardiac mortality (0.23% vs. 0.80%) and SCCP for contralateral breast vs. VMAT • CI and DHI inferior to VMAT • Patients with >0.5 cm tissue between PTV and lung benefited most	[108]
RT (X-rays): 6 Gy; NIR light (730 nm): 0.4–0.8 W/cm² for 5–8 min; UCNP@NBOF-FePc-PFA at 80–100 μg/mL	Murine breast cancer cells (4T1.2), U251 glioma cells; BALB/c mice (tumor-bearing)	Tumor cell apoptosis, ROS generation, photothermal effect, imaging-guided therapy	• Highly synergistic tri-modal effect (radiotherapy + photothermal + photodynamic therapy) • ~96% tumor inhibition in vivo • Massive cell apoptosis • ↑ ROS and temperature under dual irradiation	[109]
X-rays (6 MV): 4 Gy; NIR laser (808 nm): 1 W/cm² for 3 min at ~ 42 °C; RT applied 4–6 h after the first laser irradiation	Mouse 4T1 TNBC tumor model (BALB/c nude mice); 4T1 cells in vitro	ROS generation; tumor growth delay; colony formation; apoptosis (TUNEL)	• Strong synergistic effect: 60% complete tumor eradication in vivo • Highest ROS production in combined group • Lowest colony survival and strongest apoptosis in vitro • INS NPs showed excellent tumor targeting and magnetic guidance	[110]
NIR-PIT (690 nm laser): External exposure (50 + 100 J/cm²); Interstitial exposure (50 + 100 J/cm); Combined exposure (25 + 50 J/cm² external + 25 + 50 J/cm interstitial)	EGFR-positive A431-luc tumor xenografts in nude mice	Tumor volume, bioluminescence (viability), survival	• Combined external/interstitial light led to greatest tumor volume reduction and survival vs. either alone • Improved light delivery and tumor coverage enhanced treatment efficacy	[111]
Electron beams (25–100 MeV): up to ~73 Gy to gross tumor; Photon beams (5 MV, 15 MV, 50 MV): up to ~75 Gy to gross tumor; used alone or in combination in RT. Doses optimized per plan and energy-modality combination.	Cervical cancer and astrocytoma patient geometries (simulated)	Probability of complication-free cure (P^+), dose conformity	• Combined e^- + X-ray plans achieved higher P^+ than X-rays alone for shallow tumors • Optimized direction and energy critical • X-ray addition sharpened penumbra and improved target coverage	[112]
Carbon ions (12C, 226.5–248.5 MeV/u): up to ~1.8 Gy per field (SOBP); Helium ions (4He, 226.5 MeV/u): ~1% of carbon dose added for online range verification. Used	Cubic plastic scintillator (20 cm) + CCD-based optical system; beam scanned across scintillator surface	Bragg peak position; light intensity (photons/pixel); FLUKA-based Monte Carlo validation of detector models	• Mixed C+He beam enables sub-mm range verification via emerging He signal • Optical detection validated with proton beams	[113]

 doi:10.20944/preprints202506.2020.v1

simultaneously in mixed-beam therapeutic RT with real-time imaging potential.			• Monte Carlo models accurate within 20% • Proposed method suitable for in-treatment range control during carbon ion therapy	
Carbon ions (320 MeV/n, LET = 46.6 keV/μm): 0.8–4.4 Gy; X-rays (4 MV): 2–8 Gy; carbon 0.4–2.2 Gy + X-ray 1–4 Gy; exposures within 15 min or 72 h apart	Human salivary gland cancer cells (HSG)	Clonogenic survival (colony formation assay); survival fraction at 2 Gy (SF2); RBE	• No synergistic effect observed • Combined exposures followed additive prediction model based on GyE • Survival curves and parameters aligned with additive model • Effect independent of irradiation sequence	[114]
Carbon ions (290 MeV/u, LET 13–100 keV/μm): 2.0–6.8 Gy; Silicon ions (490 MeV/u, LET 55 keV/μm): 3.0 Gy; Argon ions (500 MeV/u, LET 85 keV/μm): 2.5–3.0 Gy; Iron ions (500 MeV/u and 200 MeV/u, LET 200–860 keV/μm): 1.75–3.5 Gy; X-rays (150 or 200 kVp): 8.0 Gy (priming or test dose)	V79 Chinese hamster cells	Clonogenic survival, sublethal damage repair (SLDR), RBE analysis	• ↑ Cell killing with sequential ion + X-ray exposure vs single beams • ↓ SLDR with increasing LET; high-LET ions (≥80 keV/μm) cause largely irreparable damage • LET-dependent reduction in repairable fraction • Evidence of combinatorial suppression of SLDR	[115]
XRT (6–24 MV) + FNT (66 MeV proton- or 8 MeV deuteron-induced fast neutrons); whole pelvis: ~50 Gy photon-equivalent; boost to prostate: 15–20 Gy eq.; mix: 60% photons, 40% neutrons; 3 fx/week photons, 2 fx/week neutrons	Patients with bulky Stage B2, Stage C, Stage D1, or post-op recurrence (n=45); treated 1978–1991 at Univ. of Chicago & Fermilab	Overall survival, disease-free survival, local control, PSA kinetics, histology (biopsy/autopsy), RTOG toxicity (Grades 1–5)	• 5-yr survival 72%, disease-free survival 45% • Local control 89% • 72% of biopsies post-RT were tumor-free • 36% had Grade 3–5 toxicity • Dose >70 Gy eq. linked to higher complications • Neutron source and field arrangement affected outcomes	[116]
Fast neutrons (22–66 MeV, various cyclotrons and linacs): 7.5–10 Gy (RBE-adjusted); Photons (megavoltage X-rays): 40–44 Gy in mixed beam arm, or 66–74 Gy in photon-only arm. Mixed beam RT delivered over 7–8 weeks using 2 neutron + 3 photon fractions per week	Patients with unresectable squamous cell carcinoma (T2–T4, any N) of oral cavity, oropharynx, supraglottic larynx, or hypopharynx (n=306)	Primary tumor control; nodal response; overall survival; 2-year DFS; toxicity (RTOG criteria)	• No significant difference in local/regional control or survival • Mixed beam improved nodal CR rate (69% vs. 55%, p=0.024) • Higher severe toxicity (16% vs. 8%) • Mixed beam feasible but not superior overall	[117]
RT (megavoltage X-rays): 66–74 Gy in 1.8–2.0 Gy/fx; FNT (neutrons, high-LET, d→Be or p→Be cyclotron): 7.5–10 Gy RBE-adjusted dose in 1.8–2.0 Gy photon-equivalent/fx); Mixed beam (Photons 40–44 Gy + Neutrons 7.5–10 Gy), 7–8 weeks total duration	327 patients (297 evaluable) with oral cavity, oropharynx, supraglottic larynx, or hypopharynx tumors; randomized at 5 U.S. neutron facilities	Primary and nodal tumor clearance, loco-regional control, survival, RTOG toxicity, recurrence patterns	• Mixed beam improved nodal control vs. photons in node + patients (45% vs. 26%, p=0.004) • But worse primary control in node– patients (27% vs. 60%, p=0.006) • No overall survival	[118]

 doi:10.20944/preprints202506.2020.v1

			difference • Higher Grade 3+ toxicity with mixed beam (18% vs. 10%)	
Fast Neutrons (30 MeV d-Be, <5% gamma contribution): up to 35.78 Gy (fractionated, 5 n); gamma rays (60Co, 1.00 Gy/min): up to 104.4 Gy (fractionated, 5 gamma); Mixed Beam (2 n + 3 gamma over 5 days): neutrons ~6.78–7.66 Gy, gamma ~66 Gy total	C3H mice bearing syngeneic NFSa fibrosarcoma; tumors irradiated locally	Tumor control dose (TCD50); lung colony assay (cell survival); Do and n from survival curves	• Mixed-beam (N-γ-γ-γ-N) yielded survival and TCD50 curves indistinguishable from calculated additive effects • No interaction observed • Neutron RBE ~3 vs. gamma rays • Fractionation increased Do and extrapolation number for gamma rays but not neutrons	[119]
BNCT. Mixed Neutron Beam (Thermal: 22.4%, Epithermal: 2.4%, Fast: 16.7%); gamma rays (58.5% of total dose): 1.25 Gy; gamma Rays (60Co or equivalent): 2 Gy	CHO-K1 cells (Chinese hamster ovary); fixed 3 h post-irradiation; foci quantified via immunofluorescence and ImageJ	Cell survival (clonogenic), 53BP1 foci number and size (DNA DSBs), D0/D10 values for single vs. fractionated exposure	• Fractionated neutron IR led to fewer foci but larger size • Higher D0 vs. single dose • Suggests persistent clustered DSBs due to high LET • Gamma IR showed less foci size difference • Importance of damage complexity in fractionated high-LET fields highlighted	[120]
BNCT. Alpha (3.2 MeV, LET ~120 keV/μm): 0.5–2.0 Gy; Gamma (60Co): 3.4–8.6 Gy; mixed doses matched for equivalent biological effect (e.g., 0.5 Gy alpha + 3.4 Gy gamma); simultaneous exposure using dual-source setup at 10 °C	V79-4 Chinese hamster cells	Clonogenic survival (colony formation assay)	• No significant synergistic effect observed • Mixed beam survival closely matched additive prediction • Results suggest lack of sub-lethal damage interaction with alpha particles under these conditions	[121]
BNCT. Alpha particles: 2 or 2.5 Gy; X-rays: variable doses; simultaneous vs non-simultaneous delivery assessed	V79 Chinese hamster lung fibroblast cells	Cell survival (clonogenic assay)	• Strong synergistic effect on cell killing observed only at 2.5 Gy alpha when combined simultaneously with X-rays • Survival curve steepened, suggesting alpha exposure impairs DNA repair from low-LET X-rays	[122]
BNCT. Neutron Mixed Beam (Thermal <0.5 eV: 25%, Epithermal 0.5–10 keV: ~2.6%, Fast >10 keV: 18–19%, LET range not specified): 0.9–1.0 Gy; gamma rays (60Co, 40 mGy/min): 0.9–1.0 Gy (controls)	CHO-K1 (wild-type) and xrs5 (Ku80-deficient) Chinese hamster ovary cells	Clonogenic survival; DNA double-strand breaks (53BP1 foci count, size, spatial distribution)	• RBE at 10% survival: 3.3 (CHO-K1) and 1.2 (xrs5) • Foci number and size similar to gamma rays, but neutron-induced foci were spatially clustered • Indicates potential for more complex DNA damage from neutron components	[123]
Cf-252 neutrons (0.2–0.3 Gy/hr), 137Cs gamma rays (0.7–0.85 Gy/hr) and 60Co gamma rays (1.25–2 Gy/min); total body irradiation with doses up to ~13 Gy,	Balb/c mice, whole-body irradiation model; gastrointestinal and bone marrow systems assessed	GI-50 (6–10 day survival) and BM-50 (30 day survival) syndromes after single and fractionated exposures	• Dose required to cause syndromes ↓ sharply up to 35% neutron contribution, then plateaued • Minimal repair in neutron-	[124]

 doi:10.20944/preprints202506.2020.v1

depending on endpoint and mix ratio			rich exposures • Mixed beams ≥35% neutrons behaved like high LET radiation • Fractionation and dose rate effects negligible for Cf-252 but substantial for photons	

Table 5. Space Radiation Studies Involving Combined Radiation.

Type & Dose	Biological systems	Biological endpoints	Effects	Ref.
40Ar (550 MeV/n, 86 keV/μm), 28Si (100 MeV/n, 150 keV/μm), 56Fe (115 MeV/n, 442 keV/μm); X-rays (150 kVp); dose combinations ranged from 1–11 Gy total; simultaneous exposure	Hamster V79 fibroblasts; Human lymphocytes	Clonogenic survival (V79); Chromosome 2 aberrations (FISH-PCC, lymphocytes)	• Additive effects for Ar and Si ions with X-rays • Slight non-additive deviation (mild synergy) observed for Fe ions, especially at 1:1 dose ratio • Fe + X-ray survival and chromosomal damage slightly exceeded predicted additive response	[125]
Gamma rays (661.7 keV): 0.4 Gy; carbon-12 ions (450 MeV/n, 10.3 keV/μm): 0.14 Gy; whole-body gamma ray exposure followed 24 h later by head-only C-12 ions	Adult male Wistar rats; nucleus accumbens (NAc) and dorsal striatum (dST) analyzed	Locomotor activity, grip strength, monoamine and choline metabolism (HPLC), gene/protein expression of STX1A and SNCA (qPCR, immunoblotting)	• IR caused hyperlocomotion and enhanced intrasession habituation • ↑ choline and α-synuclein, ↓ STX1A in NAc • ↓ 5-HIAA • STX1A protein ↓ in dST • Suggests link to vesicle trafficking and neurotransmission modulation	[126]
Gamma rays (661.7 keV): 0.4 Gy; carbon-12 ions (450 MeV/n, 10.3 keV/μm): 0.14 Gy; whole-body gamma-irradiation daily for 3 days, followed by acute C-12 head-only exposure on day 4;	Wistar rats (n=14), pituitary gland analyzed post-mortem	qPCR and Western blot for C/EBP-β isoforms (LAP*, LAP, LIP); mRNA and protein quantification	• No change in mRNA levels, but 1.76× increase in C/EBP-β LIP isoform protein in irradiated rats • Suggests translation-stage regulation • Indicates ER stress and potential apoptosis signaling via HPA axis modulation	[127]
Beta radiation (10 MeV): 0.5, 25, 250 kGy; Gamma rays (3 MeV): 0.5, 25, 250 kGy (sequential exposures for combined treatment)	Various biological polymers and small molecules immobilized on slides (e.g., proteins, peptides, spores)	Structural/chemical epitope integrity via immunoassay	• Combined exposure caused cumulative immunoidentification loss • Effect similar to separate treatments • Pattern closer to electrons-only group • Radiolysis varied with molecule type	[128]
1H (150 MeV/n): 0.5 Gy; Oxygen ions (16O, 600 MeV/n): 0.1 Gy; whole-body irradiation with a 1-hour interval	Male mice; hippocampus (dentate gyrus, CA1); Y-maze for cognition; Golgi staining, qRT-PCR, spine and dendritic morphology	Short-term spatial memory (Y-maze); dendritic complexity (Sholl); spine density (mushroom, stubby); synaptic markers (Nr2a,	• Impaired memory and ↓ novel arm recognition • ↓ mushroom spines, ↑ stubby spines in DG and CA1 • Altered dendritic	[129]

 doi:10.20944/preprints202506.2020.v1

		Nr2b, GluR1, synapsin-1, drebrin, SAP97)	arborization and complexity • ↑ GluR1, Nr2a, synapsin-1, drebrin • Hippocampal remodeling consistent with cognitive dysfunction	
Protons (150 MeV/n): 0.5 Gy; 16O (600 MeV/n): 0.1 Gy	Male C57Bl/6J mice, hippocampal neurons	Y-maze (short-term memory), novel object recognition, dendritic morphology, spine density, SNP analysis	• Memory deficits • Reduced novel object recognition • ↓ mushroom spine density • Altered dendritic morphology (↑ in dentate gyrus, ↓ in CA1) • ↑ SNPs in Txnrd2/3	[130]
Protons (1 GeV, 60%); 16O ions (250 MeV/n, 20%); 28Si ions (263 MeV/n, 20%); total doses: 0, 25, 50, or 200 cGy; sequentially delivered in rapid succession to mimic cosmic radiation exposure	B6D2F1 (C57BL/6J × DBA2/J F1) male and female mice	Behavioral (home cage activity, depressive behavior), cognitive (object recognition, fear conditioning), molecular (BDNF, CD68, MAP-2 levels), microbiome diversity	• 50–200 cGy impaired object recognition • 50 cGy ↑ depressive behavior and activity (males) • Radiation altered BDNF (↓ in males), CD68 (↑ in females) • Gut microbiome diversity ↑ in dose-dependent fashion	[131]
Protons (120 MeV/n): 20 cGy; helium (250 MeV/n): 5 cGy; silicon (300 MeV/n): 5 cGy; whole-body irradiation in 3 orders (H→He→Si, Si→He→H, and H→He +24h→Si); total dose: 30 cGy; CDDO-EA given 3 days pre-IR to 1 day post-IR	K-rasLA1 lung cancer-susceptible mice; lung tissue and plasma; histology, lipid peroxidation assay, 1-year survival	Lesion number (hyperplasia, adenoma, atypia, carcinoma); MDA levels; impact of ion order and CDDO-EA on oxidative stress and tumorigenesis	• H→He→Si sequence ↑ premalignant lesions, MDA, and adenocarcinomas • Delaying Si by 24h or using Si→H→He sequence ↓ effects • CDDO-EA countermeasure normalized lesion count and MDA • Sequence- and timing-dependent cancer risk highlighted	[132]
Protons (1000 MeV, LET 0.24 keV/μm): 1.2 Gy; 28Si ions (500 MeV/n, LET 54 keV/μm): 0.15 Gy; 56Fe ions (600 MeV/n, LET 190 keV/μm): 0.15 Gy; total dose: 1.5 Gy (whole-body, sequential rapid switching)	WAG/RijCmcr male rats (6 mo); heart, kidney, blood; 270-day follow-up; histology, echocardiography, cytokine panels	Perivascular cardiac fibrosis, blood pressure, serum cholesterol, renal histology, cytokines (IL-5, IL-18, IL-17A), macrophage (CD68+) infiltration	• 1.5 Gy → perivascular fibrosis and ↑ systolic BP • ↑ CD68+ cells in heart/kidney • Cytokine shifts at 30–60 d • Single-ion beams did not induce pathology • Threshold for fibrosis likely between 0.75–1.5 Gy	[133]
Smf-GCR (protons 1000 MeV/n, He 250 MeV/n, 16O 325 MeV/n, 28Si 300 MeV/n; LET 0.22–69 keV/μm); total dose of 0.5 Gy (0.3 Gy H, 0.1 Gy He, 0.05 Gy O, 0.05 Gy Si) delivered in sequence over ~15 min	Male and female *Apc*^1638N/+ mice (intestinal tumor model); tissues collected 150 days post-irradiation	Intestinal tumor count and classification (adenoma vs. carcinoma); histopathology; risk estimation; contribution analysis of ion components	• Smf-GCR induced more GI tumors and carcinomas than gamma rays • Heavy-ion fraction (O + Si) accounted for >95% of tumorigenic effect • Males had higher tumor burden • Data highlight heavy-ion dominance in GCR-associated GI cancer risk	[134]

 doi:10.20944/preprints202506.2020.v1

Total dose of 15 or 50 cGy (GCRsim; 5-ion simplified beam; protons 250/1000 MeV, 4He 250 MeV/n, 16O 350 MeV/n, 28Si 600 MeV/n, 56Fe 600 MeV/n)	Male and female C57Bl/6J mice, immune and endocrine systems (blood, adrenal glands)	Organ weights (thymus, spleen, adrenals), plasma hormones (aldosterone, corticosterone), immune cell profiles (phagocytosis, NLR), transcriptomics	• ↓ Thymus/spleen/adrenal weights in males • ↓ Aldosterone in males • ↑ NLR in females (3 days) • ↑ Phagocytosis in males • Sex-specific gene expression changes at 14 days	[135]
Protons (1 GeV, 250 MeV); 4He (250 MeV/n); 16O (350 MeV/n); 28Si (600 MeV/n); 56Fe (600 MeV/n); total dose of 50 cGy; whole-body irradiation using the 5-ion simGCR beam at NASA Space Radiation Lab;	Male BALB/c mice (n=12, irradiated vs. sham); hippocampus and bone marrow; tissues analyzed 3 months post-IR	Y-maze, Morris water maze (MWM); flow cytometry (astrocytes, NPCs, microglia, oligodendrocytes); cytogenetics (G-banding, SKY); proteomics (TMT + IPA)	• GCR exposure impaired short-term and spatial memory • No glial cell changes • Chromosome aberrations ↑4× vs. sham • 113 proteins differentially expressed (fold change >1.5) • Network analysis linked protein shifts to cognition and neurodegeneration	[136]
Protons (1000 MeV, LET 0.20 keV/μm): 17.5 cGy; Si (600 MeV/n, LET 50.4 keV/μm): 0.5 cGy; He (250 MeV/n, LET 1.60 keV/μm): 9 cGy; O (350 MeV/n, LET 20.9 keV/μm): 3 cGy; Protons (250 MeV, LET 0.40 keV/μm): 19.5 cGy; Fe (1000 MeV/n): 0.5 cGy; total: 50 cGy or 100 cGy depending on group.	Male and female mice; hippocampus, blood, cortex; flow cytometry, synaptocytometry, RAWM, PCA analysis	Spatial learning (RAWM), sociability, social memory, recognition memory; microglia phenotype (CD68, CD107a), synaptic density (PSD-95, Synapsin-1), blood monocytes	• GCRsim caused sex-specific spatial learning deficits (males only) • Linked to microglia activation and ↑ synapses • Microglia depletion reversed deficits • Early blood monocyte levels predicted late cognitive decline in males	[137]
5-ion GCRsim (H, He, O, Si, Fe): 0.5 or 0.75 Gy; gamma rays: 0.75 or 2 Gy; whole-body irradiation	Male and female AD-model (APP/PS1) and WT mice; brain (MRI, amyloid), heart and kidney (gene expression, fibrosis), plasma (cytokines)	Spatial memory (Y maze), anxiety (EPM, OFT), sensorimotor gating (PPI), rotarod, MRI volumes, gene expression (VLCAD, Casp3, GLUT4), cytokines	• No effect on Aβ • GCRsim and gamma caused sex-specific MRI and behavior changes • GCRsim ↓ VLCAD, Casp3, GLUT4 • Male Tg mice more affected neurologically • GCRsim ↑ hippocampal volumes and ventricular enlargement • Minor kidney/heart fibrosis and altered cytokines	[138]
5-ion GCRsim (1H, 4He, 16O, 28Si, 56Fe); total dose of 500 mGy delivered over ~4.5 h in 6 sequential beams; TGF-βRI inhibitor (IPW-5371) administered in diet pre- and post-IR	BALB/c (male) and CD1 (male/female) mice; cardiac tissue and plasma collected 12–20 weeks post-IR; cardiac function via echocardiography	Cardiac structure/function, collagen deposition, capillary density, immune markers (CD2, CD4, CD45, TLR4), TGF-β1 expression	• GCRsim caused minor cardiac changes • ↑ collagen and ↓ TLR4 in CD1 males mitigated by TGF-β inhibition • CD1 females showed ↑ capillaries and ↓ ventricular mass • Combined GCRsim + inhibitor altered immune cell marker profiles in both sexes	[139]

 doi:10.20944/preprints202506.2020.v1

5-ion GCRsim (H 1000 MeV/n, He 250 MeV/n, O 350 MeV/n, Si 600 MeV/n, Fe 600 MeV/n); total dose of 5, 15, or 50 cG; whole-body irradiation	Male and female mice; undisturbed homecage behavior; hippocampus and prefrontal cortex-related tasks	Species-typical behaviors: burrowing, grooming, rearing, nest building (Deacon score); Neuroscore test battery (7 tasks)	• No sensorimotor deficits detected • Sex- and dose-specific changes in burrowing (↑ at 15 cGy in females) and grooming (↑ at 50 cGy in females) • Nestlet construction differed by sex and dose • More robust female performance • Delayed effects subtle and behavior-dependent	[140]
15 cGy (GCRsim; 5-ion simplified beam, 0.5 cGy/min over ~20 min)	Male Wistar rats, sleep regulation and thermoregulation systems (brain, core body)	Sleep architecture (NREM, REM, TST), EEG spectral power (delta, theta, alpha, sigma, beta bands), core body temperature (CBT)	• ↓ Dark period TST • ↓ NREM • ↓ REM • ↓ NREM delta power • ↓ REM theta power • ↑ NREM/REM alpha and sigma power • ↓ CBT during light period	[141]
Total dose of 0.5 Gy delivered over ~ 20 min (GCRsim; 5-ion simplified beam)	Human 3D microvessel cultures (HUVEC-derived), female C57Bl/6 mice (liver, heart, plasma, soleus muscle)	Microvessel integrity (angiogenesis, collapse), DNA double strand breaks (53BP1 foci), mitochondrial function, inflammatory pathways (cytokines, ISGs)	• ↓ Microvessel collapse • ↓ DNA DSBs • ↓ inflammatory signaling (TNF-α, IL-6) • ↑ mitochondrial function rescue after miRNA antagomir treatment	[142]
GCRsim (5-ion simplified beam): total dose of 0.75 Gy; gamma rays: 2 Gy; whole-body irradiation	Male and female transgenic mice (APP;E3F, APP;E4F); sham, traveled, and non-traveled controls; hippocampus, plasma, feces	Open field, rotarod, NOR, spatial novelty Y-maze; hippocampal Aβ pathology, ApoE, plasma cytokines, lipids; microbiome (16S rRNA)	• Modest cognitive and neuropathological effects of GCRsim vs. sham • Radiation interacted with sex, genotype, travel • GCRsim ↓ plasma IL-6, TNF-α, HDL • Long-term microbiome shifts correlated with plaque burden and memory • ApoE genotype shaped responses	[143]
Total dose of 10 cGy (GCRsim; 1 GeV/n protons 35%, 250 MeV/n protons 39%, 250 MeV/n helium 18%, 350 MeV/n oxygen 6%, 600 MeV/n silicon 1%, 600 MeV/n iron 1%)	Male and female Wistar rats	Risk-taking propensity (RTP), decision-making performance, processing speed	• ↑ Risk-taking in females (↓ profitable choices at 30–60 days) • ↑ Decision latency in males (~2× slower at 30 days) • Performance recovery by 90 days	[144]
Total dose of 5 or 30 cGy (5- or 6-ion GCR simulation); whole-body irradiation	Male C57BL/6J mice; hippocampus, cortex; electrophysiology, behavioral assays	Hippocampal inhibitory synaptic activity, LFP oscillations, spatial and recognition memory, anxiety behavior	• Mixed-ion exposure disrupted hippocampal GABAergic signaling • Slowed sharp-wave ripple frequency • Impaired memory and ↑ anxiety-like behavior at 30 cGy	[145]

 doi:10.20944/preprints202506.2020.v1

Total dose of 10 cGy (GCRsim; 74% protons, 18% helium, 6% oxygen, 1% silicon, 1% iron)	Male Wistar rats	Approach time, pull duration, movement accuracy (misses/contacts), reach endpoint concentration	• ↑ Pull duration • Mild ↑ approach time (some individuals) • No significant change in movement accuracy or reach concentration vs Sham at 72h	[146]
Total dose of 10 cGy (GCRsim; 1 GeV/n protons 35%, 250 MeV/n protons 39%, 4He 18%, 16O 6%, 28Si 1%, 56Fe 1%)	Female Wistar rats	Task switching performance, stimulus-response training success, switch cost errors	• ↓ Switch task accuracy (−20%) • ↑ Perseverative errors (anterograde interference) • ↑ Failure to complete training stages • No change in response times	[147]
Total dose of 50 cGy (GCRsim; 1 GeV/n protons 17.5 cGy, 250 MeV protons 19.5 cGy, 4He 9 cGy, 16O 3 cGy, 28Si 0.5 cGy, 56Fe low dose)	Male and female CD1 mice, retina tissue	BRB integrity (AQP-4, PECAM-1, ZO-1 expression), oxidative stress (4-HNE), apoptosis (TUNEL assay)	• ↑ AQP-4 expression (female > male) • ↑ PECAM-1 expression (male > female) • ↓ ZO-1 expression • ↑ Oxidative stress (4-HNE) • ↑ Retinal apoptosis	[148]
Total dose of 75 cGy (GCRsim; 1 GeV/n protons 35%, 250 MeV/n protons 39%, 4He 18%, 16O 6%, 28Si 1%, 56Fe 1%)	H9c2 myoblasts, ES-D3 pluripotent cells, Hy926 endothelial cells	Mitochondrial function (MTT, TMRE), oxidative stress (DHE), cell senescence (ONPG), neoplastic transformation (Afp-tdTomato expression)	• ↓ Mitochondrial function • ↑ Oxidative stress • ↑ Senescence markers • ↑ Neoplastic transformation markers (Afp-tdTomato)	[149]
X-rays (160 kVp): 0.1–1.0 Gy pretreatment, 8 Gy challenge; 5-ion GCRsim [1000 MeV/n proton: 26.25 cGy; 250 MeV/n proton: 29.25 cGy, helium (250 MeV/n): 13.50 cGy, oxygen (350 MeV/n): 4.50 cGy, silicon (600 MeV/n): 0.75 cGy, iron (600 MeV/n): 0.75 cGy]: 75 cGy challenge	H9c2 rat cardiomyoblast cells; analyzed for viability, oxidative stress, and mitochondrial integrity	Cell doubling time, MTT viability, DHE/MitoSox fluorescence, TMRE, flow cytometry (cell size/complexity)	• X-ray pretreatment restored replicative capacity and ↓ cytosolic superoxide after GCRsim • Strongest adaptive effect at 0.5–1.0 Gy • Mitochondrial metrics unaffected • Supports low-dose X-ray hormesis as potential countermeasure	[150]
Protons (1 GeV, LET 0.24 keV/μm); 4He (250 MeV/n, LET 1.6 keV/μm); 16O (250 MeV/n, LET 25 keV/μm); 28Si (263 MeV/n, LET 78 keV/μm); 48Ti (1 GeV/n, LET 107 keV/μm); 56Fe (1 GeV/n, LET 151 keV/μm); total dose of 25, 50, or 200 cGy; rapid sequential whole-body irradiation	B6D2F1 male and female mice (n=99); cortical and hippocampal brain tissue, feces (microbiome)	Open field, object recognition, forced swim, fear conditioning, passive avoidance; BDNF, CD68, MAP-2 (ELISA); microbiome (16S rRNA sequencing)	• 50 & 200 cGy impaired object recognition and passive avoidance memory in females • Altered BDNF/CD68 patterns in males • Microbiome composition changed in sex- and dose-dependent ways • Strong link between microbiota and behavioral metrics	[151]
GCRsim [H (1 GeV); Si (600 MeV/n); He (250 MeV/n); O (350 MeV/n); Fe (600 MeV/n); H (250 MeV)]; total dose: 5 cGy or 30 cGy; whole-body irradiation	Middle-aged male mice; hippocampus (CA1); object location memory (“Objects in Updated Locations” task); LTP analysis in hippocampal slices	Memory updating, discrimination index (DI), long-term potentiation (LTP), p-cofilin expression, HDAC3 inhibition (RGFP 966)	• 30 cGy GCR impaired memory updating and LTP • 5 cGy had mild or no effect • Systemic HDAC3 inhibition reversed LTP impairment • ↓ p-cofilin suggests	[152]

 doi:10.20944/preprints202506.2020.v1

			cytoskeletal mechanism • First evidence of epigenetic rescue of GCR-induced synaptic dysfunction	
4He (250 MeV/n, LET 1.6 keV/μm): 10 cGy; 5-ion GCRsim: 10 cGy; whole-body irradiation of male Wistar rats; comparisons between single-ion (He) and complex-ion (GCRsim) groups	Male Wistar rats; performance assessed on ATSET (attentional set shifting) and UCFlex (unconstrained cognitive flexibility) tasks	Executive function measures: time to solve tasks, error rate, cue relevance discrimination, practice effect (PE) analysis	• GCRsim and He exposure both impaired SD stage of ATSET • GCRsim-exposed rats required more time/iterations to solve tasks • PE ↓ (50% slower than pretest vs. 30% improvement in sham) • UCFlex deficits also observed • Findings suggest diminished cognitive flexibility and ↓ learning from repetition after space-radiation exposure	[153]
Gamma (137Cs): 0.1–2.0 Gy; proton (150 MeV, LET 0.54 keV/μm): 0.1–2.0 Gy; carbon ion (600 MeV/n, LET 9.18 keV/μm): 0.1–2.0 Gy; iron ion (600 MeV/n, LET 172.4 keV/μm): 0.1–2.0 Gy; GCRsim (simplified 6-beam field): 0.1–2.0 Gy	Latently CMV-infected Kasumi-3 human myeloblast cells; viral load, cell viability, cell size, genomic and transcriptomic assays	CMV reactivation via DNA qPCR; cell viability and morphology; gene expression (UL49)	• All IR types induced CMV reactivation in dose- and time-dependent fashion • GCRsim triggered UL49 upregulation (logFC 1.48) • Carbon/iron led to strongest CMV load • No genomic variation • Cell viability and size affected by LET	[154]
7-ion GCRsim (1H, 2He, 6C, 16O, 28Si, 44Ti, 26Fe; 20–1000 MeV/n); chronic exposure: 2.08 cGy/day × 6 days/week × 4 weeks (total 50 cGy)	Female *Apc*^Min/+ mice; whole-body irradiated; mammary tissues and serum collected 100–110 days post-IR	Mammary tumor incidence, ductal morphology, serum estradiol and SPP1, ERα/ERRα expression (IHC/qPCR)	• ↑ ductal overgrowth, ↑ mammary tumors (24% vs. 5%) • ↑ serum estradiol, ERα, ERRα, SPP1 expression • Estrogen and inflammatory signaling linked to tumorigenesis • Conserved expression patterns in human breast cancer tissues	[155]
33-ion GCRsim (H, He, C, O, Si, Ti, Fe, and others; various LETs and energies); acute dose: ~40 cGy in 2 h; chronic dose: ~50 cGy over 24 sessions; whole-body irradiation	C57BL/6J mice (n=178 male, 91 female); hippocampus, mPFC, corpus callosum; behavioral, electrophysiological, and EM analyses	Object in updated location (OUL), novel object recognition (NOR), light–dark box (LDB), social interaction (SIT), tube dominance; LTP, sEPSC/sIPSC, EM (PSD, myelin)	• Chronic GCR impaired memory updating in both sexes • Acute exposure disrupted excitatory synaptic signaling • LTP ↓ in both sexes • Chronic GCR thinned PSD in large spines, altered myelination in small/large axons • Sex-specific deficits in behavior and synaptic function	[156]

 doi:10.20944/preprints202506.2020.v1

33-ion GCRsim (H, He, C, O, Si, Ti, Fe, etc.; 40–49.9 cGy total); acute dose: 40 cGy in 2 h; chronic dose: ~50 Gy over 4 weeks; whole-body irradiation	Male C57BL/6 mice; prefrontal cortex (PFC); touchscreen-based cognitive tasks; in vivo PFC microdialysis with LC-MS/MS	Touchscreen-based economic demand and psychomotor vigilance tasks; PFC dopamine (DA), 5-HT, NE, Glu, GABA levels; network modeling and Granger causality	• No change in motivation, but attentional deficits and slowed reaction times in GCR groups • DA signaling blunted in PFC • Chronic GCR ↑ all neurotransmitters under stimulation • Acute and chronic GCR reorganized neurotransmitter networks (DA, 5-HT, NE) • DA-GABA-Glu connectivity disrupted • Suggests persistent PFC network dysfunction	[157]
33-ion GCRsim (H, He, C, O, Si, Ti, Fe, etc.); acute dose: 40 cGy in 1 day; chronic: 50 cGy over 24 days (2.08 cGy/day)	Male and female C57BL/6J mice; whole-body irradiated at 6 months; open field behavior assessed 3.5–4.5 months post-IR	Open field progression, stopping behavior, home base clustering, speed, path circuity, edge preference	• Acute exposure caused slower, more circuitous return paths under light conditions • Chronic exposure had less disruption • Light-dependent deficits in spatial navigation emerged only with acute irradiation	[158]
33-ion GCRsim (H, He, O, Si, Ti, Fe, etc.) ± neutrons (10 cGy); acute (1.5–2 h) or chronic (4–6 week) exposure to 50, 75, or 100 cGy; 10 cGy neutron added 6 mo after acute 75 cGy GCRsim	K-rasLA1 lung cancer-susceptible mice (male/female); lung tissue and plasma; 1-year follow-up and histology	Adenocarcinoma incidence, premalignant lesion number/size, survival, lipid peroxidation (MDA assay)	• GCRsim dose- and schedule-dependent ↑ in lung adenocarcinoma • Chronic exposure > acute • 10 cGy neutrons post-GCRsim ↑ malignancy • No survival impact except with neutrons • Lesion size ↑ at 100 cGy • Implications for Mars mission cancer risk	[159]
33-ion GCRsim; acute dose: 0.75 Gy over ~1.5 h, whole-body irradiation ± antioxidant CDDO-EA pre/post	6-month-old female C57BL/6J mice; 14.25-month follow-up; dentate gyrus, cortex; touchscreen and arena-based behavioral tests	Location discrimination reversal (LDR), stimulus–response acquisition/extinction, social interaction, NOR, open field, DCX+ neurogenesis index	• GCRsim caused deficits in cognitive flexibility and ↓ DCX+ neurons • CDDO-EA mitigated LDR impairments • Anxiety, sociability, and locomotion unaffected • Female resilience differed from male studies	[160]
33-ion GCRsim: acute dose: 0.75 Gy over 1.5 h; whole-body irradiation	Male C57BL/6J mice (n = 22–24/group); behavior: open field, EPM, NOR, 3-Chamber Social Interaction (3-CSI)	Sociability, social novelty preference, anxiety-like behavior, object recognition memory (NOR)	• 33-GCR did not alter NOR or anxiety but blunted preference for social novelty • CDDO-EA did not prevent this effect • CDDO-EA+GCR also impaired sociability • Findings highlight CNS vulnerability to complex mixed-field space radiation and need for targeted	[161]

 doi:10.20944/preprints202506.2020.v1

			neuroprotective countermeasures	
Total dose of 50 cGy (GCRsim; 33 beams including 7 ion species across 20–1000 MeV/n)	Female $Apc^{Min/+}$ mice, mammary gland tissues	Ductal proliferation, ductal overgrowth, preneoplasia markers (Spp1, Rrm2)	• ↑ Ductal branching and hyperplasia • ↑ Cyclin D1+ cell proliferation • ↑ Spp1 expression (gene and protein) • ↑ Rrm2 expression (mRNA and protein)	[162]
Protons (1 GeV); titanium ions (1 GeV/n, LET 108.1 keV/μm) or iron ions (1 GeV/n, LET 151.3 keV/μm); protons: 0–20 cGy; HZE dose: 20 cGy; sequential exposure with 15 min delay;	Primary human fibroblasts	Neoplastic transformation (anchorage-independent growth in soft agar); clonogenic survival	• Marked synergistic ↑ in transformation when protons preceded HZE by 15 min • Effect evident even at 1 cGy proton + 20 cGy HZE • Split doses of same ion species did not replicate synergy • Results emphasize protons' role in sensitizing to subsequent HZE exposure	[163]
Protons (1 GeV/n); iron or titanium ions (both 1 GeV/n; Fe LET 151.3 keV/μm, Ti LET 108.1 keV/μm; protons: 20 cGy; Fe or Ti ions: 20 cGy; 2.5 min to 48 h in-between irradiations; reverse order also tested	Primary human neonatal fibroblasts	Anchorage-independent growth (soft agar assay); clonogenic survival	• Marked synergistic effect when protons preceded Fe or Ti by 2.5 min–1 h (Fe) or up to ~6 h (Ti) • Transformants per survivor ~3× additive prediction • No synergy when HZE delivered first or at longer intervals • Survival unaffected, suggesting transformation-specific interaction	[164]
Protons (1 GeV/n, 0.5 Gy/min): 2Gy; Fe ions (1 GeV/n, 1 Gy/min): 0.75 Gy; sequential exposure with intervals of 2, 30, or 60 minutes; cells kept at 37°C between exposures	Human mammary epithelial cells (CH184B5F5/M10)	Chromosome aberrations (mBAND on chromosome 3); intra- and inter-chromosomal exchanges; inversion, deletion, translocation frequency	• Highest aberration frequency observed at 30 min interval • Dual exposure yielded more damage than predicted sum • Supports enhanced susceptibility to Fe damage during early repair phase post-proton exposure • Synergy likely driven by interaction of partially repaired lesions	[165]
Protons (1 GeV, LET 0.223 keV/μm): 3 × 17 cGy; 56Fe (1 GeV/n, LET 151.4 keV/μm): 15 cGy; whole-body irradiation	Cardiovascular system (murine heart)	Myocardial infarction model; echocardiographic and histological evaluation	• Sequence-dependent cardiac effects: increased fibrosis and LV hypertrophy (56Fe+1H) • Impaired post-MI recovery and increased infarct size (1H+56Fe)	[166]
Protons (1 GeV/amu): 1 cGy; Fe ions (1 GeV/amu): 1cGy;	AG01522 normal human skin fibroblasts; co-culture transwell system for bystander analysis	Micronucleus formation and 53BP1 foci induction in	• Direct exposure → similar DNA damage levels regardless of single or	[167]

 doi:10.20944/preprints202506.2020.v1

applied sequentially with intervals from 3 min to 24 h		irradiated and bystander cells	combined exposure • Bystander response unchanged in signaling cells • Prior proton exposure suppressed bystander response in recipient cells	
UV-B: 25–100 J/m²; protons (LET ~4.7 keV/μm): 0.25–0.5 Gy; gamma rays: 0.5 Gy; sequential exposure (≤20 min apart)	Human non-malignant cells: HaCaT keratinocytes, Hs27 fibroblasts, CRL 9855 monocytes, PBMCs	DNA damage (γH2AX, dicentrics), gene expression, viability (MTS, LDH), genomic instability	• Marked synergistic effects in co-exposed fibroblasts and keratinocytes • ↑ γH2AX foci, pan-nuclear staining, stress gene upregulation, and ↓ viability • Synergy less evident in UV-B-sensitive monocytes • Gamma + UV-B mimicked proton + UV-B responses	[168]
Neutrons (5 MeV p/d on Be target, LET 10–200 keV/μm): 0.33 Gy; photons (concomitant): 0.07 Gy (acute); neutrons/photons (^{252}Cf, LET ~100 keV/μm): 0.4 Gy total at ≤1 mGy/day (chronic); GCRsim (H, He, C, O, Si, Ti, Fe ions, various energies): 0.4 Gy (acute ~2 h or 19 fractions over 1 month)	C3H male and BALB/c female mice; behavioral testing 400–600 days post-IR; aspirin tested as dietary intervention in some groups	Open field (anxiety, exploration), novel object recognition, contextual/cued fear conditioning	• Chronic mixed-field exposure impaired novel object recognition • Acute GCRsim ↓ exploratory behavior • Fractionated GCRsim → trend toward lower fear learning • Aspirin failed to mitigate radiation effects and worsened object recognition in sham controls	[169]
Gamma rays (137Cs source, ~0.97 Gy/min): 2 Gy; 28Si-ions (300 MeV/n, 69 keV/μm): 0.1 Gy	Male *Apc*^1638N/+ mice (C57BL/6), gastrointestinal epithelium	Tumor burden, carcinoma frequency, senescent cells (p16+), SASP (IL6+), cytokine expression, β-catenin signaling	• ↑ GI tumor incidence (adenoma & carcinoma) • ↑ Senescence & SASP (p16+/IL6+) • ↑ Systemic cytokines (TNFRSF1B, CCL20, etc.) • ↑ β-catenin & cyclin D1 • Mitigated by ABT-263	[170]
X-rays (190 kVp): 0–2 Gy; alpha particles (LET 90.9 keV/μm): 0–2 Gy; mixed beam (X-rays + Alpha, 1:1 dose ratio): 0–2 Gy total (0–1 Gy each component)	Human peripheral blood lymphocytes (2 male donors, in vitro)	Chromosomal aberrations, mRNA expression (FDXR, CDKN1A, MDM2), alternative transcription	• Synergistic increase in chromosomal aberrations and gene expression across seasons • Alpha > X-ray effectiveness • No synergism in alternative transcription • Inter/intra-donor variability observed	[171]
Galactic cosmic rays (GCRs); microgravity, circadian disruption, and other spaceflight stressors; estimated GCR dose: ~76 mGy (physical), ~146 mSv (effective) over 340 days; complex exposure mix including HZE particles;	One monozygotic twin in space (TW) vs. Earth-based twin (HR); human longitudinal, multi-omics profiling	Multi-system effects: transcriptomic, epigenetic, proteomic, metabolomic, immune, cardiovascular, ocular, microbiome, cognitive	• Multiple synergistic effects inferred • Persistent chromosomal inversions (DNA damage), gene dysregulation, telomere elongation → rapid shortening • Altered immune networks, inflammation, cognitive decline	[172]

 doi:10.20944/preprints202506.2020.v1

environmental stressors act in parallel	• Consistent with complex biological interaction of radiation with other spaceflight stressors

3.1. Radiobiological Studies

3.1.1. Combinations of Non-Ionizing and Ionizing Radiation

Table 1 compiles several studies on combined exposures, with many reporting significant synergistic effects from pairing UV radiation with X-rays, γ-rays, β-particles, or protons [1–15]. In one such study, no detectable synergy between UV and X-rays was observed among investigated G_1-phase human lymphocytes, as dicentric chromosome yields were equivalent to those from X-rays alone. This suggests that G_1-phase cells may possess sufficient DNA repair capabilities to independently manage lesions induced by each modality, preventing interactive effects [1]. In contrast, when G_0-phase human lymphocytes were examined, a pronounced ~2-fold increase in dicentric chromosome formation was observed when UV and X-rays were applied within 30 seconds of each other. The synergy was independent of exposure order, indicating a likely mechanistic overlap in lesion processing or repair pathway inhibition [2].

Expanded analysis of the role of timing revealed that when UV irradiation preceded X-rays, the synergistic induction of dicentrics remained constant across time intervals up to 90 minutes. In contrast, when X-rays were administered prior to UV, the synergistic effect decayed exponentially with a half-life of approximately 20 minutes. This suggests that short-lived DNA lesions generated by X-rays may be critical for synergistic exchange formation and are subject to rapid repair or dissipation. Lesion persistence and repair kinetics thus play an important role in controlling the extent and nature of interactive radiation responses [6].

In human peripheral blood lymphocytes, sequential exposures to UV and X-rays induced dicentric chromosome yields up to two-fold higher than X-rays alone, with the order and timing of exposure critically modulating the magnitude of the effect [7]. In HeLa cells, UV and X-rays were shown to induce distinct but complementary forms of damage—X-rays causing chromosomal fragmentation, and UV leading to DNA synthesis and elongation of chromosomes. Their combination intensified cellular damage profiles, supporting the concept that synergy can result not only from lesion overlap but also from convergence of disparate stress responses [9].

Altogether, these studies demonstrate that synergistic interactions between UV and X-rays are highly dependent on factors such as cell cycle stage, DNA repair competence, order of exposure, and the biochemical nature of radiation-induced lesions. These parameters must be carefully considered when evaluating the risks or therapeutic potential of mixed radiation exposures.

Beyond mammalian systems, synergistic interactions were also noted in microbial models. For instance, in bacteria, UV pretreatment sensitized *Escherichia coli* to X-ray–induced lethality, particularly in wild-type and *uvr* mutants. In contrast, no synergy was detected in *recA*, *recB*, and *polA* mutants, implicating DNA repair mechanisms in mediating interaction [3,4]. In yeast models, UV exposure prior to gamma irradiation resulted in more than 100-fold reductions in survival beyond additive predictions [10], whereas UV pretreatment enhanced the lethality of β-radiation in *E. coli* and *Salmonella*, with synergy abolished upon photoreactivation [14]. The combination of UV and proton radiation also produced synergistic decreases in bacterial survival when UV preceded protons, suggesting order-dependent DNA repair interference [15].

In *Schizosaccharomyces pombe*, gamma and UV-C exposure produced strong synergy in wild-type cells but not in recombination-deficient mutants, implicating homologous recombination in mediating interaction [10]. Applied microbial studies further demonstrated that combined UV and gamma radiation increased antifungal activity and mutagenesis in *Bacillus* strains used in bioindustrial screening, including enhanced secondary metabolite profiles [12].

 doi:10.20944/preprints202506.2020.v1

While many of these interactions amplify biological damage, some combinations exhibit the opposite effect. Notably, in a full-thickness human skin model, pre-irradiation with water-filtered infrared-A radiation (wIRA, a subtype of near-infrared radiation) prior to X-ray exposure significantly attenuated the DNA damage response, as evidenced by reduced γH2AX and 53BP1 foci. This was accompanied by lowered pro-inflammatory cytokine expression and preserved tissue viability [16]. Thereby, wIRA may be of a certain importance in activating adaptive or protective signaling pathways, offering a potential avenue for radioprotection in normal tissues. Mixed radiation exposures therefore carry a dual potential—to either amplify or mitigate biological damage depending on wavelength, timing, and cellular context.

3.1.2. Combinations of Non-Ionizing Radiation Types

In Table 2, synergistic effects were reported for UV–UV and UV–visible light combinations. For instance, simultaneous UV-A and UV-B exposure in *E. coli* produced 100-fold greater inactivation than UV-B alone, mediated by s^4U modifications in tRNA [18]. In human skin tissue models, simultaneous exposure to UV-B, UV-A, and near-infrared light produced marked synergistic effects on photoaging biomarkers, oxidative stress, and gene expression. These responses were distinct from those induced by single or sequential exposures, suggesting molecular cross-talk across photoreactive pathways, including MAPK signaling and DNA repair [21].

In a study involving ragweed-allergic patients, combined UV and visible light exposures significantly inhibited allergen-induced wheal formation, whereas neither UV-A nor visible light alone produced this effect. The mixed exposure (mUV/VIS) showed a strong, dose-dependent suppression of mast cell–mediated responses, even at suberythematous doses [33].

Additional synergistic effects were observed in diverse biological systems. In tomato plants, UV-B and UV-C exposure enhanced disease resistance and antioxidant gene expression [20]. Marine invertebrate models exposed to long-term UV-A and UV-B irradiation exhibited reduced reproductive and feeding capacity [22], demonstrating chronic toxicity. In environmental disinfection studies, complete microbial inactivation of *Enterococcus faecalis* and *E. coli* was achieved in synthetic water matrices using dual-UV systems, with synergy modulated by fluence and pH [27]. Furthermore, predictive modeling of microbial inactivation revealed that combining UV-C radiation from excimer lamps (222–285 nm) with low-pressure mercury lamps (254 nm) produced the highest energy efficiency, supporting a dose- and sequence-dependent basis for synergy [29].

These results indicate that non-ionizing radiation combinations can, at times, amplify biological effects through complementary damage mechanisms or overlapping signaling responses. The diversity of observed outcomes across bacterial, plant, invertebrate, and human systems accentuates the broad applicability of these combinations—from environmental sterilization to therapeutic and dermatological contexts. Additive and supra-additive effects, depending on exposure configuration and biological context, reinforce the importance of wavelength interaction in determining damage outcomes across both experimental and applied settings.

3.1.3. Combinations of Ionizing Radiation Types

Table 3 presents extensive data on combinations of ionizing radiation types—particularly alpha particles, X-rays, gamma rays, protons, and neutrons. These studies reveal a broad range of interaction outcomes, with synergistic effects being frequently observed across multiple biological endpoints.

A recurring finding involves persistent or amplified DNA damage responses. In human peripheral blood lymphocytes, combined alpha and X-ray exposure induced a significant increase in complex chromosomal aberrations, with evidence of non-additive interactions and a linear-quadratic dose–response relationship at higher combined doses [39]. In U2OS osteosarcoma cells, alpha and X-ray co-exposure resulted in delayed decay of small and large 53BP1 foci, along with prolonged ATM and p53 signaling. These findings suggest a synergistic disruption of DNA repair kinetics, with the most pronounced effects observed at lower total doses [42]. Similar synergy was observed in other

 doi:10.20944/preprints202506.2020.v1

beam combinations, including alpha followed by gamma radiation, where foci were larger and more persistent than in the reverse sequence [49].

Mixed-exposure effects on clonogenic survival varied substantially by system and irradiation parameters. In V79 Chinese hamster lung fibroblasts, neutron–gamma co-exposure produced supra-additive reductions in survival, particularly under simultaneous delivery. Survival curves fitted better with quadratic models, indicating interaction between damage types [71]. In rat lung epithelial cells (LECs), combined alpha (high-dose, 1 Gy) and X-ray exposure eliminated the survival curve shoulder and reduced clonogenic survival beyond additive expectations. Micronuclei frequencies were also elevated under combined exposure, consistent with non-linear interaction effects [41]. In contrast, a study in Chinese hamster ovary (AA8) cells using mixed alpha and X-ray beams reported no evidence of synergy, with survival data aligning closely with predictions from mathematical additivity models [36]. This difference illustrates the context-dependent nature of mixed-radiation effects, where factors such as cell type, DNA repair capacity, dose composition, and exposure geometry critically shape biological responses. It shows why system-specific investigations are essential when evaluating potential synergy in combined radiation settings.

At the transcriptional level, combined radiation exposures modulated key stress and damage response genes across multiple systems. In human lymphocytes, combined alpha–X-ray exposure increased FDXR, GADD45A, and MDM2 expression beyond levels induced by alpha radiation alone in most donors, with synergy confirmed in 3 out of 4 cases using envelope-of-additivity analysis. Furthermore, ATM inhibition reduced this response, implicating checkpoint signaling [38]. Neutron–photon mixtures elicited strong transcriptomic effects even at low neutron fractions. In murine models, as little as 5% neutron contribution suppressed EIF2/mTOR signaling and ribosomal protein expression—alterations not observed with X-rays alone [55]. In human peripheral blood, increasing neutron percentages led to enhanced TP53 signaling and broader immune dysregulation [60]. Other studies reported dose-dependent modulation of BAX, DDB2, and FDXR expression following neutron–gamma co-exposure [75]. Mixed radiation fields can thus reshape transcriptional networks even in the absence of overt cytotoxicity, reflecting subtle but potentially consequential molecular responses.

Beyond transcriptional responses, several studies show that mixed-field irradiation can also trigger broader cellular and physiological adaptations. In murine blood cells, neutron–gamma exposure altered membrane architecture and lectin-binding patterns, with lymphocytes and platelets showing the most marked ultrastructural remodeling [73]. In separate mouse models, combined exposures impaired hippocampus-dependent memory and shifted neuroimmune profiles toward an anti-inflammatory state [74]. These organism-level effects reinforce observations at the cellular and molecular levels, and underline the significance of mixed-field research in clinical and spaceflight contexts, where heterogeneous radiation fields are the norm.

A rare entry in the dataset examined neutron–proton co-exposure in human breast cancer cell lines, offering insight into mixed-beam effects on cancer stem cell (CSC) populations. The response varied by cell line: CSC fractions declined additively in MCF-7 cells but antagonistically in MDA-MB-231, with no significant changes in canonical stemness gene expression [80]. This study stands out as one of the few to explore neutron–proton co-exposure, emphasizing the need to investigate underrepresented beam combinations that may yield distinct biological responses relevant to radiation protection and therapy.

Additional underrepresented combinations include alpha–beta inhalation in rats, which elicited additive impairments in pulmonary function [52], and mixed radionuclide exposure in plants, where barley grown in contaminated soil accumulated mutations at rates exceeding those predicted by dose alone [53]. Though differing in species and context, these models reflect real-world exposure scenarios—from internal contamination to chronic environmental irradiation—and illustrate why investigating complex mixtures that challenge conventional assumptions about radiation risk matters.

 doi:10.20944/preprints202506.2020.v1

3.2. Therapeutic Studies

The therapeutic potential of mixed radiation modalities is explored in a wide variety of publications, ranging from clinical trials to preclinical and in vitro studies. These studies, compiled in Table 4, reveal nuanced biological outcomes depending on beam combinations, timing, sequencing, and tumor context.

Clinical investigations involving mixed proton–carbon ion therapies have demonstrated encouraging results in managing difficult-to-treat malignancies. In locally advanced pancreatic cancer (LANC), a mixed-beam regimen of proton therapy (50.4 GyE) and a carbon ion boost (12–18 GyE) yielded a 1-year overall survival of 80% and median survival of 17.3 months without dose-limiting toxicities, suggesting carbon ions may enhance local control over protons alone [86]. Similarly, in skull base and cervical spine chordomas and chondrosarcomas, a combined Intensity Modulated Proton Therapy (IMPT) and Intensity Modulated Carbon Therapy (IMCT) approach achieved 2-year local control of 86.2% with low-grade toxicities, although outcomes declined with larger tumors or re-irradiation [87]. For small cell lung cancer, a regimen combining protons and carbon ions with concurrent chemotherapy proved feasible, with a 2-year OS of 81.7% and manageable toxicities [88].

Preclinical models offer mechanistic insights into these effects. In Chinese hamster fibrosarcoma cells, sequential carbon-to-proton irradiation with a 45% carbon contribution induced significant synergy, while reversing the order diminished the effect or led to antagonism, indicating how dose fraction, timing, and sequence modulate therapeutic efficacy [89]. A related study using mixed 16O/28Si/proton beams demonstrated that elevated high-LET contributions suppressed cell survival more effectively, especially when delivered before protons. Notably, a proton-to-high-LET sequence permitted partial recovery, reinforcing the importance of beam order [92].

Several studies evaluated neutron-based combinations. Fast neutron therapy followed by proton boost in salivary gland tumors produced high local control (89.7%) with acceptable toxicity, albeit with notable late effects such as vision and hearing loss [91]. In another, murine study, neutron–proton sequencing influenced both toxicity and tumor outcomes in solid Ehrlich ascites carcinoma. Neutron-first exposures exacerbated skin damage and reduced survival, while the reverse sequence was better tolerated [93]. These findings were echoed in vitro, where neutron-before-proton combinations consistently outperformed proton-first in reducing clonogenic survival, supporting the sequence-dependent efficacy of mixed-beam regimens [94].

Efforts to combine external beam therapy with biologically targeted or nanotechnology-enhanced modalities have also shown promise. In mouse xenograft models, combining proton irradiation with 177Lu-labeled targeted radionuclides produced additive or synergistic tumor suppression, depending on cancer type [90]. Photodynamic therapy (PDT) integrated with photon radiotherapy (RT) has shown synergistic antitumor effects across diverse preclinical models. Studies using bladder cancer organoids, pancreatic co-cultures, and xenograft systems demonstrated enhanced tumor suppression via multimodal cell death, improved DNA and membrane damage, and—in some cases—increased immune infiltration. PDT efficacy was further potentiated using nanoparticle carriers or photosensitizers such as indocyanine green (ICG), supporting its radiosensitizing potential across tumor types [97–101]. X-ray-triggered UV-C via nanoscintillators further potentiated DNA damage and cell killing, particularly in UV-sensitive fibroblasts, suggesting a potential radiosensitization strategy [102,103].

In prostate and nasopharyngeal cancer, clinical application of mixed beams combining photon-based IMRT with carbon ions or protons reduced toxicity and preserved efficacy. These regimens yielded favorable PSA kinetics and quality-of-life scores, and in some cases reduced radiation doses to organs at risk compared to IMRT-only protocols [105–107]. Similar approaches using photon-electron VMAT combinations improved sparing of cardiac and pulmonary tissues in breast cancer radiotherapy, highlighting dosimetric advantages of multi-modality planning [108].

Some studies focused on biological outcomes in the context of boron neutron capture therapy (BNCT), which typically combines high-LET components such as thermal, epithermal, or fast

 doi:10.20944/preprints202506.2020.v1

neutrons with accompanying low-LET gamma or X-ray radiation. Across in vitro models, these mixed-field exposures generally produced additive effects, particularly in survival outcomes following alpha–gamma or neutron–gamma co-irradiation [120,121]. However, one study reported sequence-dependent synergy when alpha particles and X-rays were delivered simultaneously at higher alpha doses, suggesting interference with DNA repair capacity [122]. Additionally, BNCT-associated mixed-beam exposures induced spatially clustered and persistent DNA damage, particularly in wild-type but not repair-deficient cell lines, emphasizing damage complexity as a key determinant of biological response [123].

Taken together, these studies show that combining radiation modalities can improve tumor control, reduce side effects, and help elucidate mechanisms of cell damage. The choice of beams, their sequencing, and the tumor environment all play a decisive role in shaping outcomes—supporting the case for ongoing research into mixed-field radiotherapy.

3.3. Space Radiation Studies

The biological complexity of space-relevant radiation exposures has been increasingly modeled using mixed-field simulations of galactic cosmic rays (GCRs), incorporating protons, helium, and high-LET heavy ions such as oxygen, silicon, titanium, and iron. These ion combinations, delivered either acutely or fractionated over time, approximate the heterogeneous radiation profile encountered beyond low Earth orbit.

A central point discussed in related publications presented in Table 5 is the vulnerability of the central nervous system (CNS) to structural, behavioral, and synaptic disruptions following GCR-like exposures. Multiple studies using simplified and complex GCRsim beams reported dose- and sex-specific deficits in short-term memory, spatial learning, and cognitive flexibility at total doses as low as 15–50 cGy [129,130,136]. These effects were associated with dendritic simplification, reduced mushroom spine density, and altered expression of synaptic proteins such as GluR1, NR2A, and Synapsin-1. In another 5-ion beam study, male-specific cognitive impairments were causally linked to activated microglia and hippocampal synaptic remodeling, with early circulating monocyte levels serving as predictors of late-stage spatial learning deficits [137].

Other studies focused on complex behaviors, including grooming, burrowing, and risk-based decision-making, where low-dose GCRsim exposure produced sex-dependent performance shifts and increased risk-taking in females [140,144]. In related work using a touchscreen-based switch task, female rats exposed to 10 cGy of GCRsim showed reduced task-switch accuracy (~20% below controls), increased perseverative errors, and a higher failure rate during training stages that required greater cognitive load [147].

Larger ion fields, including 33-ion GCR simulations, reinforced these CNS findings. Chronic and acute exposures impaired memory updating and object recognition in a sex-dependent manner. Long-term potentiation (LTP) was reduced, and changes in postsynaptic density and axonal myelination were observed [156]. Complementary touchscreen-based testing showed that male mice developed attentional deficits and slower response times, alongside disrupted prefrontal dopamine signaling and altered neurotransmitter network organization [157]. Importantly, one study utilizing 6-ion exposures demonstrated that pharmacological HDAC3 inhibition reversed LTP deficits and restored behavioral performance, identifying an epigenetic pathway of functional recovery [152].

Parallel investigations assessed cancer risk and tissue remodeling under space-relevant mixed radiation. In K-rasLA1 mice, chronic 33-ion GCRsim exposure increased lung adenocarcinoma incidence, an effect further enhanced by a delayed neutron dose [159]. In *Apc*^1638N/+ mice, combined gamma and silicon ion exposure elevated gastrointestinal tumor burden, senescence-associated signaling (p16, IL-6), and β-catenin pathway activation, with these effects mitigated by senolytic treatment [170]. Mammary gland studies in *Apc*^Min/+ mice showed increased ductal hyperplasia and overgrowth, along with elevated expression of ERα, ERRα, and SPP1—markers associated with estrogen signaling and tumor development [155,162].

 doi:10.20944/preprints202506.2020.v1

Mechanistic studies in primary human fibroblasts and epithelial cells revealed that exposure timing critically shapes biological outcomes following mixed-beam irradiation. When proton exposure preceded titanium or iron ions by as little as 15 minutes, a strong synergistic increase in anchorage-independent growth was observed—even at near-threshold doses—an effect not replicated by same-ion split doses or reversed sequences [163]. This pattern was reinforced in neonatal fibroblasts, where transformation rates were up to three times higher than additive predictions when protons were followed by HZE ions within a 2.5-minute to 6-hour window, but not when the order was reversed [164]. In human mammary epithelial cells, chromosome aberration frequency peaked when iron was delivered 30 minutes after protons, revealing the role of unresolved proton-induced DNA lesions in sensitizing cells to complex damage from subsequent high-LET ions [165].

Radiation-induced cardiovascular and systemic effects were documented across multiple models. In WAG/RijCmcr rats, whole-body exposure to a mixed field of protons, silicon, and iron ions led to perivascular cardiac fibrosis, increased systolic blood pressure, and infiltration of CD68+ macrophages in the heart and kidneys—effects not observed with single-ion exposures [133]. In BALB/c and CD1 mice, 5-ion GCRsim caused sex- and strain-specific changes in cardiac structure, including increased collagen deposition, altered capillary density, and modulation of immune markers such as CD2 and TLR4 [139]. Another study using a myocardial infarction model showed that the sequence of proton and iron irradiation significantly influenced myocardial fibrosis and infarct size, with proton-first exposure exacerbating cardiac damage [166]. Peripheral immune alterations included changes in leukocyte profiles and phagocytic activity, with notable sex-specific transcriptional shifts [135]. Additional GCRsim studies reported reduced circulating cytokines and genotype-dependent inflammatory responses, reinforcing the relevance of immune modulation under space radiation [143].

Studies also implicated the microbiome as a sensitive and interactive component. In several mouse models, microbiota composition changed after GCRsim in a sex- and dose-dependent manner and correlated with cognitive and affective outcomes [131,151]. Gut–brain signaling may thus amplify radiation effects on neural circuitry and behavior.

Other systemic interactions included viral reactivation, endocrine modulation, and altered intercellular communication. In latently infected human myeloblasts, GCRsim and high-LET ions reactivated CMV and induced viral gene expression in a dose- and LET-dependent fashion [154]. In co-culture systems, proton pre-exposure suppressed the bystander response to iron ions in human fibroblasts, underscoring the impact of prior radiation history on intercellular signaling dynamics [167].

A uniquely translational lens is provided by the emblematic NASA Twins Study, which evaluated one astronaut exposed to chronic spaceflight stressors, including ~76 mGy of estimated GCR, over 340 days. Multi-omic profiling revealed persistent chromosomal inversions, immune dysregulation, cognitive decline, altered microbiome signatures, and telomere dynamics (elongation followed by rapid shortening). These effects—many of which mirror patterns in rodent and cellular GCR models—support the idea that space radiation interacts synergistically with other flight stressors, such as microgravity, circadian disruption, and isolation.

Finally, several studies evaluated countermeasures for radiation-induced damage. For instance, the antioxidant CDDO-EA mitigated cognitive flexibility deficits and restored neurogenesis following GCRsim in female mice, although its effects on social behavior were mixed and context-dependent [160,161]. Furthermore, HDAC3 inhibition was shown to reverse synaptic plasticity impairment [152], while low-dose X-ray pretreatment reportedly improved viability and reduced ROS in cardiomyocytes subjected to GCRsim [150]. Conversely, the use of aspirin failed to confer benefit and even worsened cognitive performance in control animals [169], stressing the need for carefully validated interventions.

Viewed collectively, the compiled studies of this section reveal that space-relevant mixed radiation fields elicit widespread, tissue-specific, and often synergistic biological responses. As is

 doi:10.20944/preprints202506.2020.v1

common in combined radiation exposures, these effects are shaped by radiation quality, order of exposure, dose rate, biological sex, genetic predisposition, and environmental co-factors. With the convergence of rodent GCRsim models, human cellular systems, and longitudinal astronaut studies, the field is now poised to generate predictive frameworks for long-duration spaceflight risk and precision countermeasures. The integration of mechanistic insight, translational relevance, and systems-level biology marks the next frontier in space radiation research.

4. Discussion

The systematic collection, classification, and synthesis of studies on combined irradiation of biological systems conducted in this review provided critical insights into the current state of the field. The research landscape is consistently structured around three main contexts: Radiobiology, Therapeutic Applications, and Space Radiation Research. This tripartite framework reflects fundamentally distinct objectives—mechanistic elucidation, clinical application, and astronaut health risk mitigation, respectively.

4.1. Mechanistic Basis of Mixed Radiation Effects

Radiobiological studies have consistently revealed that combinations of ionizing and non-ionizing radiation produce distinctive biological effects compared to single-modality exposures. These effects are shaped by variables such as radiation type, dose, timing, and cellular context. As summarized in Figure 1, such interactions often lead to complex DNA damage, saturation of repair capacity, and the emergence of genomic instability.

Multiple studies involving UV and ionizing radiation exposures in mammalian systems reported synergistic increases in dicentric chromosome formation, particularly when UV preceded X-rays or gamma rays. For example, in human G_0-phase lymphocytes, combined UV and X-ray exposures produced synergistic increases in dicentric chromosome yield, particularly when UV preceded X-rays and the interval between exposures was short [2,6,7]. This synergy diminished when the order was reversed, suggesting that repair interference plays a role in amplifying damage. In contrast, this effect was absent in G_1-phase cells, indicating a key role for the DNA repair landscape in dictating interactive outcomes [1]. Further support for this comes from HeLa cells synchronized in G_1, for which detailed chromosomal condensation analysis showed that UV and X-rays triggered fundamentally distinct responses: while X-rays induced dose-dependent fragmentation, UV elongated chromosomes into an "S-like" morphology and triggered unscheduled DNA synthesis—suggesting complementary, rather than overlapping, mechanisms of genomic stress [9].

More insights have emerged from microbial systems, where genetic manipulation enables precise dissection of DNA repair pathways. In *E. coli*, synergistic lethality from combined UV and X-ray exposures was observed in wild-type and polA mutants, but abolished in recA, recB, and recC mutants, implicating homologous recombination (Type III repair) as essential for synergy. The partial effect seen in polA mutants suggests that base excision or Type II repair may also modulate the response, though they are not sufficient on their own [3,4]. Additional work confirmed that UV pretreatment sensitizes *E. coli* to ionizing radiation by interfering with repair of strand breaks. Using B/r and Bs-1 strains, it was shown that synergistic X-ray sensitization occurred only in wild-type B/r cells, and was abolished when DNA metabolism was perturbed via 5-bromouracil substitution or purine starvation—conditions known to inhibit DNA repair [5]. In human leukocytes, combined UV and X-ray exposure led to greater chromosome damage in both healthy and Down syndrome donors, with diminished DNA repair synthesis observed in the latter. It can thus be deduced that overlapping repair pathways mediate synergistic outcomes and are modulated by cellular repair competence [6].

Critically, the temporal arrangement of UV and ionizing radiation exposures emerged as a key determinant of synergistic response in mammalian cells. In peripheral human lymphocytes, a substantial, two-fold increase in dicentric chromosome yield was consistently observed when UV exposure preceded X-rays—even with inter-exposure intervals extending to 90 minutes. This stability suggests that UV-induced lesions can persist long enough to interfere with the repair of subsequent

 doi:10.20944/preprints202506.2020.v1

ionizing damage. In contrast, reversing the order of exposure led to a rapid decay in synergistic effect, with a half-life of ~20 minutes, implicating short-lived intermediates—such as unrepaired single-strand breaks or stalled replication forks—in facilitating synergy [7]. Therefore, the interaction between lesions is time-sensitive, with DNA repair kinetics playing a central role in shaping the outcome.

Moreover, this temporal dependence aligns with cell cycle–specific differences in DNA repair dynamics. In G_0-phase lymphocytes, synergy was consistently observed, whereas in G_1-phase cells, no increase beyond additive expectations was detected [1]. This shift likely reflects the relative abundance and efficiency of lesion-processing pathways between quiescent and actively cycling cells. Further support comes from HeLa cells synchronized in G_1, where simultaneous UV and X-ray exposure triggered fundamentally distinct chromosomal responses: X-rays produced dose-dependent fragmentation, while UV induced elongation and unscheduled DNA synthesis—pointing to complementary, rather than overlapping, stress responses [9]. Analysis of this dataset leads to the inference that synergy may not simply reflect lesion quantity but rather the convergence of lesion type, repair timing, and cellular repair state.

Temporal modulation of synergistic effects appears to be governed not only by repair capacity but also by the kinetic properties of radiation-induced lesions. Parameters such as lesion half-life and inter-exposure interval critically shape the outcome of combined exposures. When interactions occur within narrow time windows, unrepaired lesions or repair intermediates from the first radiation may persist and interfere with responses to the second, thereby amplifying biological damage. Conversely, extended intervals may allow for lesion resolution and pathway recovery, reducing the potential for synergy. Intriguingly, certain mixed exposures can even attenuate damage. For instance, as mentioned previously, pretreatment with water-filtered infrared-A radiation (wIRA) before X-ray exposure was shown to reduce DNA damage foci and inflammatory signaling in full-thickness skin models, suggesting activation of protective or adaptive stress responses [16].

In non-ionizing radiation combinations, synergistic effects have been observed across both environmental and biological systems, often involving complementary mechanisms of photodamage. In *E. coli*, simultaneous UV-A and UV-B exposure resulted in a nearly 100-fold increase in inactivation compared to UV-B alone, driven by UV-A absorption through thiouridine (s^4U) residues in tRNA, which impaired translation and thereby reduced the cell's capacity to repair subsequent DNA damage [18]. In human skin models, co-exposure to UV-A, UV-B, and near-infrared radiation produced a distinct biomolecular response characterized by heightened oxidative stress, elevated MMP-1 expression, and activation of MAPK signaling—effects not reproduced by individual or sequential exposures, suggesting wavelength-dependent crosstalk between damage and repair pathways [21]. In microbial systems, sequential UV-A and UV-C exposure produced persistent translational arrest and synergistic inactivation in wild-type *E. coli*, an effect absent in strains lacking *thiI*-dependent tRNA modifications, highlighting the role of non-DNA targets in modulating radiation sensitivity [23]. In a human skin model of allergen challenge, mixed ultraviolet and visible light (mUV/VIS) exposure produced dose-dependent suppression of mast cell–mediated wheal formation at suberythematous doses—an effect not seen with UV-A or visible light alone—indicating that non-ionizing combinations can modulate immune responsiveness and may hold translational potential for therapeutic or immunomodulatory strategies [33]. A key deduction from these findings is that synergy in non-ionizing radiation exposures arises from converging damage mechanisms affecting DNA, RNA, and proteins, as well as from temporally coordinated activation of cellular stress signaling pathways.

Mechanistic insights from combinations of ionizing radiation types reveal that synergy frequently stems from the intersection of distinct lesion types and the breakdown of repair coordination. When alpha particles are combined with X-rays or gamma rays, the resulting DNA damage is not merely greater in magnitude but also altered in quality—evidenced by persistent 53BP1 foci, complex chromosomal aberrations, and sustained ATM and p53 signaling [39,42]. These

 doi:10.20944/preprints202506.2020.v1

features suggest that repair mechanisms become overwhelmed or misregulated under combined irradiation—especially at lower total doses, where synergy tends to be most apparent.

Transcriptional reprogramming offers insight into how cells perceive and prioritize competing damage signals. Co-exposures such as alpha–X-ray and neutron–photon combinations induced distinct expression signatures, including upregulation of DNA damage response genes (e.g., FDXR, GADD45A, MDM2) and suppression of translation-related pathways such as EIF2/mTOR signaling [38,55]. Importantly, these effects occur even in the absence of cell death, highlighting how transcriptional signatures may serve as early markers of synergistic stress before overt damage is visible—crucial for diagnostics and biodosimetry.

Clonogenic survival data link these molecular changes to functional outcomes. Supra-additive losses in colony formation under combined neutron–gamma or alpha–X-ray exposure reflect cumulative disruptions to proliferation and genome stability [41,71]. However, not all systems respond synergistically; for instance, in AA8 cells, survival aligned with additive predictions [43]. These discrepancies reinforce the role of cell-specific repair competence and exposure sequence in shaping whether synergy manifests—an essential consideration in therapeutic planning and radioprotective modelling.

Beyond the nucleus, mixed-field exposures have been shown to impact both membrane integrity and neuroimmune function. In erythrocytes and lymphocytes, neutron–gamma irradiation altered membrane architecture and lectin-binding profiles in a dose- and time-dependent manner [73]. Furthermore, in hippocampal circuits, similar exposures disrupted memory performance and shifted neuroinflammatory tone, marked by reduced pro-inflammatory cytokines and glial activation following gamma priming [74]. These organism-level effects show that synergy is not limited to genotoxic endpoints but can propagate through structural and signaling networks—especially relevant in complex exposures such as spaceflight or nuclear incidents.

Interestingly, even rarely tested combinations such as neutron–proton co-exposure have revealed tumor-specific effects on cancer stem cell populations, suggesting that unconventional radiation pairings may uncover selective biological vulnerabilities not detected under standard protocols [80]. Likewise, environmental models involving complex or atypical exposure scenarios—such as mixed radionuclide contamination in plants or alpha–beta inhalation in rodents—demonstrate that chronic, low-dose synergy can lead to mutation accumulation and functional tissue impairment over time [52,53]. It thus becomes evident that radiation synergy is not merely a byproduct of experimental design but a genuine biological phenomenon that occurs in real-world contexts. As such, mixed-field effects must be integrated into predictive models of environmental risk, long-term health outcomes, and radiological protection—especially in scenarios dominated by chronic, low-dose exposures.

Radiobiological findings such as those discussed here indicate that combined radiation exposures frequently lead to amplified or qualitatively distinct biological outcomes, driven by interactions at the levels of DNA damage formation, repair kinetics, and stress response signaling. A deeper understanding of these dynamics is essential for refining risk assessment models and for effectively harnessing combinatorial effects in both therapeutic interventions and protective strategies in space exploration.

 doi:10.20944/preprints202506.2020.v1

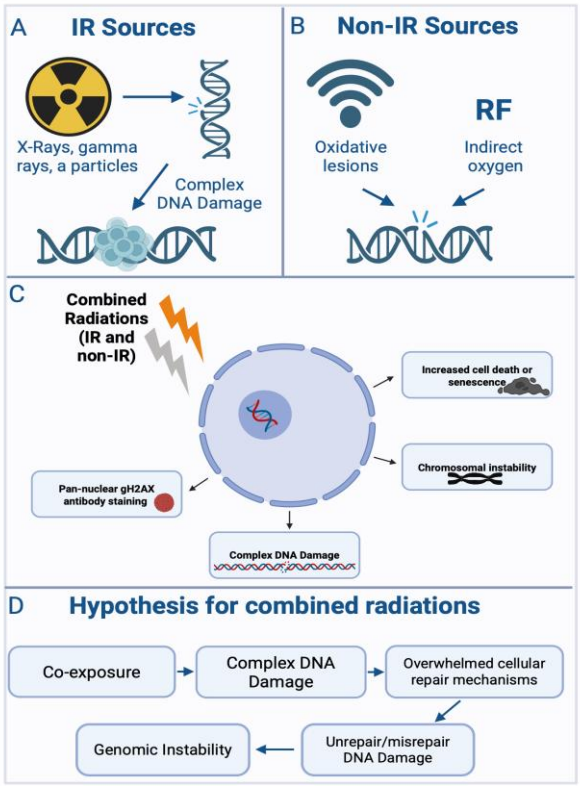

Figure 1. : Hypothesis for results of combined radiation exposure. A. Effects of IR on DNA level; B. Effects of non-IR on DNA level; C. Effects of combined exposures; D. Main hypothesis for results of combined radiation exposure. The figure was created using Biorender, available at https://app.biorender.com/illustrations.

4.2. Determinants and Mechanisms of Synergy

Synergy—defined in this review as a biological effect exceeding the sum of individual radiation exposures—emerged as a recurring observation across diverse radiation combinations. These interactions spanned ionizing and non-ionizing sources and were seen in endpoints such as DNA damage, cell survival, chromosomal aberrations, transcriptomic shifts, and organ-level function.

A key determinant of synergy was exposure sequence and timing. For instance, in studies concerning the combination of UV and X-rays, synergistic increases in dicentric chromosome yields were most pronounced when UV preceded ionizing radiation, such as X-rays or gamma rays, suggesting that early UV-induced DNA lesions or repair processes sensitize cells to subsequent damage [2,6,7]. Similar sequence sensitivity was observed in fibroblast and tumor models exposed to carbon–proton [89], heavy-ion–proton, and neutron–proton combinations [92,94]. In each case, initiating exposure with high-LET radiation—such as carbon, oxygen/silicon, or neutrons—resulted in more pronounced reductions in survival or increased cytotoxicity compared to reverse sequences, underscoring the influence of damage complexity and repair kinetics on synergistic outcome.

Cell state also modulated synergy potential. G_0-phase lymphocytes showed strong synergistic dicentric formation following UV–X-ray exposure, while G_1-phase cells did not [1,2], and microbial models lacking key repair genes (e.g., recA, polA) lost their synergistic response altogether [3,4,10]. Deductively, it can be stated that DNA repair capacity and the cell cycle context are of great importance in determining whether mixed exposures interact.

At the molecular level, co-exposures frequently led to persistent DNA damage signaling, including prolonged 53BP1 and ATM/p53 activity [42,49]. Transcriptionally, synergy was reflected in non-linear expression shifts, with combined alpha–X-ray or neutron–photon exposures enhancing genes like FDXR, GADD45A, and MDM2 in lymphocytes [38,55,60].

 doi:10.20944/preprints202506.2020.v1

Finally, synergistic effects were shown to extend beyond cellular systems. Mixed β–γ, α–X-ray, or GCRsim combinations in mice and plants induced non-additive impairments in behavior, tissue function, and mutagenesis [123–127,129–132]. In these studies, synergy is shown to be a system-wide phenomenon driven by lesion interplay, repair saturation, and signaling crosstalk—not a fixed trait of any single radiation type. As such, it offers both a mechanistic lens for radiation biology and a potential tool for optimizing radiotherapy or predicting complex exposure risks.

4.3. Therapeutic and Protective Strategies

Mixed radiation exposures are not only of biological interest but also hold considerable translational potential in therapeutic and protective contexts. Clinical studies using combinations of particle beams—such as protons and carbon ions—demonstrate that beam mixing can improve tumor control while maintaining or reducing toxicity. As presented earlier, dual-beam protocols in pancreatic, skull base, and lung cancers have been shown to achieve high local control and survival rates, with tolerable side effect profiles, suggesting synergistic gains in therapeutic index when carbon ion boosts are added to proton regimens [86–88].

Preclinical and in vitro studies deepen mechanistic understanding. Here, the timing and order of beam delivery emerge as critical factors. In fibrosarcoma cells, carbon-first protocols induced more effective cytotoxicity than reverse sequences, implicating LET-driven modulation of repair kinetics [89]. Similarly, mixed high-LET and proton beam combinations show that reversing the order can blunt or amplify survival outcomes depending on how cells process clustered damage [92,94]. To add to these, neutron-based regimens—used either alone or with protons—have shown promise in both human tumors and murine models, though late toxicity and sequence sensitivity remain concerns [91,93].

Beyond external beams, hybrid approaches that integrate radiation with nanotechnology or molecular targeting are being explored. PDT combined with photon RT enhances tumor killing in multiple models, and radiosensitization via targeted radiopharmaceuticals or nanoscintillator-triggered UV damage suggests that combinatorial designs can exploit biological vulnerabilities in novel ways [97–103].

Protective strategies related to combined radiation exposures are also gaining interest. One notable approach involves adaptive conditioning: in cardiomyocyte models, low-dose X-ray pretreatment prior to GCRsim exposure improved cell viability and reduced oxidative stress, suggesting that pre-exposure can induce protective pathways mitigating subsequent high-LET damage [150]. Similar protective mechanisms have been observed across diverse radiation types. In particular, photobiomodulation with near-infrared (NIR) or laser pretreatment prior to X-ray or gamma exposure improved leukocyte counts, enhanced antioxidant enzyme activity, and increased tissue oxygenation in full-thickness human skin models. These interventions also reduced DNA damage and apoptosis in keratinocytes and fibroblasts [16,17].

Altogether, mixed-field approaches offer significant promise for increasing treatment specificity, minimizing collateral damage, and revealing tumor-selective response windows. Future strategies may benefit from personalizing beam selection and delivery sequence based on tumor type, molecular profile, and repair capacity. In parallel, the development of radioprotective interventions—such as photobiomodulation or adaptive preconditioning—may help safeguard healthy tissues across a range of exposure contexts, from clinical radiotherapy to occupational, environmental, and spaceflight scenarios. As mechanistic understanding of these interactions deepens, such approaches could become integral components of comprehensive radiation management strategies.

4.4. Space and Environmental Risk Contexts

Space radiation studies increasingly demonstrate that mixed-field exposures—particularly GCRsim combinations of protons and high-LET ions—trigger system-wide biological disruptions that go beyond linear dose effects. The central nervous system is especially susceptible, with low-

 doi:10.20944/preprints202506.2020.v1

dose exposures impairing cognition, synaptic structure, and behavior, with sex-dependent outcomes observed in several studies[131,157]. The induced effects are frequently synergistic, shaped by radiation sequence and timing, emphasizing the role of unresolved DNA damage and repair interference [163–165]. Similar order-dependent sensitivities have also emerged in cancer models; in one study, proton-first regimens was shown to amplify tumorigenesis compared to reversed sequences [132]

In space-related research, chronic exposure has emerged as a key determinant of biological risk. For instance, in K-rasLA1 mice, chronic GCRsim regimens increased lung tumor incidence more than acute exposures, with the addition of neutrons further exacerbating malignancy [159]. In the cardiovascular domain, proton-first exposure sequences worsened myocardial fibrosis and infarct size compared to iron-first regimens, highlighting how radiation order governs tissue-level outcomes in the context of space radiation [166]. Meanwhile, microbiome alterations were found to parallel these physiological disruptions, with GCRsim exposures producing sex- and dose-dependent dysbiosis that influenced cognitive and immune phenotypes [131,151].

The NASA Twins Study provided translational support, revealing telomere elongation followed by rapid shortening, chromosomal inversions, immune dysregulation, cognitive performance changes, altered microbiome profiles, and widespread transcriptomic remodeling in the flight-exposed astronaut. Many of these effects mirrored those seen in rodent and cell-based GCR simulations, reinforcing that space radiation acts not in isolation, but synergistically with other spaceflight stressors—such as microgravity, circadian disruption, and confinement—to drive complex, system-wide biological responses.

These insights reflect a pivotal turning point in space radiation biology, enabled in large part by NASA's strategic investment in GCRsim technology and the development of multibeam irradiation platforms like those at the NASA Space Radiation Laboratory (NSRL). The ability to deliver rapid, sequential exposures of biologically relevant ions—mirroring real cosmic ray compositions—has transformed the field from single-ion approximations to nuanced, systems-level modeling. Coupled with omics-driven analyses, behavioral assays, and translational studies like the NASA Twins Study, this technological leap allows for integrative frameworks that capture the interactive, nonlinear nature of spaceflight stressors. As long-duration missions to the Moon and Mars approach, future research will increasingly depend on refining these models, identifying individual susceptibility markers, and testing personalized or adaptive countermeasures that address the cumulative burden of mixed-radiation and environmental exposures.

While the spaceflight context has catalyzed some of the most advanced modeling of mixed radiation effects, such scenarios are not directly representative of terrestrial conditions. Nevertheless, the principles uncovered—such as synergistic interactions, timing-dependent outcomes, and system-level disruption—stress the broader need to investigate combined exposures on Earth. Although everyday environments do not involve showers of galactic ions, people are routinely subjected to overlapping or sequential low-LET sources, radionuclide mixtures, and co-exposures with chemical, thermal, or biological stressors. The insights from GCRsim studies thus should act as a scientific impetus, urging environmental radiation research to move beyond isolated-dose models and account for real-world exposure complexity.

On Earth, mixed radiation exposures can arise in various contexts, such as ultraviolet radiation in combination with background gamma fields in high natural radiation areas, or beta–gamma emissions associated with radionuclide contamination from industrial or military activity. Although these exposures differ in scale and composition from those encountered in space or laboratory models, they may still present layered biological challenges. As evidence suggests that interactions between radiation types can diverge from simple additive expectations, closer examination is in order. Continued investigation into such terrestrial scenarios is important for refining our understanding of mixed exposure effects, supporting environmental protection strategies, and strengthening risk assessment and remediation frameworks.

 doi:10.20944/preprints202506.2020.v1

4.5. Methodological Challenges and Experimental Gaps

This review identifies major gaps in combinatorial radiation research. Some radiation pairings—such as protons with UV or beta ([13]–[15], [168])—remain virtually unstudied despite potential biological significance. Even for well-explored combinations like X-ray – neutron or gamma – heavy ions, systematic mapping of dose-effect relationships and mechanistic modeling is often lacking.

Moreover, although timing, dose ratio, and radiation order have emerged as critical parameters modulating synergy, many studies treat these variables as secondary rather than primary design features. Systematic investigations of inter-exposure intervals, particularly in time-resolved or cell cycle–synchronized systems, are rare but urgently needed. Cross-comparative work that spans cell type, species, or tissue specificity is also scarce, making it difficult to generalize findings across biological contexts.

Another under-addressed area involves combinatorial exposures including more than two radiation types. While many studies have tested complex mixtures such as 5- or 33-ion beams in space radiation models, terrestrial analogs involving triplet exposures (e.g., UV – gamma – alpha/beta) are largely missing. The field also lacks integrative studies combining ionizing and non-ionizing modalities in realistic exposure sequences, such as low-dose UV exposure followed by diagnostic imaging or therapeutic irradiation

Finally, many existing studies are limited to acute, high-dose exposures, whereas real-world scenarios—whether medical, environmental, or space-related—increasingly involve chronic or fractionated mixed exposures. This disparity suggests the need for experimental paradigms that mirror complex human exposure patterns more closely. Addressing these gaps will be essential to construct predictive models of mixed-radiation effects, optimize therapeutic combinations, and refine risk estimates for spaceflight and environmental contamination scenarios.

To bridge these gaps, interdisciplinary collaboration and standardization of experimental protocols will be critical. Advances in dosimetry, high-throughput assays, and computational modeling now offer the tools to systematically dissect combinatorial radiation effects across biological systems and exposure conditions. Harnessing these capabilities will allow the field to evolve from descriptive observations to mechanistic understanding and predictive accuracy.

4.6. Limitations and Future Directions

One of the main challenges in mixed radiation research lies not only in the scarcity of data, but also in how current studies are designed, conducted, and contextualized. Investigations into radiobiological, medical, and space-related exposures are often pursued within separate research domains, each shaped by its own priorities, methodologies, and regulatory frameworks. This disciplinary isolation makes it difficult to compare results, integrate findings, or construct unified frameworks for understanding biological response. As a result, efforts to build predictive models—whether theoretical, computational, or mechanistic—face significant hurdles. Such models are essential not only for estimating health risks, but also for developing effective radioprotection strategies. Yet their development is hindered by fragmented data, inconsistent endpoints, and a lack of shared experimental standards. Compounding this, most studies prioritize acute or short-term outcomes, with far fewer addressing how mixed radiation effects evolve over time, across generations, or within realistic ecological and clinical contexts.

To move the field forward, we need better coordination between disciplines, along with shared databases that connect radiation types, biological systems, and outcomes. These could support larger comparisons and help identify patterns across experiments. Building international collaborations, agreeing on common protocols, and using simulation platforms will also be important. Collectively, these steps can help the field go beyond scattered case studies and work toward a deeper, more predictive understanding of how different kinds of radiation interact with life.

5. Conclusions

 doi:10.20944/preprints202506.2020.v1

This systematic review—drawing on over 170 studies and encompassing an exceptional variety of radiation pairings—demonstrates that the biological effects of combined radiation exposures are neither trivial nor reliably additive. From fundamental radiobiology to medical applications and spaceflight scenarios, evidence consistently shows that interactions between different radiation types can yield emergent effects, including both synergistic and antagonistic responses. These outcomes are often shaped by radiation quality, dose ratio, sequence, and the biological system in question.

Crucially, the findings challenge the assumption that total dose alone can predict biological risk. Instead, they point to the need for a better understanding of how different radiation types interact over time and across levels of biological organization—from molecular repair mechanisms to whole-organism physiology. Although the field remains fragmented and methodologically uneven, the available data support the development of integrative models and coordinated research strategies that more accurately reflect the complexity of mixed radiation exposures.

Conclusively, the evidence presented in this review reflects a pressing need to rethink how we approach radiation exposure in both research and practice. Whether in medical, space, or environmental contexts, the biological impact of radiation cannot be fully understood without accounting for interactions across type, order, timing, and biological scale. This complexity is not merely theoretical—it is central to designing safer therapies, preparing for deep space missions, and protecting life on Earth. Moving beyond reductionist models is essential to predict, mitigate, and ultimately manage the multifaceted nature of mixed radiation effects.

Author Contributions: Conceptualization, A.G.G; methodology, O.P-P., A.G., A.G.G.; validation, O.P-P., A.G. and S.N.V.; formal analysis, O.P-P. and A.G.; investigation, O.P-P. and A.G.; writing—original draft preparation, O.P-P., A.G., A.A, G.M., C.B.,A.G.G. G.I.T., S.H., F.K.; writing—review and editing, All authors; supervision, A.G.G.; funding acquisition, A.G.G. and F.K.. All authors have read and agreed to the published version of the manuscript."

Funding: The project No. 21GRD02 BIOSPHERE has received funding from the European Partnership on Metrology, co-financed by the European Union's Horizon Europe Research and Innovation Programme and by the Participating States. Views and opinions expressed are, however, those of the author(s) only and do not necessarily reflect those of the European Union or EURAMET. Neither the European Union nor the granting authority can be held responsible for them.

Acknowledgments: All authors acknowledge funding from project BIOSPHERE (No. 21GRD02) that has received funding from the European Partnership on Metrology.

Conflicts of Interest: The authors declare no conflicts of interest.

Abbreviations

The following abbreviations are used in this manuscript:

EURAMET	European Association of National Metrology Institutes
Europe PMC	Europe PubMed Central

References

1. Holmberg, M. Lack of synergistic effect between X-ray and UV irradiation on the frequency of chromosome aberrations in PHA-stimulated human lymphocytes in the G1 stage. *Mutation Research/Fundamental and Molecular Mechanisms of Mutagenesis* **1976**, *34*, 141–147, doi:10.1016/0027-5107(76)90267-0.
2. Holmberg, M.; Jonasson, J. Synergistic effect of X-ray and UV irradation on the frequency of chromosome breakage in human lymphocytes. *Mutation Research/Fundamental and Molecular Mechanisms of Mutagenesis* **1974**, *23*, 213–221, doi:10.1016/0027-5107(74)90141-9.
3. Martignoni, K.D.; Smith, K.C. The synergistic action of ultraviolet and X radiation on mutants of *Escherichia coli* K-12. *Photochemistry and Photobiology* **1973**, *18*, 1–8, doi:10.1111/j.1751-1097.1973.tb06385.x.

 doi:10.20944/preprints202506.2020.v1

4. Tyrrell, R.M. The interaction of near U.V. (365 nm) and X-radiations on wild-type and repair-deficient strains of *Escherichia coli* K-12: physical and biological measurements. *International Journal of Radiation Biology and Related Studies in Physics, Chemistry and Medicine* **1974**, *25*, 373–390, doi:10.1080/09553007414550441.
5. Baptist, J.E.; Haynes, R.H. The U.V.-X-ray synergism in *Escherichia coli* B-r. I. Inhibition by the incorporation of 5-bromouracil and by purine starvation. *Photochemistry and Photobiology* **1972**, *16*, 459–464, doi:10.1111/j.1751-1097.1972.tb06314.x.
6. Lambert, B.; Hansson, K.; Bui, T.H.; Funes-Cravioto, F.; Lindsten, J.; Holmberg, M.; Strausmanis, R. DNA repair and frequency of X-ray and U.V.-light induced chromosome aberrations in leukocytes from patients with Down's syndrome. *Annals of Human Genetics* **1976**, *39*, 293–303, doi:10.1111/j.1469-1809.1976.tb00133.x.
7. Holmberg, M.; Strausmanis, R. The repair of chromosome aberrations in human lymphocytes after combined irradiation with UV-radiation (254 nm) and X-rays. *Mutation Research Letters* **1983**, *120*, 45–50, doi:10.1016/0165-7992(83)90072-6.
8. Schneider, E.; Kiefer, J. Interaction of ionizing radiation and ultraviolet-light in diploid yeast strains of different sensitivity. *Photochemistry and Photobiology* **1976**, *24*, 573–578, doi:10.1111/j.1751-1097.1976.tb06875.x.
9. Waldren, C.A.; Johnson, R.T. Analysis of interphase chromosome damage by means of premature chromosome condensation after X- and ultraviolet-irradiation. *Proceedings of the National Academy of Sciences* **1974**, *71*, 1137–1141, doi:10.1073/pnas.71.4.1137.
10. Gentner, N.E.; Werner, M.M. Synergistic interaction between UV and ionizing radiation in wild-type *Schizosaccharomyces pombe*. *Molecular and General Genetics MGG* **1978**, *164*, 31–37, doi:10.1007/BF00267595.
11. Lewis, N.F.; Shah, A.R.; Kumta, U.S. Synergistic killing effect in pre-UV-irradiated *Micrococcus radiophilus*. *Photochemistry and Photobiology* **1975**, *22*, 145–146, doi:10.1111/j.1751-1097.1975.tb08827.x.
12. Farooq, S.A.; Khaliq, S.; Ahmad, S.; Ashraf, N.; Ghauri, M.A.; Anwar, M.A.; Akhtar, K. Application of combined irradiation mutagenesis technique for hyperproduction of surfactin in *Bacillus velezensis* strain AF_3B. *International Journal of Microbiology* **2025**, *2025*, 5570585, doi:10.1155/ijm/5570585.
13. Okuda, A. Inhibition of the UV-ionizing radiation synergism in *Escherichia coli* B/r by liquid holding between the two irradiations. *Photochemistry and Photobiology* **1973**, *18*, 335–337, doi:10.1111/j.1751-1097.1973.tb06429.x.
14. Yan, Y.; Kondo, S. Synergistic effects of P32 decay and ultraviolet irradiation on inactivation of *Salmonella*. *Radiation Research* **1964**, *22*, 440, doi:10.2307/3571730.
15. Neary, G.J.; Bance, D.A.; Cox, R.; Preston, R.J.; Richards, V.; Stephens, M.A.; Stretch, A.; Wilkinson, R.E. A synergistic interaction between U.V. and protons in causing loss of reproductive capacity in *Escherichia coli* B/r. *International Journal of Radiation Biology and Related Studies in Physics, Chemistry and Medicine* **1974**, *26*, 187–192, doi:10.1080/09553007414551131.
16. König, A.; Zöller, N.; Kippenberger, S.; Bernd, A.; Kaufmann, R.; Layer, P.G.; Heselich, A. Non-thermal near-infrared exposure photobiomodulates cellular responses to ionizing radiation in human full thickness skin models. *Journal of Photochemistry and Photobiology B: Biology* **2018**, *178*, 115–123, doi:10.1016/j.jphotobiol.2017.11.003.
17. Zalesskaya, G.A.; Batay, L.E.; Koshlan, I.V.; Nasek, V.M.; Zilberman, R.D.; Milevich, T.I.; Govorun, R.D.; Koshlan, N.A.; Blaga, P. Combined impact of gamma and laser radiation on peripheral blood of rats in vivo. *Journal of Applied Spectroscopy* **2017**, *84*, 796–803, doi:10.1007/s10812-017-0547-7.
18. Probst-Rüd, S.; McNeill, K.; Ackermann, M. Thiouridine residues in tRNAs are responsible for a synergistic effect of UVA and UVB light in photoinactivation of *Escherichia coli*. *Environmental Microbiology* **2017**, *19*, 434–442, doi:10.1111/1462-2920.13319.
19. Nakahashi, M.; Mawatari, K.; Hirata, A.; Maetani, M.; Shimohata, T.; Uebanso, T.; Hamada, Y.; Akutagawa, M.; Kinouchi, Y.; Takahashi, A. Simultaneous Irradiation with Different Wavelengths of Ultraviolet Light has Synergistic Bactericidal Effect on *Vibrio parahaemolyticus*. *Photochemistry and Photobiology* **2014**, *90*, 1397–1403, doi:10.1111/php.12309.

 doi:10.20944/preprints202506.2020.v1

20. Cheang, W.K.; Wong, G.R.; Rahim, A.N.; Kethiravan, D.; Harikrishna, J.A.; Tan, B.C.; Ramakrishnan, N.; Mazumdar, P. Synergistic effects of UV-B and UV-C in suppressing *Sclerotinia sclerotiorum* infection in tomato plants. *Journal of Crop Health* **2024**, *76*, 1383–1402, doi:10.1007/s10343-024-01033-4.
21. Krutmann, J.; Sondenheimer, K.; Grether-Beck, S.; Haarmann-Stemmann, T. Combined, simultaneous exposure to radiation within and beyond the UV spectrum: a novel approach to better understand skin damage by natural sunlight. *Environment and Skin* **2018**, 11–16, doi:10.1007/978-3-319-43102-4_2.
22. Johnson, L.E.; Treible, L.M. Hanging under the ledge: synergistic consequences of UVA and UVB radiation on scyphozoan polyp reproduction and health. *PeerJ* **2023**, *11*, e14749, doi:10.7717/peerj.14749.
23. Probst-Rüd, S.; Nyangaresi, P.O.; Adeyeye, A.A.; Ackermann, M.; Beck, S.E.; McNeill, K. Synergistic effect of UV-A and UV-C light is traced to UV-induced damage of the transfer RNA. *Water Research* **2024**, *252*, 121189, doi:10.1016/j.watres.2024.121189.
24. Nyangaresi, P.O.; Qin, Y.; Chen, G.; Zhang, B.; Lu, Y.; Shen, L. Effects of single and combined UV-LEDs on inactivation and subsequent reactivation of *E. coli* in water disinfection. *Water Research* **2018**, *147*, 331–341, doi:10.1016/j.watres.2018.10.014.
25. Woo, H.; Beck, S.; Boczek, L.; Carlson, K.; Brinkman, N.; Linden, K.; Lawal, O.; Hayes, S.; Ryu, H. Efficacy of inactivation of human enteroviruses by dual-wavelength germicidal ultraviolet (UV-C) light emitting diodes (LEDs). *Water* **2019**, *11*, 1131, doi:10.3390/w11061131.
26. Sun, Z.; Li, M.; Wu, Z.; Wang, Y.; Blatchley, E.R.; Xie, T.; Qiang, Z. Water disinfection with dual-wavelength (222 + 275 nm) ultraviolet radiations: microbial inactivation and reactivation. *Environmental Science & Technology* **2025**, *59*, 1448–1456, doi:10.1021/acs.est.4c10128.
27. Beck, S.E.; Ryu, H.; Boczek, L.A.; Cashdollar, J.L.; Jeanis, K.M.; Rosenblum, J.S.; Lawal, O.R.; Linden, K.G. Evaluating UV-C LED disinfection performance and investigating potential dual-wavelength synergy. *Water Research* **2017**, *109*, 207–216, doi:10.1016/j.watres.2016.11.024.
28. Tsenter, I.; Garkusheva, N.; Matafonova, G.; Batoev, V. A novel water disinfection method based on dual-wavelength UV radiation of KrCl (222 nm) and XeBr (282 nm) excilamps. *Journal of Environmental Chemical Engineering* **2022**, *10*, 107537, doi:10.1016/j.jece.2022.107537.
29. Hull, N.M.; Linden, K.G. Synergy of MS2 disinfection by sequential exposure to tailored UV wavelengths. *Water Research* **2018**, *143*, 292–300, doi:10.1016/j.watres.2018.06.017.
30. Song, K.; Mohseni, M.; Taghipour, F. Mechanisms investigation on bacterial inactivation through combinations of UV wavelengths. *Water Research* **2019**, *163*, 114875, doi:10.1016/j.watres.2019.114875.
31. Lu, Y.; Yang, B.; Zhang, H.; Lai, A.C. Inactivation of foodborne pathogenic and spoilage bacteria by single and dual wavelength UV-LEDs: Synergistic effect and pulsed operation. *Food Control* **2021**, *125*, 107999, doi:10.1016/j.foodcont.2021.107999.
32. Chen, H.; Moraru, C. Synergistic effects of sequential light treatment with 222-nm/405-nm and 280-nm/405-nm wavelengths on inactivation of foodborne pathogens. *Applied and Environmental Microbiology* **2023**, *89*, e00650-23, doi:10.1128/aem.00650-23.
33. Koreck, A.; Csoma, Z.; Borosgyevi, M.; Ignacz, F.; Bodai, L.; Dobozy, A.; Kemeny, L. Inhibition of immediate type hypersensitivity reaction by combined irradiation with ultraviolet and visible light. *Journal of Photochemistry and Photobiology B: Biology* **2004**, *77*, 93–96, doi:10.1016/S1011-1344(04)00121-6.
34. Guffey, J.S.; Wilborn, J. *In Vitro* Bactericidal Effects of 405-nm and 470-nm Blue Light. *Photomedicine and Laser Surgery* **2006**, *24*, 684–688, doi:10.1089/pho.2006.24.684.
35. Sollazzo, A.; Shakeri-Manesh, S.; Fotouhi, A.; Czub, J.; Haghdoost, S.; Wojcik, A. Interaction of low and high LET radiation in TK6 cells—mechanistic aspects and significance for radiation protection. *Journal of Radiological Protection* **2016**, *36*, 721–735, doi:10.1088/0952-4746/36/4/721.
36. Staaf, E.; Brehwens, K.; Haghdoost, S.; Pachnerova-Brabcova, K.; Czub, J.; Braziewicz, J.; Nievaart, S.; Wojcik, A. Characterisation of a setup for mixed beam exposures of cells to 241Am alpha particles and X-rays. *Radiation Protection Dosimetry* **2012**, *151*, 570–579, doi:10.1093/rpd/ncs024.
37. Raju, M.R.; Jett, J.H. RBE and OER Variations of Mixtures of Plutonium Alpha Particles and X-Rays for Damage to Human Kidney Cells (T-1). *Radiation Research* **1974**, *60*, 473, doi:10.2307/3574026.

 doi:10.20944/preprints202506.2020.v1

38. Cheng, L.; Brzozowska-Wardecka, B.; Lisowska, H.; Wojcik, A.; Lundholm, L. Impact of ATM and DNA-PK inhibition on gene expression and individual response of human lymphocytes to mixed beams of alpha particles and X-rays. *Cancers* **2019**, *11*, 2013, doi:10.3390/cancers11122013.
39. Staaf, E.; Deperas-Kaminska, M.; Brehwens, K.; Haghdoost, S.; Czub, J.; Wojcik, A. Complex aberrations in lymphocytes exposed to mixed beams of 241Am alpha particles and X-rays. *Mutation Research/Genetic Toxicology and Environmental Mutagenesis* **2013**, *756*, 95–100, doi:10.1016/j.mrgentox.2013.05.001.
40. Staaf, E.; Brehwens, K.; Haghdoost, S.; Nievaart, S.; Pachnerova-Brabcova, K.; Czub, J.; Braziewicz, J.; Wojcik, A. Micronuclei in human peripheral blood lymphocytes exposed to mixed beams of X-rays and alpha particles. *Radiation and Environmental Biophysics* **2012**, *51*, 283–293, doi:10.1007/s00411-012-0417-x.
41. Brooks, A.L.; Newton, G.J.; Shyr, L.-J.; Seiler, F.A.; Scott, B.R. The combined effects of α-particles and X-rays on cell killing and micronuclei induction in lung epithelial cells. *International Journal of Radiation Biology* **1990**, *58*, 799–811, doi:10.1080/09553009014552181.
42. Sollazzo, A.; Brzozowska, B.; Cheng, L.; Lundholm, L.; Haghdoost, S.; Scherthan, H.; Wojcik, A. Alpha particles and X rays interact in inducing DNA damage in U2OS cells. *Radiation Research* **2017**, *188*, 400, doi:10.1667/RR14803.1.
43. Staaf, E.; Brehwens, K.; Haghdoost, S.; Czub, J.; Wojcik, A. Gamma-H2AX foci in cells exposed to a mixed beam of X-rays and alpha particles. *Genome Integrity* **2012**, *3*, doi:10.1186/2041-9414-3-8.
44. Cheng, L.; Brzozowska, B.; Sollazzo, A.; Lundholm, L.; Lisowska, H.; Haghdoost, S.; Wojcik, A. Simultaneous induction of dispersed and clustered DNA lesions compromises DNA damage response in human peripheral blood lymphocytes. *PLOS ONE* **2018**, *13*, e0204068, doi:10.1371/journal.pone.0204068.
45. Sollazzo, A.; Brzozowska, B.; Cheng, L.; Lundholm, L.; Scherthan, H.; Wojcik, A. Live dynamics of 53BP1 foci following simultaneous induction of clustered and dispersed DNA damage in U2OS cells. *International Journal of Molecular Sciences* **2018**, *19*, 519, doi:10.3390/ijms19020519.
46. McNally, N.J.; De Ronde, J.; Folkard, M. Interaction between X-ray and α-particle damage in V79 cells. *International Journal of Radiation Biology* **1988**, *53*, 917–920, doi:10.1080/09553008814551281.
47. Karimi Roshan, M.; Belikov, S.; Ix, M.; Protti, N.; Balducci, C.; Dodel, R.; Ross, J.A.; Lundholm, L. Fractionated alpha and mixed beam radiation promote stronger pro-inflammatory effects compared to acute exposure and trigger phagocytosis. *Frontiers in Cellular Neuroscience* **2024**, *18*, 1440559, doi:10.3389/fncel.2024.1440559.
48. Lee, U.-S.; Lee, D.-H.; Kim, E.-H. Characterization of γ-H2AX foci formation under alpha particle and X-ray exposures for dose estimation. *Scientific Reports* **2022**, *12*, 3761, doi:10.1038/s41598-022-07653-y.
49. Tartas, A.; Lundholm, L.; Scherthan, H.; Wojcik, A.; Brzozowska, B. The order of sequential exposure of U2OS cells to gamma and alpha radiation influences the formation and decay dynamics of NBS1 foci. *PLOS ONE* **2023**, *18*, e0286902, doi:10.1371/journal.pone.0286902.
50. Akuwudike, P.; López-Riego, M.; Ginter, J.; Cheng, L.; Wieczorek, A.; Życieńska, K.; Łysek-Gładysińska, M.; Wojcik, A.; Brzozowska, B.; Lundholm, L. Mechanistic insights from high resolution DNA damage analysis to understand mixed radiation exposure. *DNA Repair* **2023**, *130*, 103554, doi:10.1016/j.dnarep.2023.103554.
51. Murthy, M.S.S.; Madhvanath, U.; Subrahmanyam, P.; Rao, B.S.; Reddy, N.M.S. Synergistic effect of simultaneous exposure to 60Co gamma rays and 210Po alpha rays in diploid yeast. *Radiation Research* **1975**, *63*, 185, doi:10.2307/3574318.
52. Scott, B.R.; Hahn, F.F.; Snipes, M.B.; Newton, G.J.; Eidson, A.F.; Mauderly, J.L.; Boecker, B.B. Predicted and observed early effects of combined alpha and beta lung irradiation. *Health Physics* **1990**, *59*, 791–805, doi:10.1097/00004032-199012000-00003.
53. Bubryak, I.; Vilensky, E.; Naumenko, V.; Grodzisky, D. Influence of combined alpha, beta and gamma radionuclide contamination on the frequency of waxy-reversions in barley pollen. *Science of The Total Environment* **1992**, *112*, 29–36, doi:10.1016/0048-9697(92)90235-K.
54. Killion, D.D.; Constantin, M.J. Effects of separate and combined beta and gamma irradiation on the soybean plant. *Radiation Botany* **1974**, *14*, 91–99, doi:10.1016/S0033-7560(74)90248-8.

 doi:10.20944/preprints202506.2020.v1

55. Broustas, C.G.; Harken, A.D.; Garty, G.; Amundson, S.A. Identification of differentially expressed genes and pathways in mice exposed to mixed field neutron/photon radiation. *BMC Genomics* **2018**, *19*, 504, doi:10.1186/s12864-018-4884-6.
56. Miller, R.C.; Geard, C.R.; Marino, S.A.; Richards, M.; Randers-Pehrson, G. Oncogenic transformation following sequential irradiations with monoenergetic neutrons and X rays. *Radiation Research* **1991**, *125*, 338, doi:10.2307/3578121.
57. Joiner, M.C.; Bremner, J.C.; Denekamp, J.; Maughan, R.L. The interaction between X-rays and 3 MeV neutrons in the skin of the mouse foot. *International Journal of Radiation Biology and Related Studies in Physics, Chemistry and Medicine* **1984**, *46*, 625–638, doi:10.1080/09553008414551811.
58. Masuda, K. Effects of 14 MeV neutrons and X-rays, singly or combined on the reproductive capacity of L cells. *Journal of Radiation Research* **1970**, *11*, 107–112, doi:10.1269/jrr.11.107.
59. Marples, B.; Skov, K.A. Small doses of high-linear energy transfer radiation increase the radioresistance of chinese hamster V79 cells to subsequent X irradiation. *Radiation Research* **1996**, *146*, 382, doi:10.2307/3579300.
60. Mukherjee, S.; Grilj, V.; Broustas, C.G.; Ghandhi, S.A.; Harken, A.D.; Garty, G.; Amundson, S.A. Human transcriptomic response to mixed neutron-photon exposures relevant to an improvised nuclear device. *Radiation Research* **2019**, *192*, 189, doi:10.1667/RR15281.1.
61. McNally, N.J.; De Ronde, J.; Hinchliffe, M. The effect of sequential irradiation with X-rays and fast neutrons on the survival of V79 chinese hamster cells. *International Journal of Radiation Biology and Related Studies in Physics, Chemistry and Medicine* **1984**, *45*, 301–310, doi:10.1080/09553008414550441.
62. Ngo, F.Q.H.; Han, A.; Elkind, M.M. On the repair of sub-lethal damage in V79 chinese hamster cells resulting from irradiation with fast neutrons or fast neutrons combined with X-rays. *International Journal of Radiation Biology and Related Studies in Physics, Chemistry and Medicine* **1977**, *32*, 507–511, doi:10.1080/09553007714551291.
63. Hornsey, S.; Andreozzi, U.; Warren, P.R. Sublethal damage in cells of the mouse gut after mixed treatment with X rays and fast neutrons. *The British Journal of Radiology* **1977**, *50*, 513–517, doi:10.1259/0007-1285-50-595-513.
64. Suzuki, S. Survival of chinese hamster V79 cells after irradiation with a mixture of neutrons and 60 co g rays: experimental and theoretical analysis of mixed irradiation. *Radiation Research* **1993**, *133*, 327, doi:10.2307/3578217.
65. Posypanova, G.A.; Ratushnyak, M.G.; Semochkina, Y.P.; Strepetov, A.N. Response of murine neural stem/progenitor cells to gamma-neutron radiation. *International Journal of Radiation Biology* **2022**, *98*, 1559–1570, doi:10.1080/09553002.2022.2055802.
66. Wojcik, A.; Obe, G.; Lisowska, H.; Czub, J.; Nievaart, V.; Moss, R.; Huiskamp, R.; Sauerwein, W. Chromosomal aberrations in peripheral blood lymphocytes exposed to a mixed beam of low energy neutrons and gamma radiation. *Journal of Radiological Protection* **2012**, *32*, 261–274, doi:10.1088/0952-4746/32/3/261.
67. Wang, C.-K.C.; Zhang, X.; Gifford, I.; Burgett, E.; Adams, V.; Al-Sheikhly, M. Experimental validation of the new nanodosimetry-based cell survival model for mixed neutron and gamma-ray irradiation. *Physics in Medicine and Biology* **2007**, *52*, N367–N374, doi:10.1088/0031-9155/52/17/N01.
68. Railton, R.; Lawson, R.C.; Porter, D. Interaction of γ-ray and neutron effects on the proliferative capacity of chinese hamster cells. *International Journal of Radiation Biology and Related Studies in Physics, Chemistry and Medicine* **1975**, *27*, 75–82, doi:10.1080/09553007514550071.
69. Palmqvist, T.; Lopez-Riego, M.; Bucher, M.; Oestreicher, U.; Pojtinger, S.; Giesen, U.; Toma-Dasu, I.; Wojcik, A. Biological effectiveness of combined exposure to neutrons and gamma radiation applied in two orders of sequence: Relevance for biological dosimetry after nuclear emergencies. *Radiation Medicine and Protection* **2025**, *6*, 1–10, doi:10.1016/j.radmp.2024.10.004.
70. Higgins, P.D.; DeLuca, P.M.; Pearson, D.W.; Gould, M.N. V79 survival following simultaneous or sequential irradiation by 15-MeV neutrons and 60Co photons. *Radiation Research* **1983**, *95*, 45–56.
71. Higgins, P.D.; DeLuca, P.M.; Gould, M.N. Effect of pulsed dose in simultaneous and sequential irradiation of V-79 cells by 14.8-MeV neutrons and 60Co photons. *Radiation Research* **1984**, *99*, 591–595.

 doi:10.20944/preprints202506.2020.v1

72. Skidmore, W.D.; McHale, C.G. Fluorescence of serum and urine from rats exposed to mixed gamma-neutron radiations. *Radiation Research* **1969**, *38*, 357, doi:10.2307/3572778.
73. Kubasova, T.; Antal, S.; Somosy, Z.; Kœteles, G.J. Effects of mixed neutron-gamma irradiation in vivo on the cell surfaces of murine blood cells. *Radiation and Environmental Biophysics* **1984**, *23*, 269–277, doi:10.1007/BF01407598.
74. Rodina, A.V.; Semochkina, Y.P.; Vysotskaya, O.V.; Romantsova, A.N.; Strepetov, A.N.; Moskaleva, E.Y. Low dose gamma irradiation pretreatment modulates the sensitivity of CNS to subsequent mixed gamma and neutron irradiation of the mouse head. *International Journal of Radiation Biology* **2021**, *97*, 926–942, doi:10.1080/09553002.2021.1928787.
75. Yuan, Y.; Chai, D.; Zhang, R.; Cheng, J.; Dong, J.; Liu, H.; Zhang, Z.; Dang, X.; Ning, K. Effects of neutron and gamma rays combined irradiation on the transcriptional profile of human peripheral blood. *Radiation Research* **2023**, *200*, doi:10.1667/RADE-22-00147.2.
76. Jervis, H.R.; McLaughlin, M.M.; Johnson, M.C. Effect of neutron-gamma radiation on the morphology of the mucosa of the small intestine of germfree and conventional mice. *Radiation Research* **1971**, *45*, 613–628.
77. Iliakis, G.; Ngo, F.Q.; Roberts, W.K.; Youngman, K. Evidence for similarities between radiation damage expressed by beta-araA and damage involved in the interaction effect observed after exposure of V79 cells to mixed neutrons and gamma radiation. *Radiation Research* **1985**, *104*, 303–316.
78. Mason, A.J.; Giusti, V.; Green, S.; Af Rosenschöld, P.M.; Beynon, T.D.; Hopewell, J.W. Interaction between the biological effects of high- and low-LET radiation dose components in a mixed field exposure. *International Journal of Radiation Biology* **2011**, *87*, 1162–1172, doi:10.3109/09553002.2011.624154.
79. Laiakis, E.C.; Canadell, M.P.; Grilj, V.; Harken, A.D.; Garty, G.Y.; Astarita, G.; Brenner, D.J.; Smilenov, L.; Fornace, A.J. Serum lipidomic analysis from mixed neutron/X-ray radiation fields reveals a hyperlipidemic and pro-inflammatory phenotype. *Scientific Reports* **2019**, *9*, 4539, doi:10.1038/s41598-019-41083-7.
80. Matchuk, O.N.; Yakimova, A.O.; Saburov, V.O.; Koryakin, S.N.; Ivanov, S.A.; Zamulaeva, I.A. Effects of combined action of neutron and proton radiation on the pool of breast cancer stem cells and expression of stemness genes in vitro. *Bulletin of Experimental Biology and Medicine* **2022**, *173*, 749–753, doi:10.1007/s10517-022-05635-8.
81. Ngo, F.Q.; Blakely, E.A.; Tobias, C.A. Sequential exposures of mammalian cells to low- and high-LET radiations. I. Lethal effects following X-ray and neon-ion irradiation. *Radiation Research* **1981**, *87*, 59–78.
82. Ngo, F.Q.; Blakely, E.A.; Tobias, C.A.; Chang, P.Y.; Lommel, L. Sequential exposures of mammalian cells to low- and high-LET radiations. II. As a function of cell-cycle stages. *Radiation Research* **1988**, *115*, 54–69.
83. Bird, R.P.; Zaider, M.; Rossi, H.H.; Hall, E.J.; Marino, S.A.; Rohrig, N. The sequential irradiation of mammalian cells with X rays and charged particles of high LET. *Radiation Research* **1983**, *93*, 444–452.
84. Tenforde, T.S.; Montoya, V.J.; Afzal, S.M.J.; Parr, S.S.; Curtis, S.B. Response of rat rhabdomyosarcoma tumors to split doses of mixed high- and low-LET radiation. *International Journal of Radiation Oncology*Biology*Physics* **1989**, *16*, 1529–1536, doi:10.1016/0360-3016(89)90958-9.
85. Yamamoto, N.; Ikeda, C.; Yakushiji, T.; Nomura, T.; Katakura, A.; Shibahara, T.; Mizoe, J. Genetic effects of X-ray and carbon ion irradiation in head and neck carcinoma cell lines. *The Bulletin of Tokyo Dental College* **2007**, *48*, 177–185, doi:10.2209/tdcpublication.48.177.
86. Yu, Z.; Hong, Z.; Zhang, Q.; Lin, L.-C.; Shahnazi, K.; Wu, X.; Lu, J.; Jiang, G.; Wang, Z. Proton and carbon ion radiation therapy for locally advanced pancreatic cancer: A phase I dose escalation study. *Pancreatology* **2020**, *20*, 470–476, doi:10.1016/j.pan.2020.01.010.
87. Guan, X.; Gao, J.; Hu, J.; Hu, W.; Yang, J.; Qiu, X.; Hu, C.; Kong, L.; Lu, J.J. The preliminary results of proton and carbon ion therapy for chordoma and chondrosarcoma of the skull base and cervical spine. *Radiation Oncology* **2019**, *14*, 206, doi:10.1186/s13014-019-1407-9.
88. Ma, N.-Y.; Chen, J.; Ming, X.; Jiang, G.-L.; Lu, J.J.; Wu, K.-L.; Mao, J. Preliminary safety and efficacy of proton plus carbon-ion radiotherapy with concurrent chemotherapy in limited-stage small cell lung cancer. *Frontiers in Oncology* **2021**, *11*, 766822, doi:10.3389/fonc.2021.766822.
89. Troshina, M.V.; Koryakina, E.V.; Potetnya, V.I.; Solov'ev, A.N.; Saburov, V.O.; Lychagin, A.A.; Ivanov, S.A.; Kaprin, A.D.; Koryakin, S.N. Biological response of chinese hamster B14-150 cells to sequential combined

 doi:10.20944/preprints202506.2020.v1

exposure to protons and 12C ions. *Bulletin of Experimental Biology and Medicine* **2023**, *176*, 38–41, doi:10.1007/s10517-023-05963-3.

90. Müller, C.; De Prado Leal, M.; Dominietto, M.D.; Umbricht, C.A.; Safai, S.; Perrin, R.L.; Egloff, M.; Bernhardt, P.; Van Der Meulen, N.P.; Weber, D.C.; et al. Combination of Proton Therapy and Radionuclide Therapy in Mice: Preclinical Pilot Study at the Paul Scherrer Institute. *Pharmaceutics* **2019**, *11*, 450, doi:10.3390/pharmaceutics11090450.
91. Aljabab, S.; Lui, A.; Wong, T.; Liao, J.; Laramore, G.; Parvathaneni, U. A combined neutron and proton regimen for advanced salivary tumors: early clinical experience. *Cureus* **2021**, doi:10.7759/cureus.14844.
92. Koryakina, E.V.; Potetnya, V.I.; Troshina, M.V.; Solov'ev, A.N.; Saburov, V.O.; Lychagin, A.A.; Koryakin, S.N.; Ivanov, S.A.; Kaprin, A.D. Post-irradiation recovery of B14-150 fibrosarcoma cells after combined irradiation with low and high linear energy transfer. *Bulletin of Experimental Biology and Medicine* **2022**, *173*, 641–644, doi:10.1007/s10517-022-05604-1.
93. Balakin, V.E.; Rozanova, O.M.; Smirnova, E.N.; Belyakova, T.A.; Shemyakov, A.E.; Strelnikova, N.S. Combined effect of neutron and proton radiations on the growth of solid ehrlich ascites carcinoma and remote effects in mice. *Doklady Biochemistry and Biophysics* **2021**, *498*, 159–164, doi:10.1134/S1607672921030017.
94. Koryakin, S.N.; Troshina, M.V.; Koryakina, E.V.; Potetnya, V.I.; Pichkunova, A.A.; Saburov, V.O.; Kazakov, E.I.; Lychagin, A.A.; Ivanov, S.A.; Kaprin, A.D.; et al. The study of effectiveness of combined proton—neutron irradiation of tumor cells in vitro. *Bulletin of Experimental Biology and Medicine* **2024**, *178*, 75–78, doi:10.1007/s10517-024-06285-8.
95. López-Nieva, P.; González-Vasconcellos, I.; González-Sánchez, L.; Cobos-Fernández, M.A.; Ruiz-García, S.; Sánchez Pérez, R.; Aroca, Á.; Fernández-Piqueras, J.; Santos, J. Differential molecular response in mice and human thymocytes exposed to a combined-dose radiation regime. *Scientific Reports* **2022**, *12*, 3144, doi:10.1038/s41598-022-07166-8.
96. Gao, F.; Fish, B.L.; Szabo, A.; Schock, A.; Narayanan, J.; Jacobs, E.R.; Moulder, J.E.; Lazarova, Z.; Medhora, M. Enhanced survival from radiation pneumonitis by combined irradiation to the skin. *International Journal of Radiation Biology* **2014**, *90*, 753–761, doi:10.3109/09553002.2014.922722.
97. Reinhold, A.; Glasow, A.; Nürnberger, S.; Weimann, A.; Telemann, L.; Stolzenburg, J.-U.; Neuhaus, J.; Berndt-Paetz, M. Ionizing radiation and photodynamic therapy lead to multimodal tumor cell death, synergistic cytotoxicity and immune cell invasion in human bladder cancer organoids. *Photodiagnosis and Photodynamic Therapy* **2025**, *51*, 104459, doi:10.1016/j.pdpdt.2024.104459.
98. Luksiene, Z.; Kalvelyte, A.; Supino, R. On the combination of photodynamic therapy with ionizing radiation. *Journal of Photochemistry and Photobiology B: Biology* **1999**, *52*, 35–42, doi:10.1016/S1011-1344(99)00098-6.
99. Bulin, A.-L.; Broekgaarden, M.; Simeone, D.; Hasan, T. Low dose photodynamic therapy harmonizes with radiation therapy to induce beneficial effects on pancreatic heterocellular spheroids. *Oncotarget* **2019**, *10*, 2625–2643, doi:10.18632/oncotarget.26780.
100. Wang, G.D.; Nguyen, H.T.; Chen, H.; Cox, P.B.; Wang, L.; Nagata, K.; Hao, Z.; Wang, A.; Li, Z.; Xie, J. X-Ray Induced Photodynamic Therapy: A Combination of Radiotherapy and Photodynamic Therapy. *Theranostics* **2016**, *6*, 2295–2305, doi:10.7150/thno.16141.
101. Montazerabadi, A.R.; Sazgarnia, A.; Bahreyni-Toosi, M.H.; Ahmadi, A.; Aledavood, A. The effects of combined treatment with ionizing radiation and indocyanine green-mediated photodynamic therapy on breast cancer cells. *Journal of Photochemistry and Photobiology B: Biology* **2012**, *109*, 42–49, doi:10.1016/j.jphotobiol.2012.01.004.
102. Tran, T.A.; Kappelhoff, J.; Jüstel, T.; Anderson, R.R.; Purschke, M. UV emitting nanoparticles enhance the effect of ionizing radiation in 3D lung cancer spheroids. *International Journal of Radiation Biology* **2022**, *98*, 1484–1494, doi:10.1080/09553002.2022.2027541.
103. Müller, M.; Wang, Y.; Squillante, M.R.; Held, K.D.; Anderson, R.R.; Purschke, M. UV scintillating particles as radiosensitizer enhance cell killing after X-ray excitation. *Radiotherapy and Oncology* **2018**, *129*, 589–594, doi:10.1016/j.radonc.2018.06.016.

 doi:10.20944/preprints202506.2020.v1

104. Kargar, S.; Khoei, S.; Khoee, S.; Shirvalilou, S.; Mahdavi, S.R. Evaluation of the combined effect of NIR laser and ionizing radiation on cellular damages induced by IUdR-loaded PLGA-coated Nano-graphene oxide. *Photodiagnosis and Photodynamic Therapy* **2018**, *21*, 91–97, doi:10.1016/j.pdpdt.2017.11.007.
105. Marvaso, G.; Vischioni, B.; Pepa, M.; Zaffaroni, M.; Volpe, S.; Patti, F.; Bellerba, F.; Gandini, S.; Comi, S.; Corrao, G.; et al. Mixed-beam approach for high-risk prostate cancer carbon-ion boost followed by photon intensity-modulated radiotherapy: preliminary results of phase II trial AIRC-IG-14300. *Frontiers in Oncology* **2021**, *11*, 778729, doi:10.3389/fonc.2021.778729.
106. Gugliandolo, S.G.; Marvaso, G.; Comi, S.; Pepa, M.; Romanò, C.; Zerini, D.; Augugliaro, M.; Russo, S.; Vischioni, B.; Valvo, F.; et al. Mixed-beam approach for high-risk prostate cancer: Carbon-ion boost followed by photon intensity-modulated radiotherapy. Dosimetric and geometric evaluations (AIRC IG-14300). *Physica Medica* **2020**, *76*, 327–336, doi:10.1016/j.ejmp.2020.07.012.
107. Alterio, D.; D'Ippolito, E.; Vischioni, B.; Fossati, P.; Gandini, S.; Bonora, M.; Ronchi, S.; Vitolo, V.; Mastella, E.; Magro, G.; et al. Mixed-beam approach in locally advanced nasopharyngeal carcinoma: IMRT followed by proton therapy boost versus IMRT-only. Evaluation of toxicity and efficacy. *Acta Oncologica* **2020**, *59*, 541–548, doi:10.1080/0284186X.2020.1730001.
108. Zhang, R.; Heins, D.; Sanders, M.; Guo, B.; Hogstrom, K. Evaluation of a mixed beam therapy for postmastectomy breast cancer patients: Bolus electron conformal therapy combined with intensity modulated photon radiotherapy and volumetric modulated photon arc therapy. *Medical Physics* **2018**, *45*, 2912–2924, doi:10.1002/mp.12958.
109. Liu, J.; Zhang, J.; Huang, F.; Deng, Y.; Li, B.; Ouyang, R.; Miao, Y.; Sun, Y.; Li, Y. X-ray and NIR light dual-triggered mesoporous upconversion nanophosphor/Bi heterojunction radiosensitizer for highly efficient tumor ablation. *Acta Biomaterialia* **2020**, *113*, 570–583, doi:10.1016/j.actbio.2020.06.044.
110. Zhou, Y.; Kou, J.; Zhang, Y.; Ma, R.; Wang, Y.; Zhang, J.; Zhang, C.; Zhan, W.; Li, K.; Li, X. Magnetic-guided nanocarriers for ionizing/non-ionizing radiation synergistic treatment against triple-negative breast cancer. *BioMedical Engineering OnLine* **2024**, *23*, 67, doi:10.1186/s12938-024-01263-7.
111. Maruoka, Y.; Nagaya, T.; Sato, K.; Ogata, F.; Okuyama, S.; Choyke, P.L.; Kobayashi, H. Near infrared photoimmunotherapy with combined exposure of external and interstitial light sources. *Molecular Pharmaceutics* **2018**, *15*, 3634–3641, doi:10.1021/acs.molpharmaceut.8b00002.
112. Åsell, M.; Hyödynmaa, S.; Söderström, S.; Brahme, A. Optimal electron and combined electron and photon therapy in the phase space of complication-free cure. *Physics in Medicine and Biology* **1999**, *44*, 235–252, doi:10.1088/0031-9155/44/1/017.
113. Mazzucconi, D.; Agosteo, S.; Ferrarini, M.; Fontana, L.; Lante, V.; Pullia, M.; Savazzi, S. Mixed particle beam for simultaneous treatment and online range verification in carbon ion therapy: Proof-of-concept study. *Medical Physics* **2018**, *45*, 5234–5243, doi:10.1002/mp.13219.
114. Demizu, Y.; Kagawa, K.; Ejima, Y.; Nishimura, H.; Sasaki, R.; Soejima, T.; Yanou, T.; Shimizu, M.; Furusawa, Y.; Hishikawa, Y.; et al. Cell biological basis for combination radiotherapy using heavy-ion beams and high-energy X-rays. *Radiotherapy and Oncology* **2004**, *71*, 207–211, doi:10.1016/j.radonc.2004.03.008.
115. Furusawa, Y.; Nakano-Aoki, M.; Matsumoto, Y.; Hirayama, R.; Kobayashi, A.; Konishi, T. Equivalency of the quality of sublethal lesions after photons and high-linear energy transfer ion beams. *Journal of Radiation Research* **2017**, *58*, 803–808, doi:10.1093/jrr/rrx030.
116. Haraf, D.J.; Rubin, S.J.; Sweeney, P.; Kuchnir, F.T.; Sutton, H.G.; Chodak, G.W.; Weichselbaum, R.R. Photon neutron mixed-beam radiotherapy of locally advanced prostate cancer. *International Journal of Radiation Oncology*Biology*Physics* **1995**, *33*, 3–14, doi:10.1016/0360-3016(95)00181-W.
117. Griffin, T.W.; Davis, R.; Laramore, G.E.; Maor, M.H.; Hendrickson, F.R.; Rodriguez-Antunez, A.; Davis, L. Mixed beam radiation therapy for unresectable squamous cell carcinomas of the head and neck: the results of a randomized RTOG study. *International Journal of Radiation Oncology*Biology*Physics* **1984**, *10*, 2211–2215, doi:10.1016/0360-3016(84)90225-6.
118. Griffin, T.W.; Pajak, T.F.; Maor, M.H.; Laramore, G.E.; Hendrickson, F.R.; Parker, R.G.; Thomas, F.J.; Davis, L.W. Mixed neutron/photon irradiation of unresectable squamous cell carcinomas of the head and neck: The final report of a randomized cooperative trial. *International Journal of Radiation Oncology*Biology*Physics* **1989**, *17*, 959–965, doi:10.1016/0360-3016(89)90142-9.

 doi:10.20944/preprints202506.2020.v1

119. Ando, K.; Koike, S.; Fukuda, N.; Kanehira, C. Independent effect of a mixed-beam regimen of fast neutrons and gamma rays on a murine fibrosarcoma. *Radiation Research* **1984**, *98*, 96–106.
120. Kinashi, Y.; Yokomizo, N.; Takahashi, S. DNA double-strand breaks induced by fractionated neutron beam irradiation for boron neutron capture therapy. *Anticancer Research* **2017**, *37*, 1681–1685, doi:10.21873/anticanres.11499.
121. Phoenix, B.; Green, S.; Hill, M.A.; Jones, B.; Mill, A.; Stevens, D.L. Do the various radiations present in BNCT act synergistically? Cell survival experiments in mixed alpha-particle and gamma-ray fields. *Applied Radiation and Isotopes* **2009**, *67*, S318–S320, doi:10.1016/j.apradiso.2009.03.097.
122. Green, S.; Phoenix, B.; Mill, A.J.; Hill, M.; Charles, M.W.; Thompson, J.; Jones, B.; Ngoga, D.; Detta, A.; James, N.D.; et al. The Birmingham Boron Neutron Capture Therapy (BNCT) Project:: Developments towards Selective Internal Particle Therapy. *Clinical Oncology* **2011**, *23*, S23–S24, doi:10.1016/j.clon.2011.01.378.
123. Okumura, K.; Kinashi, Y.; Kubota, Y.; Kitajima, E.; Okayasu, R.; Ono, K.; Takahashi, S. Relative biological effects of neutron mixed-beam irradiation for boron neutron capture therapy on cell survival and DNA double-strand breaks in cultured mammalian cells. *Journal of Radiation Research* **2013**, *54*, 70–75, doi:10.1093/jrr/rrs079.
124. Maruyama, Y.; Feola, J.M.; Wierzbicki, J. Study of biological effects of varying mixtures of Cf-252 and gamma radiation on the acute radiation syndromes: Relevance to clinical radiotherapy of radioresistant cancer. *International Journal of Radiation Oncology*Biology*Physics* **1993**, *27*, 907–914, doi:10.1016/0360-3016(93)90467-A.
125. Furusawa, Y.; Aoki, M.; Durante, M. Simultaneous exposure of mammalian cells to heavy ions and X-rays. *Advances in Space Research* **2002**, *30*, 877–884, doi:10.1016/S0273-1177(02)00409-X.
126. Kokhan, V.S.; Chaprov, K.; Abaimov, D.A.; Nesterov, M.S.; Pikalov, V.A. Combined irradiation by gamma-rays and carbon-12 nuclei caused hyperlocomotion and change in striatal metabolism of rats. *Life Sciences in Space Research* **2025**, *44*, 99–107, doi:10.1016/j.lssr.2024.08.005.
127. Anokhina, I.P.; Anokhin, P.K.; Kokhan, V.S. Combined Irradiation by Gamma Rays and Carbon Nuclei Increases the C/EBP-β LIP Isoform Content in the Pituitary Gland of Rats. *Doklady Biological Sciences* **2019**, *488*, 133–135, doi:10.1134/S0012496619050016.
128. Blanco, Y.; De Diego-Castilla, G.; Viúdez-Moreiras, D.; Cavalcante-Silva, E.; Rodríguez-Manfredi, J.A.; Davila, A.F.; McKay, C.P.; Parro, V. Effects of gamma and electron radiation on the structural integrity of organic molecules and macromolecular biomarkers measured by microarray immunoassays and their astrobiological implications. *Astrobiology* **2018**, *18*, 1497–1516, doi:10.1089/ast.2016.1645.
129. Kiffer, F.; Carr, H.; Groves, T.; Anderson, J.E.; Alexander, T.; Wang, J.; Seawright, J.W.; Sridharan, V.; Carter, G.; Boerma, M.; et al. Effects of ^{1}H +^{16}O charged particle irradiation on short-term memory and hippocampal physiology in a murine model. *Radiation Research* **2018**, *189*, 53–63, doi:10.1667/RR14843.1.
130. Kiffer, F.; Alexander, T.; Anderson, J.; Groves, T.; McElroy, T.; Wang, J.; Sridharan, V.; Bauer, M.; Boerma, M.; Allen, A. Late Effects of ^{1}H +^{16}O on Short-Term and Object Memory, Hippocampal Dendritic Morphology and Mutagenesis. *Frontiers in Behavioral Neuroscience* **2020**, *14*, 96, doi:10.3389/fnbeh.2020.00096.
131. Raber, J.; Yamazaki, J.; Torres, E.R.S.; Kirchoff, N.; Stagaman, K.; Sharpton, T.; Turker, M.S.; Kronenberg, A. Combined effects of three high-energy charged particle beams important for space flight on brain, behavioral and cognitive endpoints in B6D2F1 female and male mice. *Frontiers in Physiology* **2019**, *10*, 179, doi:10.3389/fphys.2019.00179.
132. Luitel, K.; Kim, S.B.; Barron, S.; Richardson, J.A.; Shay, J.W. Lung cancer progression using fast switching multiple ion beam radiation and countermeasure prevention. *Life Sciences in Space Research* **2020**, *24*, 108–115, doi:10.1016/j.lssr.2019.07.011.
133. Lenarczyk, M.; Kronenberg, A.; Mäder, M.; Komorowski, R.; Hopewell, J.W.; Baker, J.E. Exposure to multiple ion beams, broadly representative of galactic cosmic rays, causes perivascular cardiac fibrosis in mature male rats. *PLOS ONE* **2023**, *18*, e0283877, doi:10.1371/journal.pone.0283877.
134. Suman, S.; Kumar, S.; Kallakury, B.V.S.; Moon, B.-H.; Angdisen, J.; Datta, K.; Fornace, A.J. Predominant contribution of the dose received from constituent heavy-ions in the induction of gastrointestinal tumorigenesis after simulated space radiation exposure. *Radiation and Environmental Biophysics* **2022**, *61*, 631–637, doi:10.1007/s00411-022-00997-z.

 doi:10.20944/preprints202506.2020.v1

135. Burke, M.; Wong, K.; Talyansky, Y.; Mhatre, S.D.; Mitchell, C.; Juran, C.M.; Olson, M.; Iyer, J.; Puukila, S.; Tahimic, C.G.T.; et al. Sexual dimorphism during integrative endocrine and immune responses to ionizing radiation in mice. *Scientific Reports* **2024**, *14*, 7334, doi:10.1038/s41598-023-33629-7.
136. Simmons, P.; Trujillo, M.; McElroy, T.; Binz, R.; Pathak, R.; Allen, A.R. Evaluating the effects of low-dose simulated galactic cosmic rays on murine hippocampal-dependent cognitive performance. *Frontiers in Neuroscience* **2022**, *16*, 908632, doi:10.3389/fnins.2022.908632.
137. Krukowski, K.; Grue, K.; Becker, M.; Elizarraras, E.; Frias, E.S.; Halvorsen, A.; Koenig-Zanoff, M.; Frattini, V.; Nimmagadda, H.; Feng, X.; et al. The impact of deep space radiation on cognitive performance: From biological sex to biomarkers to countermeasures. *Science Advances* **2021**, *7*, eabg6702, doi:10.1126/sciadv.abg6702.
138. Varma, C.; Schroeder, M.K.; Price, B.R.; Khan, K.A.; Curty Da Costa, E.; Hochman-Mendez, C.; Caldarone, B.J.; Lemere, C.A. Long-term, sex-specific effects of GCRsim and gamma irradiation on the brains, hearts, and kidneys of mice with alzheimer's disease mutations. *International Journal of Molecular Sciences* **2024**, *25*, 8948, doi:10.3390/ijms25168948.
139. Nemec-Bakk, A.S.; Sridharan, V.; Desai, P.; Landes, R.D.; Hart, B.; Allen, A.R.; Boerma, M. Effects of simulated 5-ion galactic cosmic radiation on function and structure of the mouse heart. *Life* **2023**, *13*, 795, doi:10.3390/life13030795.
140. Puukila, S.; Siu, O.; Rubinstein, L.; Tahimic, C.G.T.; Lowe, M.; Tabares Ruiz, S.; Korostenskij, I.; Semel, M.; Iyer, J.; Mhatre, S.D.; et al. Galactic cosmic irradiation alters acute and delayed species-typical behavior in male and female mice. *Life* **2023**, *13*, 1214, doi:10.3390/life13051214.
141. Sanford, L.D.; Adkins, A.M.; Boden, A.F.; Gotthold, J.D.; Harris, R.D.; Shuboni-Mulligan, D.; Wellman, L.L.; Britten, R.A. Sleep and core body temperature alterations induced by space radiation in rats. *Life* **2023**, *13*, 1002, doi:10.3390/life13041002.
142. McDonald, J.T.; Kim, J.; Farmerie, L.; Johnson, M.L.; Trovao, N.S.; Arif, S.; Siew, K.; Tsoy, S.; Bram, Y.; Park, J.; et al. Space radiation damage rescued by inhibition of key spaceflight associated miRNAs. *Nature Communications* **2024**, *15*, 4825, doi:10.1038/s41467-024-48920-y.
143. Wieg, L.; Ciola, J.C.; Wasén, C.C.; Gaba, F.; Colletti, B.R.; Schroeder, M.K.; Hinshaw, R.G.; Ekwudo, M.N.; Holtzman, D.M.; Saito, T.; et al. Cognitive effects of simulated galactic cosmic radiation are mediated by ApoE status, sex, and environment in APP knock-in mice. *International Journal of Molecular Sciences* **2024**, *25*, 9379, doi:10.3390/ijms25179379.
144. Smits, E.; Reid, F.E.; Tamgue, E.N.; Alvarado Arriaga, P.; Nguyen, C.; Britten, R.A. Sex-dependent changes in risk-taking predisposition of rats following space radiation exposure. *Life* **2025**, *15*, 449, doi:10.3390/life15030449.
145. Klein, P.M.; Parihar, V.K.; Szabo, G.G.; Zöldi, M.; Angulo, M.C.; Allen, B.D.; Amin, A.N.; Nguyen, Q.-A.; Katona, I.; Baulch, J.E.; et al. Detrimental impacts of mixed-ion radiation on nervous system function. *Neurobiology of Disease* **2021**, *151*, 105252, doi:10.1016/j.nbd.2021.105252.
146. Blackwell, A.A.; Fesshaye, A.; Tidmore, A.; I Lake, R.; Wallace, D.G.; Britten, R.A. Rapid loss of fine motor skills after low dose space radiation exposure. *Behavioural Brain Research* **2022**, *430*, 113907, doi:10.1016/j.bbr.2022.113907.
147. Stephenson, S.; Liu, A.; Blackwell, A.A.; Britten, R.A. Multiple decrements in switch task performance in female rats exposed to space radiation. *Behavioural Brain Research* **2023**, *449*, 114465, doi:10.1016/j.bbr.2023.114465.
148. Mao, X.W.; Stanbouly, S.; Chieu, B.; Sridharan, V.; Allen, A.R.; Boerma, M. Low dose space radiation-induced effects on the mouse retina and blood-retinal barrier integrity. *Acta Astronautica* **2022**, *199*, 412–419, doi:10.1016/j.actaastro.2022.07.029.
149. Weiss, M.; Nikisher, B.; Haran, H.; Tefft, K.; Adams, J.; Edwards, J.G. High throughput screen of small molecules as potential countermeasures to galactic cosmic radiation induced cellular dysfunction. *Life Sciences in Space Research* **2022**, *35*, 76–87, doi:10.1016/j.lssr.2022.06.006.
150. Edwards, S.; Adams, J.; Tchernikov, A.; Edwards, J.G. Low-dose X-ray radiation induces an adaptive response: A potential countermeasure to galactic cosmic radiation exposure. *Experimental Physiology* **2024**, EP091350, doi:10.1113/EP091350.

 doi:10.20944/preprints202506.2020.v1

151. Raber, J.; Fuentes Anaya, A.; Torres, E.R.S.; Lee, J.; Boutros, S.; Grygoryev, D.; Hammer, A.; Kasschau, K.D.; Sharpton, T.J.; Turker, M.S.; et al. Effects of six sequential charged particle beams on behavioral and cognitive performance in B6D2F1 female and male mice. *Frontiers in Physiology* **2020**, *11*, 959, doi:10.3389/fphys.2020.00959.
152. Keiser, A.A.; Kramár, E.A.; Dong, T.; Shanur, S.; Pirodan, M.; Ru, N.; Acharya, M.M.; Baulch, J.E.; Limoli, C.L.; Wood, M.A. Systemic HDAC3 inhibition ameliorates impairments in synaptic plasticity caused by simulated galactic cosmic radiation exposure in male mice. *Neurobiology of Learning and Memory* **2021**, *178*, 107367, doi:10.1016/j.nlm.2020.107367.
153. Britten, R.A.; Fesshaye, A.; Tidmore, A.; Blackwell, A.A. Similar loss of executive function performance after exposure to low (10 cGy) doses of single (4He) ions and the multi-ion GCRSim beam. *Radiation Research* **2022**, *198*, doi:10.1667/RADE-22-00022.1.
154. Mehta, S.K.; Diak, D.M.; Bustos-Lopez, S.; Nelman-Gonzalez, M.; Chen, X.; Plante, I.; Stray, S.J.; Tandon, R.; Crucian, B.E. Effect of simulated cosmic radiation on cytomegalovirus reactivation and lytic replication. *International Journal of Molecular Sciences* **2024**, *25*, 10337, doi:10.3390/ijms251910337.
155. Kumar, K.; Angdisen, J.; Ma, J.; Datta, K.; Fornace, A.J.; Suman, S. Simulated galactic cosmic radiation exposure-induced mammary tumorigenesis in Apcmin/+ mice coincides with activation of ERα-ERRα-SPP1 signaling axis. *Cancers* **2024**, *16*, 3954, doi:10.3390/cancers16233954.
156. Alaghband, Y.; Klein, P.M.; Kramár, E.A.; Cranston, M.N.; Perry, B.C.; Shelerud, L.M.; Kane, A.E.; Doan, N.-L.; Ru, N.; Acharya, M.M.; et al. Galactic cosmic radiation exposure causes multifaceted neurocognitive impairments. *Cellular and Molecular Life Sciences* **2023**, *80*, 29, doi:10.1007/s00018-022-04666-8.
157. Desai, R.I.; Kangas, B.D.; Luc, O.T.; Solakidou, E.; Smith, E.C.; Dawes, M.H.; Ma, X.; Makriyannis, A.; Chatterjee, S.; Dayeh, M.A.; et al. Complex 33-beam simulated galactic cosmic radiation exposure impacts cognitive function and prefrontal cortex neurotransmitter networks in male mice. *Nature Communications* **2023**, *14*, 7779, doi:10.1038/s41467-023-42173-x.
158. Schaeffer, E.A.; Blackwell, A.A.; Oltmanns, J.R.O.; Einhaus, R.; Lake, R.; Hein, C.P.; Baulch, J.E.; Limoli, C.L.; Ton, S.T.; Kartje, G.L.; et al. Differential organization of open field behavior in mice following acute or chronic simulated GCR exposure. *Behavioural Brain Research* **2022**, *416*, 113577, doi:10.1016/j.bbr.2021.113577.
159. Luitel, K.; Siteni, S.; Barron, S.; Shay, J.W. Simulated galactic cosmic radiation-induced cancer progression in mice. *Life Sciences in Space Research* **2024**, *41*, 43–51, doi:10.1016/j.lssr.2024.01.008.
160. Yun, S.; Kiffer, F.C.; Bancroft, G.L.; Guzman, C.S.; Soler, I.; Haas, H.A.; Shi, R.; Patel, R.; Lara-Jiménez, J.; Kumar, P.L.; et al. The longitudinal behavioral effects of acute exposure to galactic cosmic radiation in female C57BL/6J mice: Implications for deep space missions, female crews, and potential antioxidant countermeasures. *Journal of Neurochemistry* **2025**, *169*, e16225, doi:10.1111/jnc.16225.
161. Kiffer, F.C.; Luitel, K.; Tran, F.H.; Patel, R.A.; Guzman, C.S.; Soler, I.; Xiao, R.; Shay, J.W.; Yun, S.; Eisch, A.J. Effects of a 33-ion sequential beam galactic cosmic ray analog on male mouse behavior and evaluation of CDDO-EA as a radiation countermeasure. *Behavioural Brain Research* **2022**, *419*, 113677, doi:10.1016/j.bbr.2021.113677.
162. Kumar, K.; Moon, B.-H.; Datta, K.; Fornace, A.J.; Suman, S. Simulated galactic cosmic radiation (GCR)-induced expression of Spp1 coincide with mammary ductal cell proliferation and preneoplastic changes in Apc mouse. *Life Sciences in Space Research* **2023**, *36*, 116–122, doi:10.1016/j.lssr.2022.09.006.
163. Bennett, P.V.; Cutter, N.C.; Sutherland, B.M. Split-dose exposures versus dual ion exposure in human cell neoplastic transformation. *Radiation and Environmental Biophysics* **2007**, *46*, 119–123, doi:10.1007/s00411-006-0091-y.
164. Zhou, G.; Bennett, P.V.; Cutter, N.C.; Sutherland, B.M. Proton-HZE-particle sequential dual-beam exposures increase anchorage-independent growth frequencies in primary human fibroblasts. *Radiation Research* **2006**, *166*, 488–494, doi:10.1667/RR0596.1.
165. Hada, M.; Meador, J.A.; Cucinotta, F.A.; Gonda, S.R.; Wu, H. Chromosome aberrations induced by dual exposure of protons and iron ions. *Radiation and Environmental Biophysics* **2007**, *46*, 125–129, doi:10.1007/s00411-006-0083-y.

 doi:10.20944/preprints202506.2020.v1

166. Sasi, S.P.; Yan, X.; Zuriaga-Herrero, M.; Gee, H.; Lee, J.; Mehrzad, R.; Song, J.; Onufrak, J.; Morgan, J.; Enderling, H.; et al. Different sequences of fractionated low-dose proton and single iron-radiation-induced divergent biological responses in the heart. *Radiation Research* **2017**, *188*, 191–203, doi:10.1667/RR14667.1.
167. Yang, H.; Magpayo, N.; Held, K.D. Targeted and non-targeted effects from combinations of low doses of energetic protons and iron ions in human fibroblasts. *International Journal of Radiation Biology* **2011**, *87*, 311–319, doi:10.3109/09553002.2010.537431.
168. Gkikoudi, A.; Manda, G.; Beinke, C.; Giesen, U.; Al-Qaaod, A.; Dragnea, E.-M.; Dobre, M.; Neagoe, I.V.; Sangsuwan, T.; Haghdoost, S.; et al. Synergistic effects of UVB and ionizing radiation on human non-malignant cells: implications for ozone depletion and secondary cosmic radiation exposure. *Biomolecules* **2025**, *15*, 536, doi:10.3390/biom15040536.
169. Holden, S.; Perez, R.; Hall, R.; Fallgren, C.M.; Ponnaiya, B.; Garty, G.; Brenner, D.J.; Weil, M.M.; Raber, J. Effects of acute and chronic exposure to a mixed field of neutrons and photons and single or fractionated simulated galactic cosmic ray exposure on behavioral and cognitive performance in mice. *Radiation Research* **2021**, *196*, doi:10.1667/RADE-20-00228.1.
170. Kumar, K.; Moon, B.-H.; Kumar, S.; Angdisen, J.; Kallakury, B.V.S.; Fornace, A.J.; Suman, S. Senolytic agent ABT-263 mitigates low- and high-LET radiation-induced gastrointestinal cancer development in Apc1638N/+ mice. *Aging* **2025**, *17*, 97–115, doi:10.18632/aging.206183.
171. Riego, M.L.; Meher, P.K.; Brzozowska, B.; Akuwudike, P.; Bucher, M.; Oestreicher, U.; Lundholm, L.; Wojcik, A. Chromosomal damage, gene expression and alternative transcription in human lymphocytes exposed to mixed ionizing radiation as encountered in space. *Scientific Reports* **2024**, *14*, 11502, doi:10.1038/s41598-024-62313-7.
172. Garrett-Bakelman, F.E.; Darshi, M.; Green, S.J.; Gur, R.C.; Lin, L.; Macias, B.R.; McKenna, M.J.; Meydan, C.; Mishra, T.; Nasrini, J.; et al. The NASA Twins Study: A multidimensional analysis of a year-long human spaceflight. *Science* **2019**, *364*, eaau8650, doi:10.1126/science.aau8650.